Thesis for the degree of Doctor of Philosophy in Natural Science, Specialization in Chemistry

---

How ship exhaust particles change cloud activity

Implications for Arctic mixed-phase clouds

Luis Filipe Escusa dos Santos

UNIVERSITY OF GOTHENBURG

Department of Chemistry and Molecular Biology
University of Gothenburg
Gothenburg, January 2024

How ship exhaust particles change cloud activity
Implications for Arctic mixed-phase clouds

Cover illustration: Luis Santos and Timo Söhren
Photo: Christian Metzler

ISBN: 978-91-8069-579-4 (PRINT)
ISBN: 978-91-8069-580-0 (PDF)

Department of Chemistry and Molecular Biology
University of Gothenburg
413 90 Gothenburg
Sweden

Printed by Stema AB
Borås, Sweden 2024

Abstract

The Arctic is experiencing surface warming rates that exceed those observed at lower latitudes. This is caused by a complex system of feedback mechanisms in the Arctic climate system and is referred to as Arctic Amplification. Persistent mixed-phase clouds cover large areas of the Arctic region and thus, have a substantial impact on the radiative budget in the Arctic. One consequence of the amplified warming is that Arctic sea-ice extent has been decreasing over the past decades. With the rapid decline in sea-ice extent, shipping activity is projected to significantly increase due to easier accessibility and availability of shorter transportation routes. Ships are also a significant source of atmospheric pollutants, which include greenhouse gases, sulfur oxides (SO_x) and particulate matter (PM). Increased local emissions of such pollutants may perturb the natural state of Arctic clouds and thus, can lead to further climatic feedbacks.

Simultaneous with climate change, the shipping sector is undergoing regulatory changes aimed at reducing exhaust emissions of climate- and health-affecting substances. SO_x and PM emissions have been strongly linked to tens of thousands of premature deaths worldwide. As a result, the International Maritime Organization (IMO) implemented regulations that aim to reduce emissions of SO_x and indirectly, of PM to atmosphere. Respective IMO regulations mandate ships to either use fuels with reduced fuel sulfur content (FSC) or to use exhaust aftertreatment systems, such as wet scrubbers, in instances where ships continue to utilize non-compliant high sulfur content fuels. Both, FSC reduction and exhaust wet scrubbing change physicochemical properties of exhaust particles and may therefore, lead to climate feedbacks.

A series of laboratory engine experiments were performed to characterize impacts of FSC reduction and exhaust wet scrubbing on the physicochemical properties of exhaust particles. The secondary impact of compliance choices on exhaust particles' cloud activity, including liquid droplet and ice crystal formation, was a particular focus. Results from laboratory experiments were subsequently implemented into a cloud-resolving large eddy simulation model, in an effort to quantify the impact of additional ship aerosol particles on micro- and macrophysical properties of an Arctic mixed-phase cloud.

Results presented in this study illustrate how international regulations in the shipping sector may affect atmospheric processes. We observed that FSC reduction and wet scrubbing have opposing effects on exhaust particles' ability to form liquid droplets in the atmosphere. These results are supported by observed changes in particles' chemical mixing states. Moreover, we find that the impact of wet scrubbing on exhaust particle properties varies substantially between experiments and between marine engines. Wet

scrubbing may lead to particle emission profiles, which counteract the intended aims of the IMO regulation. This may have further consequences for health- and climate-related issues.

Our modelling study suggests that ship aerosol may lead to increased cloud droplet and decreased raindrop number concentrations. Consequently, a reduction in surface precipitation and reduced longwave radiative surface cooling were observed. Nevertheless, changes in cloud properties were mostly observed when ship particle number concentrations were significantly increased and/or strongly depended on the aerosol particle properties.

Increased shipping activity in the Arctic may lead to further climate feedbacks, but as demonstrated in this thesis, the magnitude of the induced changes strongly depends on fuels and engines, and whether exhaust aftertreatment systems are utilized. Given continuous changes in the shipping sector, it becomes challenging to predict how ship exhaust emissions in the Arctic may evolve over the next decades. New regulations are emerging, and the consequences should be studied as the Arctic is one of Earth's most pristine and sensitive regions, where increased shipping activity may lead to substantial environmental impacts.

Keywords: Aerosol particles, mixed-phase clouds, ship emissions, Arctic, maritime regulations

SAMMANFATTNING

Arktis upplever en ökning av yttemperaturen som överstiger den som observerats på lägre breddgrader. Detta orsakas av ett komplext system av återkopplingsmekanismer i det arktiska klimatsystemet och kallas arktisk förstärkning. Stabila blandfasmoln (moln som innehåller både is och vätska) täcker stora delar av den arktiska regionen och har därmed en betydande inverkan på strålningsbalansen i Arktis. En konsekvens av den förstärkta uppvärmningen är att utbredningen av havsis i Arktis har minskat under de senaste decennierna. Med den snabba minskningen av havsisens utbredning förväntas sjöfartsaktiviteten öka betydligt på grund av lättare tillgänglighet och tillgång till kortare transportrutter. Fartyg är också en betydande källa till luftföroreningar, bland annat växthusgaser, svaveloxider (SO_x) och partiklar (PM). Ökade lokala utsläpp av sådana föroreningar kan störa de arktiska molnens naturliga tillstånd och därmed leda till ytterligare återkopplingar till klimatet.

Samtidigt med klimatförändringarna genomgår sjöfartssektorn regeländringar som syftar till att minska avgasutsläppen av klimat- och hälsopåverkande ämnen. Utsläpp av SO_x och partiklar har starkt kopplats till tiotusentals förtida dödsfall världen över. Därför har Internationella sjöfartsorganisationen (IMO) infört bestämmelser som syftar till att minska utsläppen av SO_x och indirekt av PM till atmosfären. Enligt IMO:s bestämmelser måste fartyg antingen använda bränslen med reducerad svavelhalt (FSC) eller använda efterbehandlingssystem för avgaser, t.ex. våtskrubbrar, i de fall där fartygen fortsätter att använda bränslen med hög svavelhalt som inte uppfyller kraven. Både reducerad svavelhalt och våtskrubbrar förändrar avgaspartiklarnas fysikalisk-kemiska egenskaper och kan därför leda till återkopplingar på klimatet.

En serie laboratorieförsök med dieselmotorer utfördes för att karakterisera effekterna av reducerad svavelhalt och våtskrubbrar på avgaspartiklarnas fysikalisk-kemiska egenskaper. Den sekundära effekten av val av efterlevnad på avgaspartiklarnas molnaktivitet, inklusive vätskedroppar och iskristallbildning, var ett särskilt fokus. Resultaten från laboratorieexperimenten implementerades därefter i en molnupplösande large eddy simulation modell, i ett försök att kvantifiera effekterna av ytterligare aerosolpartiklar från fartyg på mikro- och makrofysikaliska egenskaper hos ett arktiskt blandfasmoln.

Resultaten som presenteras i denna studie illustrerar hur internationella bestämmelser inom sjöfartssektorn kan leda till oväntade klimatåterkopplingar. Vi observerade att reducerad svavelhalt och våtskrubbrar har motsatta effekter på avgaspartiklarnas förmåga att bilda vätskedroppar i atmosfären. Dessa resultat stöds av observerade förändringar i partiklarnas kemiska blandningsförhållanden. Dessutom konstaterar vi att våtskrubberns inverkan på avgaspartiklarnas egenskaper varierar avsevärt mellan olika experiment och

mellan olika marinmotorer. Användandet av våtskrubbrar kan leda till partikelutsläppsprofiler som motverkar de avsedda syftena med IMO-förordningen. Detta kan få ytterligare konsekvenser för hälso- och klimatrelaterade frågor.

Vår modellstudie visar att fartygsaerosol kan leda till ökade koncentrationer av molndroppar och minskade antal regndroppar. Följaktligen observerades en minskning av ytnederbörden och minskad långvågig radiativ ytkylning. Ändå observerades förändringar i molnegenskaper mestadels när fartygspartikelantalskoncentrationerna ökade avsevärt och/eller berodde starkt på aerosolpartikelns egenskaper.

Ökad sjöfartsaktivitet i Arktis kan leda till ytterligare klimatåterkopplingar, men som visas i denna avhandling beror storleken på de inducerade förändringarna starkt på bränslen och motorer, och om efterbehandlingssystem för avgaser används. Med tanke på de ständiga förändringarna inom sjöfartssektorn blir det en utmaning att förutsäga hur fartygens avgasutsläpp i Arktis kan komma att utvecklas under de kommande årtiondena. Nya bestämmelser är på väg och konsekvenserna bör studeras eftersom Arktis är en av jordens mest orörda och känsliga regioner, där ökad sjöfartsaktivitet kan leda till betydande miljöpåverkan.

Nyckelord: Aerosolpartiklar, blandfasmoln, fartygsutsläpp, Arktis, sjöfartsregler

List of Publications

I **Luis F. E. d. Santos**, Kent Salo and Erik S. Thomson
Quantification and physical analysis of nanoparticle emissions from a marine engine using different fuels and a laboratory wet scrubber. Environmental Science: Processes & Impacts (**2022**), 24, 1769-1781.

II **Luis F. E. d. Santos**, Kent Salo, Xiangrui Kong, Jun Noda, Thomas Kristensen, Takuji Ohigashi, Erik S Thomson
Changes in CCN activity of ship exhaust particles induced by fuel sulfur content reduction and wet scrubbing. Environmental Science: Atmosphere (**2023**), 3, 182-195.

III **Luis F. E. d. Santos**, Kent Salo, Xiangrui Kong, Markus Hartmann, Jonas Sjöblom, and Erik S. Thomson
Ship aerosol emissions and marine fuel regulations: Impacts on physicochemical properties, cloud activity and emission factors. *Manuscript submitted to Journal of Geophysical Research: Atmospheres. Under review.*

IV **Luis F. E. d. Santos**, Hannah C. Frostenberg, Alejandro Baró Pérez, Annica M. L. Ekman, Luisa Ickes and Erik S Thomson
Arctic mixed-phase cloud responses from increased shipping activity. *Manuscript planned for submission to Atmospheric Chemistry and Physics.*

Statement of Contribution

I I planned and designed the experiment and setup. I conducted the engine experiments together with KS. I analyzed and interpreted all data in collaboration with the co-authors. I wrote the original draft of the paper and formulated responses and corrections during the peer review process with assistance from the co-authors.

II I planned and designed the experiment and setup. I conducted the engine experiments together with KS and STXM analysis with XK. I analyzed and interpreted all data in collaboration with the co-authors. I wrote the original draft of the paper and formulated responses and corrections during the peer review process with assistance from the co-authors.

III I planned and designed the experiment and setup. I operated all aerosol instrumentation during the experiments (ice nucleation measurements assisted by MH), collected all filters and TEM grids for off-line analysis and performed STXM analysis together with XK. I analyzed all data and interpreted it in collaboration with the co-authors. I wrote the original draft of the paper with assistance from the co-authors.

IV I performed model simulations together with HF, LI and ABP and suggestions from AE. I analyzed all data and interpreted it in collaboration with the co-authors. I wrote the original draft of the paper with assistance from the co-authors.

Publications not Included in this Thesis

- Wanyu Liu, Jun Li, Wenjun Gu, **Luis F. E. d. Santos**, Johan Boman, Xiying Zhang, Mingjin Tang, Sen Wang, and Xiangrui Kong
  Chemical and Hygroscopic Characterization of Surface Salts in the Qaidam Basin: Implications for Climate Impacts on Planet Earth and Mars.
  ACS Earth and Space Chemistry (**2021**), 5 (3), 651-662.

List of Abbreviations

AAC	Aerodynamic aerosol classifier
BC	Black carbon
CCN	Cloud condensation nuclei
CCNc	Cloud condensation nuclei counter
CPC	Condensation particle counter
d_{mo}	Mobility diameter
d_{ae}	Aerodynamic diameter
DMA	Differential mobility analyzer
EF_x	Emission factor of variable x
FSC	Fuel sulfur content (given in wt %, herein abbreviated with %)
FWS	Wet scrubber operated with freshwater (Paper I and Paper II)
HiS	Paper III: High sulfur content distillate fuel (0.63%)
HiS/HiS_sul	Paper IV: High sulfur content fuel cases
HGO	Heavy gas oil; High sulfur content fuel (0.86%) used in Paper I and Paper II
HVO	Hydrotreated vegetable oil; low sulfur content fuel (<0.03%) used in Paper I and Paper II
IMO	International Maritime Organization
INP	Ice nucleating particles
IWP	Ice water path
κ	Dimensionless hygroscopicity parameter
LES	Large eddy simulation
LoS	Paper III: Low sulfur content distillate fuel (0.041%)
LoS	Paper IV: Low sulfur content fuel case based on MGO
LWP	Liquid water path
MGO	Marine gas oil; low sulfur content fuel (<0.03%) used in Paper I and Paper II
MIMICA	MISU MIT Cloud and Aerosol LES model
MPC	Mixed-phase cloud
NEXAFS	Near edge X-ray absorption fine structure
PINCii	Portable Ice Nucleation Chamber II
PN	Particle number
PM	Particulate matter or mass (used synonymously)
PSD	Particle size distribution

r_e	Cloud drop effective radius
RH	Relative humidity
RH_i	Relative humidity with respect to ice
ρ_{eff}	Effective density
SFCA	Scanning flow CCN analysis (operation mode for the CCNc)
SMPS	Scanning mobility particle sizer
SS	Supersaturation
SS_c	Critical supersaturation
STXM	Scanning transmission X-ray microscopy
SWS	Wet scrubber operated with seawater (Paper I and Paper II)
WS	Wet Scrubber
WS/WS_sul	Paper IV: Wet scrubber cases

Acknowledgments

Erik, thank you so much for giving me the opportunity and the trust to work on this project. Thank you for all the helpful discussions, for being so open-minded towards new ideas for experiments, and for giving me plenty of opportunities to attend interesting experiments and conferences around the world. I still think about my first day with the CCNc at RISE in Borås and often compare it to our final engine campaign... Looking back, my own personal growth and progress is probably my greatest achievement during my PhD and you were a huge part in that! Thank you for your guidance. All the best for your future! Given that Gothenburg is the world's largest village, we will probably meet each other here and there. **Kent**, if there is one person with whom I would have liked to spend all these weeks inhaling engine exhaust fumes, being surrounded by heavy, greasy, noisy machinery and not being able to see the sun (while everyone else in Gothenburg gets to enjoy it), it was you. Thank you for my first real Midsommar experience and for hours of talking about music! Hope to see you some day with TNP on the big stage at Way Out West! All the best! **Kong**, I have no idea how you do it but you're incredible! Thank you so much for introducing me to STXM and giving me the chance to participate in all these beam times! I will never forgot these experiences (eating jellyfish and getting stranded in Yokohama is one of my favorites). It was always fun and exciting. Wish you all the best for your future.

Jan, Johan and Mattias, thank you for your help and guidance, and for making the Atmospheric Science division the way it is! It was a pleasure working in this great environment! **All present and former colleagues** of the Atmospheric Science division deserve a big Thank You! I will never forget all the fikas, AWs, lunch runs and discussions! **Nondas**, thank you for taking me under your wing and teaching me how to "fly" (up walls). You are probably the only person I've ever met who can explain in 20 minutes, how to prepare a 5 minute breakfast. **Mike**, thank you for all the Simpsons talk, concerts and jam sessions. Hope to get to see Manchester one day (with a "local" guide)! **Julia**, my German compatriot, so glad that I've gotten to know you! How do we manage to live in a country with such inferior beer brewing and bread baking culture? **Linjie, Veronica and Nicolas**, you are almost there. Kämpa på!

I would like to thank **Luisa Ickes, Hannah Frostenberg and Alejandro Baró Pérez** from Chalmers University and **Annica Ekman** from Stockholm University for all their guidance and (needed) assistance during the LES experiments. I am still learning a lot each day, so please be patient with me! **Luisa**, it was nice to meet you again after all these years and roughly 900 km away from Frankfurt. A big Thank You goes out to

Jonas Sjöblom, Anders Mattsson and Timothy Benham from Chalmers University for the opportunity to use their engine cell and all the amazing support during the final engine campaign. I would like to thank all co-authors and people who participated in the engine campaigns and beam times!

Special thanks to **Anders Lennartsson** for all the great support, organization of the student labs and teaching me more about chemistry than any text book! I also want to thank **Birgitta Svenningson** from Lund University, and **Thomas Kristensen and John Falk** for all the help and assistance with the CCNc, and helpful discussions. It has been a great journey (at least, for most of the time). I would like to thank all the people I met during the past 5 years that I forgot to mention!

Danke an alle Buben!

Josefin, vet du nu vad moln är? Tack för att du har stöttat mig under denna tid! (Eller var det jag som tog hand om dig?) Du är bäst!

Als letztes möchte ich noch meiner Familie danken! Danke für all die Unterstützung und dafür, dass es für euch ok war, all die Jahre keinen richtigen Job zu haben! Endlich könnt ihr die Frage stellen: “Bist du jetzt fertig mit deiner Arbeit?”! Obrigado por tudo!

Luis

Gothenburg, Sweden, 2024

Contents

1

BACKGROUND

1.1 Aerosol Particles, Clouds and their Impact on the Climate System

In the context of atmospheric science the term "aerosol particle" refers to particulate matter (PM) suspended in Earth's atmosphere. Atmospheric aerosol particles can have both natural and anthropogenic sources. Natural sources include, for example, wind-driven suspension of salt particles from the ocean, dust particles from deserts and biological particles, such as spores, or secondary organic aerosol formed from gaseous precursors emitted by different types of vegetation or human activity. Aerosol particles from anthropogenic sources include combustion-related particles, such as black carbon (BC), also referred to as soot, and sulfate particles formed from traffic- and industry-related SO_2 emissions and volcanoes. The size of these particles typically ranges from a few nm to several μm and depends on how they were formed and emitted into the atmosphere. PM concentrations have large spatial and temporal variability. In urban areas with a high density of anthropogenic activity concentrations are generally much greater than in remote regions and show distinct temporal patterns, with peak concentrations often around commuting hours. One remote region with comparatively low particle concentrations is the Arctic, where number concentrations are usually around or below a few hundred particles per cm^3 and show distinct seasonal variability linked to sea ice cover and biological activity.[1] Nevertheless, recent studies have shown that Arctic background aerosol concentrations are increasing due to, for example, climate-driven changes in air mass transport[2] and enhanced particle formation from biological activity in the marine surface microlayer.[3]

Not only do aerosol particles have a substantial impact on local air quality and thus, affect human health, they also play key role(s) in atmospheric processes and have a substantial impact on Earth's radiative budget and its climate.[4] Aerosol particles are necessary for cloud formation. At any given time, clouds cover about two-thirds of the Earth's surface and consist of liquid cloud droplets and/or ice crystals, depending on atmospheric conditions. Cloud droplets, which generally have diameters of a few tens of

μm, are formed when aerosol particles interact with surrounding water molecules in the atmosphere and grow in size due to molecular adsorption. Aerosol particles that serve as embryos for cloud droplets are also referred to as cloud condensation nuclei (CCN). Similar to liquid droplet formation, the formation of ice crystals most often requires preexisting aerosol particles or solution droplets. A particle can serve as an ice nucleating particle (INP) at temperatures well below 0 °C.

Both aerosol particles and clouds impact Earth's radiative budget. Aerosol particles are considered to be short-lived climate forcers, which are physically and chemically reactive compounds with atmospheric lifetimes of typically less than two decades (for aerosol particles typically on the order of a few days). In the atmosphere aerosol particles interact with electromagnetic radiation, for example, by scattering, reflecting and/or absorbing incoming solar radiation. The interaction is determined by physicochemical properties that determine whether the particles exert positive or negative radiative forcing and its magnitude. Collectively, aerosol particles have a net cooling effect (negative radiative forcing) on Earth's climate. However, this cooling is a sensitive balance between negative forcing by brighter, more reflective particles, like sulfate, and darker, absorbing particles like soot.[4]

Clouds can also have cooling and warming effects on the climate system via interactions with short- and long-wave radiation. The overall effect is determined by different factors, such as the cloud altitude, its phase and optical properties. For example, high altitude clouds tend to absorb outgoing, longwave radiation and re-emit it at lower temperatures (energy), leading to a reduction in outgoing energy compared to clear sky conditions, which creates a net warming effect. Low-level clouds, on the other hand, have a greater tendency to reflect incoming solar radiation, preventing it from reaching Earth's surface, which has a net cooling effect. Globally averaged, clouds have a net cooling effect on climate, but since the pre-industrial era contributions from human activities have been altering atmospheric conditions, which also has implications for the climate effect of clouds. How clouds will change in the future and what this implies for Earth's climate system, is subject to major uncertainties. Properties of clouds may change in different ways and a lot of processes are locally constrained and thus not well resolved in global climate models. Projected changes in general cloud properties include rising high-level cloud altitudes, which could enhance their tendency to trap longwave radiation, and a general shift towards the liquid phase for ice-containing clouds, making them optically thicker and hence, prone to reflect more solar radiation.[5] In a warm enough climate reduced low-level clouds over subtropical oceans and land may lead to a positive radiative feedback.[4,6]

Aerosol particles and clouds also interact with each other. The observed increase in aerosol concentrations since the pre-industrial era, has had effects on cloud properties and thus, on the global radiative budget. Two major interaction pathways are often identified

regarding the effects of increased aerosol particle concentrations on cloud properties. Increased aerosol number concentrations will, in most cases, simultaneously lead to an increase in CCN concentrations and thus, increase the number of cloud droplets (N_c). If the liquid water content of a cloud remains constant, an increase in N_c will cause a reduction in cloud drop effective radius (r_e), therefore increasing the cloud albedo and have a cooling effect. This aerosol-cloud interaction process is also known as the Twomey effect.[7] Smaller cloud droplets may also suppress precipitation due to deceleration of droplet coalescence and thus, increase the liquid water path (LWP; vertically integrated total amount of liquid cloud water) and extend the cloud lifetime.[4,8] According to the latest IPCC report, aerosol-cloud interactions have a net cooling effect with a -1 W m^{-2} radiative forcing. These interactions make up to 75-80% of the total aerosol effect on climate, equivalent to an estimated cooling of ≈-0.5 °C. This emphasizes why it is important to improve our understanding of the underlying mechanisms and how changes in future atmospheric aerosol concentrations may impact Earth's climate system. Especially, since worldwide air pollution policies will likely reduce total anthropogenic aerosol emissions in the future, resulting in a diminished cooling effect.[4]

1.1.1 Cloud Condensation Nuclei and κ-Köhler Theory

In order to form atmospheric cloud droplets, the presence of solid or liquid aerosol particles is required. A particle's ability to bind water molecules, grow in size and form a liquid droplet, is also referred to as hygroscopicity. Water molecules can condense or deposit onto particle surfaces or be absorbed into the bulk of a solution droplet. The relative humidity (RH) plays a crucial role in aerosol particle droplet formation. Without the presence of CCN, liquid droplet formation would require unrealistically high supersaturations (SS; RH > 100%) and would therefore not be possible.[9] The SS required for droplet growth activation strongly depends on the initial size and the physicochemical properties of the CCN.[10] For water-insoluble particles generally supersaturated conditions are required to form liquid droplets. Once onset conditions for droplet formation are met, water molecules will continue to condense onto particles and grow to be become cloud droplets. This droplet growth process is known as droplet activation and the corresponding SS required to activate particles into droplets, is referred to as the critical supersaturation (SS_c). When water vapor interacts with water-soluble particles, solution droplets already form at subsaturated conditions (RH < 100%). This process is known as deliquescence and the substance-specific relative humidity, at which a particle becomes a saturated solution droplet, is referred to as the deliquescence relative humidity (DRH). Nevertheless, the solvation process of water-soluble particles is generally initiated at RH < DRH. Deliquescence is typically observed for salt particles, which are abundant in the atmosphere, especially in

marine environments.[9]

The transition from a dry aerosol particle into a liquid droplet is described by the Köhler equation that equates the saturation ratio (s), which is the ratio between the actual vapor pressure of gas (p) and its saturation vapor pressure at a given temperature (p_0), to a function of droplet diameter (D),

$$s = \frac{p}{p_0} = a_w(D) * K(D) \ . \tag{1.1}$$

Note that s and SS are directly related,

$$SS = (s - 1) \times 100\% \ . \tag{1.2}$$

Equation 1.1 consists of a water activity or Raoult's term (a_w) and a Kelvin term (K). A majority of particles in the atmosphere contain soluble material such as salts. Once condensation of water molecules occurs and a liquid phase is formed, soluble material will dissolve and solute molecules will dissociate to form an ion containing aqueous solution. At small droplet sizes, when the ionic concentration is relatively high, the ions promote condensation of water molecules and lower the vapor pressure. This solute effect is quantified as the a_w term and is vital during the early stages of droplet activation. Once the droplet grows in size due to further condensation of water molecules, the aqueous solution becomes more dilute and hence, the solute effect becomes less dominant. The water activity of a solution droplet can be approximated as

$$a_w(D) = \left(1 + \frac{6 j_I m_s M_w}{M_s \rho_w \pi D^3}\right)^{-1} \ , \tag{1.3}$$

where j_I is the number of dissociation products, m_s is the mass of the solute, M_w is the molecular weight of water, M_s is the molecular weight of the solute and ρ_w is the density of water.[9,11]

The second term of Equation 1.1, the Kelvin term, also known as the curvature effect, describes how the vapor pressure over a curved interface differs from the vapor pressure of the same substance over a flat surface, and for an atmospheric droplet is given by,

$$K(D) = exp\left(\frac{4\sigma_{s/a} M_w}{RT\rho_w D}\right) \ , \tag{1.4}$$

where $\sigma_{s/a}$ is the surface tension at surface-air interface, R is the universal gas constant and T is the temperature. It describes the relationship between the energy, necessary for a molecule to transition from liquid phase to the gas phase, and the size- or curvature-dependent surface tension of the liquid/air interface. The vapor pressure of a liquid surface

is determined by the energy necessary to separate a molecule from the attractive forces exerted by its neighbors and to bring it into the gas phase (evaporation). In a small droplet with a curved surface, a molecule is less strongly bound to neighboring molecules than on a flat surface. Given surrounding molecules exert less attractive forces, it is easier for a molecule on a curved surface to escape into the vapor phase. As a result, the vapor pressure over a convexly curved interface is greater than that over a planar surface. The vapor pressure over a curved surface increases with decreasing D, i.e., as the curvature increases with smaller droplet diameter.

Intercomparison of CCN activity for various aerosol particles across the literature can be achieved by utilizing an alternative expression of a_w, represented by the dimensionless hygroscopicity parameter, κ. The κ-parameter was introduced by Petters and Kreidenweis [10] and is based on a modification of the Köhler equation, which relates a_w to the fraction between the volume of the dry aerosol particle and the droplet volume. κ describes the water uptake of dry aerosol particles based on their physicochemical properties. According to κ-Köhler theory the saturation ratio over an aqueous solution droplet (Equation 1.1) is alternatively,

$$s(D) = \frac{D^3 - D_p^3}{D^3 - D_p^3(1-\kappa)} \exp\left(\frac{4\sigma_{s/a} M_w}{RT\rho_w D}\right)^{-1}, \tag{1.5}$$

where D_p is the diameter of the dry particle. [10] The second term in Equation 1.5 is identical to Equation 1.4. The critical supersaturation, SS_c, of a given dry particle diameter is equal to the maximum of Equation 1.5. If the initial dry particle diameter is known and its corresponding SS_c is experimentally determined, for example, by using a cloud condensation nuclei counter (CCNc), one can alternatively, determine κ with the approximation,

$$\kappa = \frac{4A^3}{27 D_p^3 ln^2 SS_c} \quad \text{where } A = \frac{4\sigma_{s/a} M_w}{RT\rho_w}, \tag{1.6}$$

which is valid for $\kappa > 0.2$, but holds for less hygroscopic particles ($\kappa \gtrsim 0.001$) with minor numerical inaccuracies. [10] The κ values of atmospherically relevant aerosol species strongly depend on their chemical compositions. In general, soluble aerosol particles, such as salts and certain acids, have the largest κ values. Atmospherically important salts include, for example, NaCl and $(NH_4)_2SO_4$ with κ values of 1.28 and 0.61, respectively. Sulfuric acid, H_2SO_4, which is formed from combustion-related processes, has an estimated κ value of 0.90. [10] Less hygroscopic aerosol encountered in the atmosphere are, for example, SOA and soot particles. Whereas SOA typically has κ values of ≤ 0.2, pure, insoluble, carbonaceous soot particles are generally hydrophobic and require very high SS and are therefore, rather poor CCN. [12–14] Nevertheless, chemical processing and atmospheric aging

of soot particles, which can increase the amount of water soluble material on the particle surface, can significantly facilitate CCN activity. It has been shown that H_2SO_4 coatings on soot particles lower SS_c [12,13] and that soot particles, which are exposed to UV radiation to simulate photochemical aging in the atmosphere, facilitate droplet formation. This is postulated to occur due to condensation of photochemically formed SOA, which condenses onto the soot, or due to oxidation of organic material already present in the particle phase. [14]

1.1.2 Ice Nucleating Particles

At temperatures below freezing, clouds can exist in the liquid and/or ice phase. Atmospheric ice formation or nucleation can occur through different mechanisms which often require the presence of aerosol particles. Homogeneous ice nucleation describes the formation of ice from freezing of supercooled solution droplets without the presence of insoluble aerosol particles. Homogeneous freezing occurs at temperatures below ≈-38°C. [15] Nevertheless, a large fraction of clouds in the atmosphere are mixed-phase clouds (MPC) and exist at temperatures between -38°C and the melting point. [16] At these temperatures, other ice nucleation mechanisms are required to facilitate ice formation. Studies have found that certain particles can initiate ice nucleation at temperatures well above homogeneous freezing conditions. Insoluble or partially soluble particles, which facilitate ice formation, are known as INP. Ice nucleation mechanisms which involve INP are referred to as heterogeneous ice nucleation, that are often described phenomenologically as different pathways or modes.

Certain heterogeneous ice nucleation modes require the presence of supercooled liquid, i.e., immersion freezing, condensation freezing and contact freezing. Immersion freezing occurs when an aerosol particle is immersed in a droplet and subsequently freezes at temperatures below 0°C. Likewise, condensation freezing describes an aerosol particle initially acting as a CCN below the melting point of ice and subsequent droplet freezing. Deposition freezing, on the other hand, describes the nucleation of ice, when water molecules in supersaturated conditions deposit on an INP without forming bulk liquid. Ice crystals can also form when a supercooled INP, upon contact with the air-water interface of a liquid droplet, initiate freezing at temperatures below 0°C. [17] Lastly, secondary ice formation processes, such as rime splintering, also known as the Hallett-Mossop process, [18] have been able to explain to some extent discrepancies between observed INP and ice crystal number concentrations, which are often observed to be larger than those of INP. [19]

The physicochemical properties of aerosol particles are key in determining whether or not a particle is an efficient INP. One important factor is the particle size, or more precisely, the surface area of an aerosol particle. Larger particle surface areas, can increase the probability that some site on the particle surface triggers ice formation and enhances

kinetics governing intermolecular interactions. For mineral and desert dust, ice nucleation above homogeneous freezing temperature ($T_{\text{hom}} \gtrsim -38°\text{C}$) is mostly observed for larger, supermicron particles. Nevertheless, at temperatures below -38° C, dust particles can form ice at relative humidities below liquid water saturation.[20] Some primary biological aerosol particles, or bioaerosol, such as bacteria and fungal spores, have been observed to be efficient at nucleating ice, even enabling ice formation at temperatures greater than -10°C.[21] Carbonaceous soot particles, on the other hand, are rather poor ice nucleators. Although, fresh soot particles have been reported to nucleate ice in the cirrus regime between -40 and -50°C,[22,23] at warmer temperatures, or in the mixed-phase cloud regime, soot mostly nucleates ice close to liquid water saturation.[24,25] The ability of soot particles to form ice strongly depends on its physicochemical properties. Similar to the CCN activity of soot, its ice nucleation behavior may significantly change when the particles are chemically and physically altered. Several laboratory studies have shown both chemical treatment, involving sulfuric acid and organics, and physical treatment improved soot particles' ice forming abilities compared to unprocessed soot.[26–29]

1.2 Maritime Shipping - A Source of Airborne Pollutants

In 2022 roughly 12 billion tons of freight were shipped via maritime trade, including containerized cargo, gas and crude oil. The total world fleet, contributing to the trade, is estimated to consist of nearly 105,000 ships.[30] Despite rapid technological advances in the general transport sector, the global shipping fleet has been aging, with the exception of bulk carriers. Uncertainties in future fuel costs and technologies, carbon prices, maritime regulations and other technological developments, cause ship owners to delay investments.[30]

Most ships utilize compression-ignition, i.e., diesel, engines for power generation. Meaning the power is directly related to the chemical energy contained in the fuel. Conventional marines fuels are produced from crude oil and consist of mixtures of hydrocarbons, typically ≈86% carbon and ≈14% hydrogen (weight %), but also contain other elements such as sulfur and metals.[31] While a majority of the maritime fleet still operates on residual fuel oils, byproduct(s) from the production of distillate fuels, other fuels such as low sulfur distillate fuels, biodiesel, liquefied natural gas (LNG), methanol and ammonia are gaining more traction as alternative fuels in the maritime shipping sector.[30]

During the diesel combustion process, a distillate or heated residual fuel oil is directly injected and aerosolized into the engine cylinder at the end of the compression stroke. High pressure and temperature conditions cause the air-fuel mixture to self-combust. The combustion between the fuel hydrocarbons and O_2 in the air releases energy, causing the

air in the cylinder to expand and pushes the cylinder's piston into motion, generating mechanical power. Under stochiometric combustion conditions, the carbon in the fuel reacts with O_2 to produce H_2O and CO_2. Nevertheless, different factors, such as variations in combustion conditions and in the chemical composition of the fuel, as well as fuel impurities, generally lead to co-emission of combustion byproducts. Important byproducts include nitrogen oxides (NO_x; NO and NO_2), PM, and a variety of hydrocarbons, including polyaromatic hydrocarbons (PAH).[31] Combinations of trace elements present in the fuel and, when sufficient sulfur is present in the fuel, sulfur dioxide (SO_2) can also be major constituents of exhaust emissions.[31]

NO_x is strongly linked to air pollution due to its potential for tropospheric ozone (O_3) and secondary organic aerosol formation.[32] Similarly, SO_2 can be partially converted to SO_3, which can react with water vapor to form sulfuric acid droplets[31] and lead to the formation of sulfate particles. PM emitted from diesel engines are often products of incomplete hydrocarbon combustion and thermal decomposition. The hydrocarbons undergo a series of physicochemical processes, resulting in the nucleation of carbonaceous exhaust particles, which are often referred to as soot. These particles are initially formed in the high temperature regions of the combustion flame and continue to grow as exhaust cools and both, organic and inorganic species, such as SO_2 and sulfuric acid, condense onto the particles.[31,33] The bulk of exhaust particle emissions consist of soot and sulfate, while others, including mineral, ash, carbonaceous char and organic carbon particles, originating from unburned fuel and lubrication oil, are often co-emitted.[34,35] PM emissions from ships are heavily influenced by a variety of parameters such as engine type and operating conditions, lubricating oil as well as fuel type and composition.[36,37]

PM, SO_2, NO_x and other ship related exhaust emissions are strongly linked to air pollution and can therefore have a substantial impact on human health, especially near coastal areas or along major trade routes where a significant fraction of maritime shipping occurs.[38–40] Directly emitted primary or secondary particles, formed from emitted gaseous precursors, can be inhaled by human beings and cause respiratory and cardiopulmonary diseases.[38] Studies have shown that worldwide, tens of thousands of premature deaths can be attributed to shipping related exhaust emissions. Regions that are especially affected, include Europe and East Asia, where high population densities coincide with large contributions of ship-related PM concentrations. The high number of premature deaths are not only attributed to direct inhalation of PM but also to enhanced ozone pollution which is associated with NO_x emissions.[39] Moreover, shipping-related SO_2 emissions and their strong potential to form airborne particles, play a significant role in health-related issues.[40]

1.2.1 Regulations In the Shipping Sector Targeting SO_x Emission Reductions

The International Maritime Organization (IMO) is the United Nations agency responsible for safety and security of shipping and the prevention of pollution from ships. In 1973, the IMO adopted the International Convention for the Prevention of Pollution from Ships (MARPOL), which represents the legal framework addressing environmental pollution from ship operation and accidents. Initially, MARPOL focused on oil spills and leaks from ships, but over time protocols were adjusted and new regulations adopted, incorporating various issues related to environmental pollution from shipping activity. In 1997 Annex VI was adopted and came into force in 2005. Annex VI was established to prevent air pollution from ships. It sets limits on sulfur oxides (SO_x) and NO_x emissions, and prohibits deliberate emissions of ozone depleting substances.[41]

To address issues of maritime air pollution and diminish the impact of ship exhaust particle emissions on human health, the IMO has implemented international regulations which aim to reduce ship exhaust emissions of SO_x and thus, indirectly those of PM. Principally, the IMO's regulatory framework limits the sulfur content of marine fuels, and therefore, mandates ship owners and operators to use higher-grade or alternative fuels with reduced fuel sulfur content (FSC) or to use exhaust aftertreatment-systems such as wet scrubbers, which are designed to remove SO_x from exhaust.

1.2.1.1 Fuel Sulfur Content Reduction

Exhaust particle removal in maritime shipping by, for example, diesel particulate filters is not as straightforward as in road traffic, due to on-board space limitations, additional fuel consumption used for regeneration, particle removal efficiencies depending on fuel types, the corrosive nature of sulfur-containing species and the lack of strict regulations being in place. A way to indirectly limit PM emissions, is to reduce exhaust emissions of SO_x and thus, prevent formation of secondary sulfur-containing particles, which can make up a large fraction of PM emissions from ships. Consequently, IMO regulations were adopted that limit the maximum allowed FSC of marine fuels and distinguish between FSC caps for global ship traffic and shipping in designated sulfur emission control areas (SECA). Since January 2020 ships worldwide are not allowed to operate on marine fuels with FSCs exceeding 0.5 wt % (from here on %). In SECAs, which include the Baltic and North Sea area; designated coastal areas of the United States and Canada; and the United States Caribbean Sea area, stricter rules apply. There, the FSC is limited to 0.1% and has been since 2015.[41] In 2025 the entire Mediterranean Sea will also become a SECA.[42]

While historically vessels have utilized sulfur-rich residual fuel oils, commonly known as heavy fuel oil (HFO), they must now use low FSC or alternative fuels, which

usually contain little to no sulfur, such as LNG, biofuels or methanol. The transition towards higher grade or alternative fuels comes at an economic cost. The market price for compliant fuels can be two to five times that of conventional fuels with higher FSC and are often not economically viable for stakeholders within maritime shipping.[30,43] As a result, the transition towards alternative fuels is not as rapid as one would have hoped for and other more economical options are sought. The global fleet of ships operating on alternative fuels is slowly increasing. Yet, carriers have been reluctant towards associated investments due to more looming environmental regulations, fuel prices and technological developments.[30] More than 90% of the operational fleet is still utilizing conventional fuels. Nevertheless, new orders show an increasing percentage of alternative fuel ship engines (16%), with LNG being the most common alternative fuel type.[43] An alternative that provides greater market flexibility involves adapting marine vessels with dual-fuel systems. These systems are already in place in most LNG and methanol fueled ships for safety and technical reasons, and also offer increased flexibility in fuel utilization and enable swift adaptation to varying circumstances.

Shifting towards higher grade fuels with lower FSC or alternative fuels, has indeed led to a reduction in particle exhaust emissions from ships, as has been shown by several recent studies. In the Baltic Sea, for example, Zetterdahl et al.[44] compared emissions of two ships and measured exhaust particle mass reductions of about 67% but found no significant reduction in number emissions upon introduction of the 2015 0.1% FSC cap. On the other hand, Seppälä et al.[45] observed particle number reductions of around 32% and a reduction in the geometric mean diameter of measured size distributions during ship plume measurements in the Baltic Sea. Similarly, Yu et al.[46,47] reported a significant reduction in particulate mass emissions due to much lower emissions of particulate sulfate for ships utilizing fuels with FSC below 0.5% in Western Europe. A study conducted around coastal areas of North America by Anastasopolos et al.[48] reported reductions of particle mass concentrations by up to 37%, as well as reductions in PM-related vanadium and nickel concentrations, caused by the introduction of the 0.1% FSC cap. While fuel switching policies can lead to PM concentration reductions, they were also found to increase emissions of volatile organic compounds (VOC), which can lead to enhanced secondary aerosol formation and ground-level ozone pollution and thus, have other detrimental effects on human health.[49] IMO regulations associated with FSC reductions are estimated to lead to a reduction of ship-related premature mortality and morbidity by 34% and 54%, respectively, compared to business-as-usual scenarios, where FSC regulations are not in place.[50] Nevertheless, exhaust particle emissions from ships will remain a significant source of anthropogenic PM,[51] especially, in major port areas.[52] Moreover, some alternative fuels, such as LNG, are associated with other unwanted side-effects. With LNG, methane, which

is a potent greenhouse gas, is often co-emitted into the atmosphere.[53–55]

1.2.1.2 Exhaust Wet Scrubbing

IMO regulations open alternative compliance pathways, which allow ships to operate on cheaper residual fuel oils with FSCs exceeding global and SECA limits. These include the use of exhaust aftertreatment systems which reduce SO_x exhaust emissions, such as wet scrubbers (WS). SO_x emissions from ships typically consist of ≈95% SO_2 with the remaining ≈5% emitted as SO_3.[56] In a wet scrubber, exhaust gas is introduced into an absorption section, where it is exposed to a mist, typically consisting of seawater droplets. Reactions between SO_2 in the exhaust and seawater can be summarized by SO_2 solvation and subsequent reactions in liquid water.[56–58] Initially, SO_2 is dissolved in water,

$$SO_2(g) \rightleftharpoons SO_2(aq)\,, \tag{1.7}$$

and subsequently, reacts with H_2O and ionizes to form bisulfite (HSO_3^-) and sulfite (SO_3^{2-})

$$SO_2 + H_2O \rightleftharpoons HSO_3^- + H^+\,, \tag{1.8}$$

$$HSO_3^- \rightleftharpoons SO_3^{2-} + H^+\,. \tag{1.9}$$

When the oxygen content in the seawater is high enough, SO_3^{2-} will be further oxidized to sulfate, SO_4^{2-},

$$SO_3^{2-} + \frac{1}{2}O_2 \longrightarrow SO_4^{2-}\,. \tag{1.10}$$

Similarly, when gaseous SO_3 is absorbed into the aqueous phase, it will produce bisulfate (HSO_4^-), and sulfate ions (SO_4^{2-}),

$$SO_3(g) + H_2O(aq) \rightleftharpoons HSO_4^- + H^+\,, \tag{1.11}$$

$$HSO_4^- \rightleftharpoons SO_4^{2-} + H^+\,. \tag{1.12}$$

Reactions 1.8, 1.9, 1.11 and 1.12 generate excess H^+ ions, that are neutralized by the buffer capacity of the scrubbing water, which is determined by its alkalinity. Alkaline species, which are naturally present in seawater, include carbonate (CO_3^{2-}) and bicarbonate (HCO_3^-). Thus, the neutralization can proceed as,

$$HCO_3^- + H^+ \longrightarrow CO_2 + H_2O\,, \text{ and/or} \tag{1.13}$$

$$CO_3^{2-} + 2\,H^+ \longrightarrow CO_2 + H_2O\,. \tag{1.14}$$

Before exiting a wet scrubber and being emitted into the atmosphere, scrubbed exhaust gas is passed through a section containing demisters, to remove droplets and prevent subsequent emission into the atmosphere. Wet scrubbing technologies are broadly classified as open- and closed-loop systems. Open-loop scrubbers use seawater as scrubbing liquid and utilize its natural alkalinity and salinity to bind SO_x in the exhaust. In open-loop systems seawater is directly pumped into the wet scrubber and sprayed into the exhaust gas. Afterwards it can be stored and chemically treated before being released back into the sea.[59] The IMO Exhaust Gas Cleaning System Guidelines[60] outline quality criteria for wet scrubber wash-/discharge water. These state that the pH value should be ≥6.5, that the concentrations of PAHs should not exceed 50 μg L^{-1} and that the turbidity, which is a proxy for suspended particulate matter, should be ≤25 NTU (nephlometric turbidity units).[60] Because the alkalinity and salinity of seawater depends on location, open-loop wet scrubbing efficiency can vary as a ship travels. In areas where the salinity and thus, the abundance of ions, that bind SO_2 and SO_3, is relatively low, open-loop scrubbing may prove to be inefficient. Such areas include coastal regions where seawater blends with the outflow of rivers to form brackish water or, for example, the Baltic Sea.[56] In these instances, better results can be achieved by utilizing closed-loop scrubbing systems. For closed-loop systems seawater is replaced by freshwater with added sodium hydroxide (NaOH) as a scrubbing agent. The NaOH increases the SO_x uptake of the freshwater. In contrast to open-loop systems, the washwater is not discharged into the sea but instead is transferred into processing tanks, where it is cleaned, and eventually recirculated into the wet scrubber. Only small amounts of treated washwater are discharged into the sea to prevent accumulation of sodium sulfate crystal precipitate in the water, which reduces scrubbing efficiency.[59] Wet scrubbing, in general, has gained negative attention over the past years due to environmental concerns. One focus point is the potential hazardous impact of the washwater on marine lifeforms and ecosystems. A number of studies have shown that while, washwater quality criteria exist, open-loop scrubbing can lead to concentrated emissions of PAHs and metals and introduce new contaminants, such as chromium, into the marine environment.[61,62] Due to environmental concerns, open-loop scrubbing and related washwater discharges have therefore been banned or restricted by a number of countries, including many major ports.[63] Thus, closed-loop scrubbers pose an attractive alternative for ships operating in waters of low alkalinity and/or where they face regulatory constraints. Hybrid-mode scrubbers, which allow switching between open- and closed-loop scrubbing, provide flexibility for ship operators but are also more complex in their design.[59] Today, around 5,000 ships are equipped with wet scrubbers, which represents ≈4.8% of the global fleet. The largest fraction of ships with wet scrubbers are bulk carriers and container ships. Moreover, around 82% of wet scrubbers continue to be open-loop systems.[43]

Particulate matter removal efficiency is another concern, which is indirectly a goal of the IMO emissions regulations. Recent studies that quantify exhaust particle removal efficiency by wet scrubbing, yield varying results. Large particle emissions reductions were observed by Fridell and Salo [64] and Winnes et al. [65] Fridell and Salo [64] found total particle number concentrations to decrease by approximately 92% after a scrubber. Winnes et al. [65] observed wet scrubbing to significantly reduce total number emissions but found no clear reduction in the solid fraction of PM. Other studies have only shown moderate reductions in total particle number concentrations [53] or only found exhaust particle removal to be efficient for particle sizes above 1 μm. [66] Moderate reductions were also observed by Yang et al., [67] who reported particulate matter below 2.5 μm to be reduced by about 10% but found sulfate particles to be more or less unaffected. More recently, studies investigating the implementation of a wet electrostatic precipitator after a scrubber, were able to efficiently remove up to 98% of particulate matter from marine engine exhaust. [68,69]

Wet scrubbing has also been shown to affect the size, mixing state and chemical composition of particles. In Jeong et al., [68] the authors report that the dominant sulfate particle mode shifts towards larger sizes upon scrubbing and concluded, that the shift was caused by particle coagulation. Lieke et al. [70] found mixing state and chemical composition to be significantly impacted. They reported that the relative abundance of sulfate and salt in the particulate phase increased, whereas the abundance of soot decreased, after scrubbing. [70] Shifts in particle size distributions and changes to their respective mixing states can have important implications for atmospheric processes such as cloud formation.

1.2.2 Climate Impact of Shipping Emissions

Exhaust emissions from ships affect the climate system in a variety of ways. As a country, the shipping sector would rank eighth among the largest sovereign greenhouse gas emitters. [71] During the 2022 COP27 United Nations Climate Change conference several countries and stakeholders accepted the Green Shipping Challenge (GSC), whose goal is to significantly reduce carbon emissions from ships and to reach net-zero emissions by 2050. [71] This sparked the IMO to adopt the 2023 IMO GHG Strategy in July 2023 that aims to reduce GHG emissions from ships as outlined by the GSC. [72] At COP28 in December 2023, a second GSC event was hosted and included implementation of IMO's 2023 GHG Strategy for developing countries and new private commitments. [71] That said, as shown in Section 1.2, ships emit a variety of substances to the atmosphere, with impacts that are much more complicated than simple greenhouse forcing. The heterogeneity of air exhaust emissions, makes it challenging to quantify the overall climate impact of shipping. Aerosol particles can contribute to radiative forcing due to direct and indirect processes and their net impact depends on their physicochemical properties, including particle size and

chemical composition (see also Section 1.1). Whereas sulfate particles scatter shortwave radiation and thus, lead to radiative cooling, soot particles lead to net warming due to absorption. Moreover, sulfate and soot particles, which are major constituents of ship exhaust emissions, possess different abilities to interact with clouds (Section 1.1.1).

Ship particulate emissions interact with atmospheric processes in a variety of ways. A prominent effect of ship aerosol-cloud interactions, is the formation of ship tracks, which are long-lived, linear marine stratiform cloud formations with increased albedo that are visible in satellite imagery.[73,74] Major factors that contribute to the occurrence and intensity of ship tracks' formation is the amount of water soluble material in the particle phase, the size of the emitted exhaust particles and the aerosol particle background state.[73–75] Often, the brightest ship tracks are observed during cleaner conditions, when the level of background ambient aerosol particles is low.[73,75]

Studies that attempt to quantify the overall impact of ship exhaust emissions on the radiative budget, generally find them to have a net cooling effect and highlight the importance of SO_2 and sulfate aerosol emissions, which generally outweigh the warming effects of CO_2 and soot emissions.[76–79] While sulfate aerosol itself has a cooling effect, the most significant contributor to the net negative radiative effect are aerosol-cloud interactions. These correspond to up to 39% of the total indirect effect of anthropogenic aerosols.[76] In fact, projections for 2050 were estimated to cause a net cooling and a change in global-mean temperature of up to -0.33°C, despite implementation of IMO FSC regulations.[78] While most studies agree on the overall near-term cooling effect of ship exhaust emissions, some stress that atmospheric lifetimes[77] and emission reduction policies[77,79] must also be taken into account, and that these may alter the net long-term radiative effect.

Given the importance of ship sulfate aerosol particles acting as cloud seeds and the impact of SO_x emission reduction policies, it is of importance to investigate, how related compliance measures secondarily influence clouds and climate. Reductions in CCN emissions when switching to lower FSC fuels have been observed, which is attributed to emissions of comparatively smaller particles and a reduction in the more hygroscopic particle fraction.[46,47,80] The global 0.5% FSC limit has resulted in reduced observations of ship tracks and subsequently, was estimated to reduce the climate cooling effect from emitted aerosol particles.[81–83] Investigations cite sulfate aerosol as the dominant component governing the net radiative impact of shipping emissions. The detection of ship tracks also depends on the aerosol background state. Higher background aerosol concentrations can blur the impact of the additional ship aerosol, thus making their detection more problematic, which can lead to an underestimate of the indirect radiative effect.[81,83,84] Diamond[85] found a decrease in cloud brightening after implementation of the 2020 FSC cap, resulting in reduced indirect radiative forcing within a major shipping corridor in the southeastern

Atlantic. It has also been shown that the magnitude of SO_x emission reductions can be substantially larger compared to detectable corresponding ship-track frequencies, adding to the uncertainty regarding underlying processes.[83] In light of uncertainties regarding future fuel type usage and possible future marine regulations, investigating ship aerosol-cloud interactions and aiming to assess their climatic impact, remains an important task.

1.3 The Arctic

The Arctic does not have strict geographical boundaries, yet, it is often defined as the region north of the Arctic Circle, i.e., 66.5°N. Arctic climate is characterized by a low thermal energy state and strong couplings between the land, ocean and atmosphere. The Arctic Ocean occupies most of the area north of the Arctic Circle. One of its striking geographical features, is its direct connection to both, the Pacific Ocean through the Bering Strait and its link to the North Atlantic Ocean through the seas surrounding Greenland and Norway. The ocean's surface is characterized by a thin veneer of floating sea ice, which is strongly coupled with the atmosphere's energy budget and circulation, the energy budget at Earth's surface and the hydrologic budget. The year to year areal extent of sea ice cover ranges on average from ≈15 million km^2 in March to ≈8 million km^2 in September. A majority of Arctic land and the sea ice surface is covered by snow for at least 6 to 8 months of the year, which has implications for the surface energy balance. Snow has a relatively high albedo, typically between 0.8 and 0.9 for fresh snow, an insulating effect on underlying land and sea ice surfaces, and a capability to store precipitation over terrestrial regions. Surface air temperatures over the Arctic Ocean are subject to large spatial variability. Whereas January temperatures over the central part of the Arctic ocean reach values between -25°C and -32°C, temperatures around the seas of Iceland stay near 0°C during the same period, owing to strong couplings between atmosphere of oceanic circulation. During the summer months temperatures over snow-free land typically reach values between 10°C to 20°C. Over the Arctic Ocean a substantial amount of solar radiation is used to melt ice and thus, air surface temperatures are close to the freezing point.[86]

Clouds play an important role in the Arctic climate system, as cloud cover usually ranges between 60% and 80% for the summer and winter months respectively. As described in Section 1.1, clouds have the ability to reflect incoming solar radiation and to trap and re-emit longwave radiation. The latter is an important process during the polar nights, when solar radiation becomes insignificant. Thus, the magnitude of cloud-induced cooling and warming on surface air temperatures is strongly coupled to the respective seasons.[87,88] A large fraction of Arctic clouds are low-level stratus mixed-phase clouds, consisting of both supercooled liquid droplets and ice crystals.[86,89] In comparison to MPCs encountered

at lower latitudes, Arctic MPCs can persist for several days.[89] The longevity of these clouds is remarkable given that the co-existence of supercooled liquid droplets and ice crystals is thermodynamically unstable. Generally, at subfreezing temperatures the mixed-phase state is driven towards the ice phase. This is due to the lower equilibrium saturation vapor pressure of H_2O vapor over ice compared to over liquid water. As a result, ice crystals grow at the expense of liquid droplets. This glaciation process is also referred to as the Wegener-Bergeron-Findeisen process, which can transform MPCs into ice clouds within the span of a few hours. The reason for the persistence of Arctic MPCs is a complex feedback of interlinked dynamical and microphysical processes. Those include cloud-top radiative cooling driven by supercooled droplets, which produces turbulence and maintains the cloud layer in a well-mixed state, the cloud leading to enhanced radiative surface heating, which increases vertical moisture fluxes, and resupply of water vapor via sublimation of precipitating ice.[90,91] Certain cloud structures are sustained, where supercooled liquid droplets are encountered in the top part of the cloud and hydrometeors related to the ice-phase are concentrated near the cloud bottom.[90]

Anthropogenic activity and associated climate warming are impacting the Arctic substantially. Climate projections and observations over the past decades show enhanced warming rates in the Arctic region compared to the global average. These temperature trends will have significant impacts on ecosystems, the cryosphere and further amplify effects on the Arctic climate system.

1.3.1 Arctic Amplification and Decline in Sea-Ice Extent

The northern polar region has been experiencing a warming rate of about 1.36°C per century between 1875 and 2008. That rate is almost twice the northern hemisphere average. Moreover, amplified temperature anomalies are observed in recent decades.[92] The elevated warming rates are strongly linked to radiative greenhouse gas forcing and reductions in sea-ice cover and thickness, which has pronounced surface air temperature warming effects during autumn and winter.[93] Projections in the latest IPCC report show that by the end of 21st century the Arctic will on average warm by at least 3°C compared to a period from 1995 to 2014,[4] which is more than the projected global average. This phenomenon of enhanced Arctic warming as a response to radiative forcing is also known as Arctic Amplification (AA) and is an emergent feature displayed in most climate model projections.[4]

Arctic Amplification is characterized by a complex web of local and regional process interactions within the cryo-, hydro- and atmosphere under greenhouse gas forcing. One of the most prominent impacts of AA is undoubtedly the continuous decline in Arctic sea-ice extent and thickness. The Fifth Assessment Report by the IPCC stated that annual

mean Arctic sea-ice extent decreased by up to 4.1% per decade between 1979 and 2012, with summer sea-ice extent being reduced by as much as 13.6%.[94] The most amplified Arctic warming is generally observed during winter months, when heat fluxes from the ocean warm the near surface air. This warming can be further enhanced by the presence of low-level clouds, which trap outgoing longwave radiation.

While a lot of processes governing the effects of AA are locally constrained to the Arctic, others can occur on much larger spatial scales, such as changes in poleward atmospheric and oceanic heat transport due to greenhouse gas forcing. The ice-albedo effect describes how enhanced ice and snow melting exposes surfaces with lower albedo(s), which absorb more radiation and thus, enhance surface warming. Over land, this process is straightforward, i.e., enhanced warming leads to earlier melt onsets and therefore darker surfaces are exposed earlier in the year. This leads to increased absorption of solar radiation and thus, to a warmer surface and surface air temperatures, further amplifying melting. Higher temperatures also extend and intensify sea-ice melt seasons, exposing larger areas of comparatively dark ocean surface. This leads to an increase in Arctic ocean surface warming, but contrary to land surfaces, a significant portion of the absorbed energy is used for further ice melting and added sensible heat flux into the upper layer of the ocean, thus reducing the feedback on air temperature over the ocean.[95] An increase in open ocean surfaces does result in increased abundance of atmospheric moisture and cloud cover which influences downwelling longwave radiation. Clouds in the Arctic form at low altitudes and co-vary with the underlying sea ice cover.[4] While low-level clouds typically have a cooling effect due to reflection of incoming shortwave radiation, in the Arctic they tend to augment the re-emission of longwave radiation to the surface and therefore, for most of the year have a warming effect.[87,88,95] It has been shown that the intensified and extended sea ice melting periods can lead to an increase in low-level cloud formation during early fall, which can be linked to enhanced warming during the latter parts of the year.[96] Nevertheless, it has been found that while cloud-sea-ice feedback has a warming effect, it is of low magnitude compared to the surface albedo effect.[97,98] Schmale et al.[99] highlight how the impacts of AA most likely affect the abundance and composition of Arctic aerosol particles, which may alter cloud properties and therefore, impact cloud optical properties, precipitation and lifetimes.

The complexity of interacting feedback processes make projections of the magnitude of AA challenging and there is larger variability and uncertainty compared with global and tropical warming, which are mostly dominated by cloud feedbacks. Furthermore, many polar feedbacks are coupled to warming processes at lower latitudes, which themselves are influenced by other regional processes, increasing the uncertainty in future AA projections.[4]

1.4 Increased Shipping Activity in the Arctic

With the ongoing climatic changes observed in the Arctic, it is projected that the natural background state will drastically change, most notably caused by projected reductions in snow and ice cover. These changes will also affect the natural background state of Arctic aerosol particles. As the Arctic generally has low ambient aerosol concentrations deprived of CCN and therefore, relatively small perturbations in this natural state may induce significant changes in cloud formation and properties.[100] A decline in Arctic sea ice extent is associated with an increase in sea spray aerosol, increased microbial activity in the sea surface microlayer, leading to enhanced emissions of VOCs, dimethyl sulfide and bioaerosols, which lead to enhanced new particle formation.[3] Additionally, local anthropogenic aerosol emissions are projected to increase, due to increased socioeconomic activities.[99]

One anthropogenic activity, that has been gaining a substantial amount of attention from the scientific community for its projected impact on the Arctic climate system, is the likely increase in Arctic shipping activity. The reduction in sea ice extent and thickness increases ships' access to the Arctic, yielding opportunities for establishing new and shorter trading routes, for exploration and extraction of natural resources and provides easier accessibility for tourist travel. As an example, the Northern Sea Route, which follows the Northern coast line of the Eurasian continent, is projected to increase its navigation season by 80 to 90 days per year (previously 20 to 30 days), and for marine vessels with ice-breaking capabilities by approximately 150 days, by 2080.[101] Shorter transportation routes yield large economic benefits, because such routes reduce fuel consumption and save time. Although, there exists some ambiguity as to whether Arctic shipping routes are economically feasible for stakeholders compared to more traditional trade routes via the Suez and Panama Canal.[102] Nonetheless, even short time periods of ice-free Arctic Ocean conditions would likely yield significant traffic increases.

Increased Arctic shipping may result in a variety of socioeconomic and environmental challenges which need to be addressed. These include, for example, uncertainties about sovereignty over shipping routes and natural resources, growing conflicts between users of the relatively narrow waterways and a potential increase in number of shipping accidents due to challenging navigation in Arctic seas. In other words, more risk for oil spills and other environmental catastrophes related to shipping accidents.[101] A recent study has shown how sea-ice reduction also leads to increased sea fog frequency along projected Arctic shipping routes, which could impact navigational safety and cause significant delays.[103] Therefore, international regulations should focus on improving marine safety and protection of the environment in the near-future.[101]

Ship emissions of climate forcers related to Arctic transit shipping and shipping activity related to gas and oil production, are projected to increase to varying degrees until mid century.[104–106] It is obvious that the uncertainty envelope of emission factors predicted for Arctic shipping strongly depends on the methodological approaches and emission databases used for the projections. Nevertheless, shipping activity is universally anticipated to increase substantially until the mid-century. The spread in estimates is highlighted in a review by Theocharis et al.[107] Moreover, projections suggest that international regulations, that aim to reduce emissions of short-lived climate forcers, may be counteracted by the general growth in shipping volume. And this will likely, in fact, lead to significantly enhanced emissions of soot and other pollutants by the year 2050.[105]

Projecting the volume of future Arctic shipping activity is difficult in the context of prevailing uncertainties in climate-relevant processes, such as the extent and decrease in Arctic sea ice cover. Moreover, global and Arctic-related socioeconomic issues, as well as on-going developments in the maritime shipping sector, including developments in propulsion technologies, will further increase uncertainties in future projections.

1.4.1 Climate Impact of Shipping in the Arctic

While Arctic shipping activity bears a lot of potential socioeconomic and environmental risks, in terms of climatic impacts, researchers often highlight two key processes. The first, is deposition of black carbon onto snow and ice surfaces. Due to the hydrophobic nature of soot, it mostly contributes to climate forcing by absorbing shortwave radiation, both in the atmosphere but also, once deposited onto surfaces, on land. Research indicates soot emitted from anthropogenic sources in the Arctic, including ships, when deposited onto snow and ice, contributes to reductions of surface albedo and subsequently, enhances melting and amplifies surface warming.[108] It is believed that while ship exhaust soot deposition will contribute to some extent to regional warming, its effect is, to first order, very regionally dependent and also quite small in magnitude compared to other soot sources, which are transported to the Arctic from lower latitudes.[109] Namazi et al. estimated a radiative forcing of 0.45 W m^{-2} for black carbon deposition on snow in the Arctic.[110]

How ship aerosol will influence Arctic mixed-phase clouds in the future is still subject to significant uncertainty. Studies have found that the magnitude of the effect depends on emissions scenarios, mixed-phase cloud background state and how it might change in the future, and also the methods used to investigate these processes. Ship aerosol pollution may cause cloud phase to shift towards the ice phase, which has been shown to reduce precipitation and increase cloud albedo.[111,112] Possner et al.[112] also found significant increases in LWP when emitted ship CCN exceeded concentrations of 1000 cm^{-3}. Simultaneously, these changes were found to be of much smaller magnitude

than similar aerosol perturbations in warmer, liquid phase clouds. Yet, these studies do not provide a conclusive picture, as to whether ship aerosol perturbations are sufficient to affect radiative cooling or heating, or to affect overall Arctic warming rates.[111,112] While the aforementioned studies were performed using satellite data[111] and a large-eddy simulation (LES) model,[112] Gilgen et al.[113] used a global model and found ship aerosol perturbations to only significantly affect cloud properties, when exaggerated future Arctic ship emission inventories are used. Similar, to the aforementioned studies, the effect of increased shipping emissions was much more pronounced in liquid phase clouds. In contrast, Stephenson et al.[114] found trans-Arctic shipping to be able to slow down Arctic warming and calculated a shipping-induced cooling of about 1°C. It is, however, important to note, that the authors of the latter study did not take current IMO FSC regulations into account in their model, which has significant implications for hygroscopicities of emitted PM and gaseous compounds.[114] Another important aspect that should be considered, is that not only will aerosol emissions change in the Arctic, but also the background state of Arctic (mixed-phase) clouds. Changes in atmospheric conditions caused by the enhanced Arctic warming rates, will ultimately affect the radiative properties of Arctic clouds.[115] Whereas the aerosol effect of ship emissions on Arctic mixed-phase clouds may offset to some extent surface warming during the summer, it is unlikely that it will counteract warming rates over the span of a full year.[111,112,115]

In order to reduce black carbon emissions from ships in the Arctic and mitigate environmental impacts, the IMO has adapted regulations, which particularly address Arctic shipping. One of those regulations prohibits carriers and ship owners from utilizing marine fuels which exceed densities and kinematic viscosities of 900 kg m^{-3} and 150 mm^2 s^{-1} respectively.[116] This regulation will most likely have a significant impact on the fuel types used in Arctic shipping and therefore, impact the physicochemical state of exhaust emissions, which adds to the uncertainty envelope when quantifying the climatic impact of ship emissions in the Arctic.

2

Thesis Motivation and Outline

The objectives of this thesis are to enhance understanding as to how increased ship emissions can lead to further climatic feedbacks in the Arctic, taking into account international maritime fuel policies, that affect properties of exhaust particle emissions.

Laboratory engine experiments presented in this study (**Paper I**,[117] **Paper II**[118] and **Paper III**), contextualize recent changes in the shipping sector with respect to marine fuel regulations that aim to reduce emissions of SO_x and indirectly, those of PM.[41] Here, we focus on two possible pathways to comply with regulations, FSC reduction and exhaust wet scrubbing. The aim of the laboratory results was to investigate the impact of compliance measures on physicochemical properties of exhaust particles and their influence on the particles' cloud activity. Several engine measurement campaigns were conducted using different fuel types and a laboratory wet scrubber. Results from the experiments are not only useful to improve our understanding as to how maritime policies may affect exhaust particle properties and what this implies for health- and climate-related issues, but they are also essential to perform simulation studies on how ship exhaust emissions affect Arctic mixed-phase cloud properties. Individual goals of these laboratory experiments were:

1. How do fuel sulfur content reduction and exhaust wet scrubbing impact the physicochemical properties of exhaust particles, including particle size distributions, particle densities and chemical mixing states? (**Paper I to Paper III**)

2. How is the cloud activity of the exhaust particles, i.e., their ability to form liquid droplets and ice crystals, affected by compliance pathways? (**Paper II and Paper III**)

3. Quantify exhaust particle and CCN emissions from test engines. What does this imply for human health and climate? (**Paper I to Paper III**)

One way that ship activity might impact the Arctic climate is via aerosol-cloud interactions, i.e., ship exhaust particle emissions change the properties of Arctic clouds and consequently, affect the radiative budget. Having characterized the effects of FSC reduction and exhaust wet scrubbing on the properties of exhaust particles in laboratory experiments,

results have been implemented into a cloud-resolving model (**Paper IV**). Using the MIMICA LES model, an Arctic mixed-phase cloud, which was based on observations from an Arctic field campaign, is simulated and used as a reference case.[119,120] The reference case was subsequently perturbed by adding aerosol data based on Papers I to III and impacts on cloud properties were studied. The aims of the LES study (**Paper IV**) are:

1. Characterization of the Arctic mixed-phase cloud simulation, which is used as a reference case to ship perturbation experiments.

2. How can results from Paper I to III be synthesized and implemented into the MIMICA LES model?

3. What is the impact of ship aerosol perturbations on the micro- (distribution of hydrometeors) and macrophysical cloud properties (cloud albedo, precipitation and net surface radiation)?

4. How do the observations vary with ship exhaust particle properties (particle size, hygroscopicity etc.) and what does this imply for future Arctic shipping emissions?

3

Methods

3.1 Laboratory Engine Experiments

Laboratory studies presented in Paper I, II and III were based on three measurement campaigns conducted at two different laboratories using different engines and fuels. The following sections describe instrumentation and setups used during the campaigns and highlight key differences. A schematic experimental setup is illustrated in Figure 3.1, which is based on measurements from Paper III and shows the various instruments used during the campaigns.

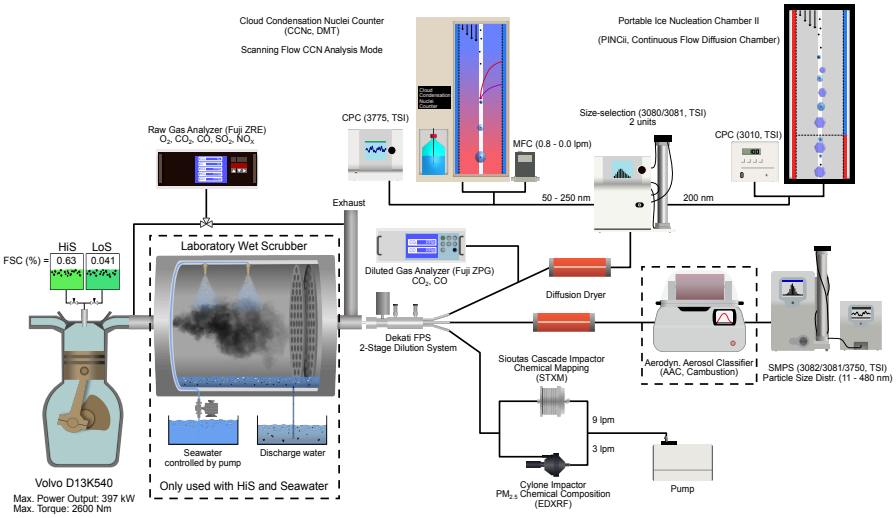

Figure 3.1: Schematic of a typical test-bed engine experiment setup. Experiments reported in Paper I excluded the CCNc, PINCii, STXM and EDXRF analysis techniques (see Figure 1, Paper I). Experiments reported in Paper II excluded the AAC, PINCii and EDXRF instruments (see Figure 1, Paper II). Reproduced from Paper III.

3.1.1 Engines, Fuels and the Model Wet Scrubber

Paper I and II are based on measurement campaigns performed between May 2019 and June 2020 at the Chalmers University of Technology's Marine Engine Laboratory in Gothenburg, Sweden. The lab features a turbocharged Volvo Penta D3-110 marine diesel test-bed engine, employing a four-stroke design with five cylinders and a common rail fuel injection system. It can achieve a peak crankshaft power of 81 kW, capable of reaching 3000 rpm. During measurements, the engine ran at a 32% load, determined by operational speed and torque. Notably, cruising and ocean-bound vessels often demand loads exceeding 60%, while coastal, port, and ice-affected ship operations commonly handle loads as low as 30%.[121]

For Paper III, measurements were conducted between May and June 2022 at Chalmers University of Technology in Gothenburg, Sweden. This study utilized a Volvo D13K540 Euro 6 common rail diesel engine, featuring six cylinders with a 131 mm bore and 158 mm stroke. Experimental operations were maintained at 1200 rpm, yielding peak torque of 2600 Nm and a maximum power output of 349 kW. To simulate various ship operational scenarios and explore engine load's impact on particle exhaust emissions, we conducted measurements at three distinct load points: 50% (≈168 kW) and 70% (≈245 kW) representing cruising conditions, and 25% (≈85 kW) simulating maneuvering, such as port operations. Engine loads were determined based on the ratios between measured torque at 1200 rpm and maximum torque.

To study the effects of IMO FSC regulations on ship exhaust particulate emissions a variety of fuels were used. In Paper I and II, heavy gas oil (HGO), a marine distillate fuel with a FSC of 0.86%, served as a proxy for fuels that do not meet IMO FSC compliance (global and SECA). Two low FSC fuels (≤ 0.03%) were used during the same experiments. Both Marine gas oil (MGO) and hydrotreated vegetable oil (HVO) are compliant with IMO FSC regulations on global and SECA levels. Marine gas oil is widely used in shipping for medium- and high-speed engines and HVO is a biodiesel, which has the lowest density and aromatic content of the three tested fuels. For Paper III, two fuels were used which correspond to HGO and MGO of the previous campaigns. To avoid confusion, fuels are named differently between campaigns. Here, the baseline case (no compliance) is a marine distillate fuel with a FSC of 0.63% (HiS). The compliant, low FSC fuel used during experiments was marine gas oil (here referred to as LoS) which had a FSC of 0.041% and was therefore SECA compliant. In contrast to HFO, both, HGO and HiS have lower viscosities and densities, and thus, do not need to be heated prior to combustion. This is expected to affect emitted particle number concentrations[36] and the physicochemical properties of the exhaust particles.[122] However, the engines were not suitable or equipped to operate with HFO. Physical and chemical characteristics of the fuels used during the

Table 3.1: Properties of fuels used in the laboratory experiments.

	Paper I + II			Paper III	
	HGO	MGO	HVO	HiS	LoS
Density at 15°C [kg/m^3]	865.3	847.4	780.0	865.7	837.3
Heat of Combustion [MJ/kg]					
Gross Heat of Combustion	45.02	45.60	46.57	45.10	45.73
Net Heat of Combustion	42.30	42.79	43.55	-	-
Carbon content [%]	86.4	86.5	85.2	-	-
Sulfur content [%]	0.86	<0.03	<0.03	0.63	0.041
Aromatic content [vol. %]					
Total aromatics	27.4	23.6	0.2	32.5	22.3
Mono-aromatics	20.2	20.5	0.2	20.8	18.3
Di-aromatics	6.46	2.60	<0.1	10.2	3.5
Poly aromatics (Tri+)	0.71	0.43	<0.02	1.5	0.5
Additive and Wear Metals [mg/kg]					
Cu	1.81	<0.1	<0.1	<0.1	<0.1
K	0.4	0.27	0.25	0.29	0.60
B	-	-	-	0.17	<0.1
Al, Ca, Cr, Fe, Pb, Ni, Na, V, Zi, Zn	<0.1	<0.1	<0.1	<0.1	<0.1

experiments are summarized in Table 3.1.

The laboratory-scale WS used in these experiments, whose design is based on those deployed on-board ships, was built at Chalmers University of Technology, with its primary purpose being the reduction of SO_2 emissions in exhaust. The stainless steel scrubber measures approximately 50 cm in length and has an inner diameter of 40 cm. Six water nozzles are evenly positioned around the inner wall, forming a concentric pattern, while an additional seventh nozzle is suspended in the center and directed towards the exhaust inlet (Figure 3.2). A pressure pump controls the water flow from a storage tank to the spray nozzles, which maintained a flow of 1.5 to 2 liters per minute during experiments. Demister plates inside the WS separate large water droplets from the exhaust gas. For Paper III experiments additional packing material was positioned between the demister plates to increase surface interactions with the exhaust and thus, enhance the particle and droplet removal efficiency. Seawater used for the scrubber was either sourced from University of Gothenburg's Kristineberg Center for Marine Research and Innovation located on the

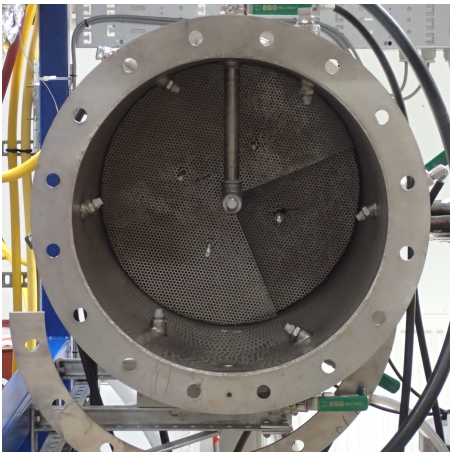

Figure 3.2: Internal view of the laboratory wet scrubber (WS) displaying the internal water nozzles (6 concentrically and one centrally mounted) and rear demister plates. Reproduced from Paper I.

Gullmar fjord in western Sweden, which has access to a seawater system with an intake depth of 32 m (Paper I to III); or from surface water near the southern archipelago of Gothenburg (Paper I and II). Seawater scrubbing cases are referred to as SWS (Paper I and Paper II) and WS (Paper III). Moreover, to investigate the effect of water salinity on the particulate emissions, freshwater provided by the municipality of Gothenburg was also used for wet scrubbing (FWS; Paper I and II). The wet scrubber was mainly operated using the high FSC fuels, HGO and HiS.

Guidelines for exhaust gas cleaning systems outlined by the IMO mandate that ships utilizing exhaust wet scrubbers must not exceed certain SO_2/CO_2 emission ratio limits. Outside of SECAs, where the FSC is limited to 0.5%, the ratio between emitted SO_2 (in ppm) and CO_2 (in %) may not exceed 21.7. In SECAs, where FSC is limited to 0.1%, this ratio needs to be below 4.3.[60] During wet scrubber experiments emission limits were continuously monitored by comparing SO_2 and CO_2 concentrations in the raw exhaust measured by the raw exhaust gas analyzers (Figure 3.1). In Paper I and II, the WS was able to achieve SECA compliance during all experiments which were performed at an engine load of ≈32%. For Paper III, when experiments were conducted using an engine with larger power output, the WS was only capable of reliably reducing the ratio below SECA limits for engine loads of ≈25%. For higher engine loads, the ratio varied between 4.3 and 8.2, and thus, compliance was achieved on global but not on SECA levels.

3.1.2 Gas Instrumentation

While this study focuses on properties of exhaust particles, it is also essential to monitor emissions of gaseous species which are relevant for engine combustion processes. For Papers I to III a variety of gas measurement instruments were used (see the publications for detailed information), which measured different compounds in the undiluted raw exhaust as well as downstream of the dilution unit. Measured raw exhaust gas species included O_2, CO_2, CO, NO_x and SO_2 and were monitored using different instruments for individual measurement campaigns. Some of the particle analysis instruments used during the experiments are sensitive to particle number concentrations, it is therefore necessary to dilute the sample gas using an appropriate unit. Dilution of raw exhaust also serves to mimic atmospheric dilution, which naturally occurs when the engine exhaust is emitted into the atmosphere. The result of dilution is that the temperature of the exhaust gas and concentrations of various components are substantially reduced, which can also have impacts on secondary particle formation. During the campaigns a 2-stage dilution system (FPS-4000, Dekati Ltd.) was used, which consisted of a first-stage temperature-controlled porous tube diluter, followed by an ejector diluter. In order to determine the actual dilution factors, it is necessary to measure a relatively inert gas species before and after the dilution step. Here, diluted CO_2 was monitored using different analyzers (see Papers I to III for details) and corrected for background CO_2 concentrations in the dilution air. Dilution factors were determined using the ratio between CO_2 concentrations in the raw and diluted exhaust gas.

3.1.3 General Aerosol Measurements

Exhaust or aerosol particles within the sample gas were analyzed downstream of the dilution unit (Figure 3.1). In some cases, for example, when measuring the cloud activity of the exhaust particles, sample aerosol was dried using silica gel diffusion dryers before reaching the respective analysis instruments. Condensation particle counters (CPC) were used to determine the total number of particles in the sample gas. In these instruments, a flow of submicron aerosol particles is exposed to supersaturated conditions with respect to either liquid water or butanol (depending on the instrument model). Sample gas is passed through growth sections, where vapors diffuse and condense onto the particles, which serve as condensation nuclei. This leads to rapid growth of the immersed particles into enlarged droplets, which are detected and counted by optical systems. Electrostatic classifiers allow size-selection of naturally polydisperse aerosol sample and generate monodisperse aerosol streams of given mobility diameters (d_{mo}). These classifiers use charging sources, to establish a known bipolar particle charge distribution. The charged particles then

pass through a differential mobility analyzer (DMA), which separates the particles based on their electrical mobility. Within the DMA, the sample flow together with a sheath air flow pass through the annular DMA chamber where the charged aerosol particles experience an electric field. In this section, consisting of two concentric electrodes, particles are either attracted by the outer electrode (negative charge), are removed with the sheath air flow (neutral charge) or are carried axially downward with the sheath airflow while also being attracted by the inner electrode (positive charge). Depending on the electrode settings, particles within a narrow band of electrical mobility are able to exit the DMA as a quasi-monodisperse aerosol flow, from which they can be passed to other instruments. This method allows selection of a monodisperse aerosol in the range of ≈2 to ≈1000 nm (depending on the DMA model). Before entering the classifier, aerosol particles larger than the upper limit of the DMA's size range are removed by an impactor. If an electrostatic classifier is coupled and synchronized with a CPC, it can be used as scanning mobility particle sizer (SMPS), which automates repeated changes in the electric field of the DMA, allowing for continuous measurements of particle size distributions (PSD) of the polydisperse aerosol flow.[123]

3.1.4 Effective Density Measurements and Calculations

The particle mobility (B) is a measure of the ease of producing steady particle motion and is the ratio between the settling velocity of the particle and the force producing this steady motion. It follows that,

$$B = \frac{C_c(d_{\mathrm{mo}})}{3\pi\mu d_{\mathrm{mo}}}\,, \tag{3.1}$$

where $C_c(d_{\mathrm{mo}})$ is the size-dependent Cunningham slip correction factor and μ is the viscosity of the carrier gas.[124] Whereas a DMA size-selects particles based on d_{mo}, instruments, such as the aerodynamic aerosol classifier (AAC), select particles based on a relaxation time (τ).[125] This τ describes the time required for a particle to adjust its velocity to new conditions,

$$\tau \equiv Bm = \frac{C_c(d_{\mathrm{ae}})\rho_0 d_{\mathrm{ae}}^2}{18\mu}\,. \tag{3.2}$$

It is defined as the product between B and the mass of the respective particle (m), where ρ_0 is the standard density (1 g cm^{-3}), and d_{ae} is the aerodynamic diameter, defined as the diameter of a sphere with standard density and the same settling velocity as the particle of interest.[124] If d_{mo} and d_{ae} are known, as can be measured with coupled AAC-SMPS or DMA-AAC systems, then Equations 3.1 and 3.2 can be used to derive the mass of a particle,[126]

$$m = \frac{\pi \rho_0}{6} \frac{C_c(d_{\mathrm{ae}}) d_{\mathrm{ae}}^2 d_{\mathrm{mo}}}{C_c(d_{\mathrm{mo}})} \,. \tag{3.3}$$

The effective density (ρ_{eff}) of a particle,

$$\rho_{\mathrm{eff}} = \frac{6m}{\pi d_{\mathrm{mo}}^3} = \rho_0 \frac{C_c(d_{\mathrm{ae}}) d_{\mathrm{ae}}^2}{C_c(d_{\mathrm{mo}}) d_{\mathrm{mo}}^2} \,, \tag{3.4}$$

is by definition the particle mass divided by a sphere of the particle's mobility diameter.

During experiments ρ_{eff} was determined from tandem measurements using an AAC (Cambustion Ltd., UK) and a SMPS or DMA. One of the instruments was used for size-selecting the polydisperse aerosol, while the other instrument determined the corresponding equivalent diameter by scanning the monodisperse aerosol downstream. These measurements were repeated for sizes between 50 and 250 nm and allowed for determination of ρ_{eff} over a wide size range.

While for spherical, homogeneous particles the effective density equals the material density. This is not the case for irregularly-shaped particles. For example, soot agglomerates in diesel engine exhaust often become less dense with increasing size, resulting in decreasing ρ_{eff}. That often follows a power-law function and is referred to as the mass-mobility relationship,

$$\rho_{\mathrm{eff,\,MB}} = \frac{6k}{\pi} d_{\mathrm{mo}}^{D_m - 3} \,, \tag{3.5}$$

where k is a constant pre-factor and D_m is the mass-mobility exponent, which is indicative of the shape of a particle.[127]

3.1.5 Energy Dispersive X-Ray Fluorescence

Energy Dispersive X-ray Fluorescence (EDXRF) is an analytical technique used for elemental analysis for either solid or liquid samples. This method relies on the re-emission of characteristic X-rays from elements when exposed to high-energy X-rays. Hereby, samples are exposed to a beam of X-rays generated from a X-ray tube. Upon exposure, atoms in the sample will interact with photons. If the energy of the incident photon is large enough to create a vacancy in the atom's inner shells, it may lead to the emission of characteristic, element-specific fluorescence radiation. The result is an emission spectrum of fluorescence radiation, which serves as chemical fingerprint of the sample.

Fluorescence radiation is caused by the difference in binding energies, when electrons in higher shells transition into the vacancy spot of the lower shell. When atoms of lower atomic number are excited, the probability increases that Auger electrons are emitted instead

of fluorescence radiation. This is because electrons in smaller atoms have lower binding energies compared to those of larger atoms.[128] This limits the fluorescence detection of elements of smaller atomic numbers. The smallest atomic number detected with our lab-based EDXRF was Mg.

EDXRF measurements were utilized to measure trace-element concentrations of exhaust particles and are reported in Paper III. Samples of PM2.5 (particulate matter smaller than 2.5 μm) were collected on filters, using a cyclone impactor with a 50% efficiency cut-off diameter of 2.5 μm. EDXRF analysis was performed with a SPECTRO XEPOS analyzer (SPECTRO Analytical Instruments GmbH, Germany) and controlled with the XRF Analyzer Pro software (AMETEK, USA). Filters were repeatedly analyzed and all results were corrected for elemental background concentrations using a blank filter membrane. Element-specific emission factors were derived from the data output, after normalizing for sampling duration, dilution ratio, and fuel consumption specific to each sample.

3.1.6 Scanning Transmission X-Ray Microscopy and Near-Edge X-Ray Absorption Fine Structure

Scanning transmission X-ray microscopy (STXM) in combination with near-edge X-ray absorption fine structure spectroscopy (NEXAFS) allows for chemical analysis and morphological examination of individual aerosol particles. The combined approach allows for characterization of functional groups, the assessment of mixing states, and the investigation of the structure and morphology of collected particles. Aerosol particle samples are collected on transmission electron microscopy (TEM) grids and are exposed to soft X-rays of tunable energy at STXM endstations in synchrotron facilities. At energies close to an atom's ionization threshold, photons with sufficient energy can cause inner-shell electrons to be ejected from the atom or transition to higher unoccupied orbitals. This phenomenon is observed in X-ray absorption spectroscopy as an absorption edge. Absorption edges are specific to both the element and energy level and thus can be used to identify the chemical composition of samples, including the detection of specific functional groups.[129] These techniques were utilized in analyses reported in Paper II and Paper III.

Sample collection onto standard TEM copper mesh grids (Ted Pella Inc.) was conducted using the Zurich Electron Microscope Impactor (ZEMI;[23] Paper II) and a Sioutas five-stage cascade impactor (Paper III). Measurements for Paper II and III were conducted at the BL4U beamline at the UVSOR Synchrotron Facility in Okazaki, Japan and at the SoftiMAX beamline at MAX IV laboratory in Lund, Sweden. These synchrotron facilities cover energy ranges from 75 eV to 1 keV and from 275 eV to 2.5 keV respectively. This enables measurements at the carbon (280-300 eV), nitrogen (393-425 eV), oxygen

(525-550 eV) and sodium (1068-1095 eV; only at MAX IV) K-edges as well as the sulfur L-edge (159-196 eV; only at UVSOR).

Data was processed using aXis 2000[130] and included image alignment, correction for background signals and conversion of flux data to optical densities.

3.1.7 Cloud Condensation Nuclei Measurements

Measuring exhaust particles proclivity to form liquid droplets under supersaturated conditions, their CCN activity, was an integral part of the laboratory experiments. In our experiments we used a DMT Cloud Condensation Nuclei Counter (CCNc; CCNC-100, DMT) which is a cylindrical continuous-flow thermal-gradient diffusion chamber.[131] The CCNc consists of a vertical cylindrical column with wetted walls to which a streamwise increasing thermal gradient is applied. This section is also referred to as the growth chamber. Sample flow, which is surrounded by a particle free annular sheath flow to minimize wall interactions, enters the growth chamber at its top, from where it flows downstream and is exposed to a thermal gradient and supersaturated conditions with respect to liquid water. Water vapor supersaturation in the sample flow region is achieved due to the different diffusion coefficients for heat in air (0.21 $cm^2\ s^{-1}$) and mass, i.e., water vapor in air, (0.25 $cm^2\ s^{-1}$) at 294 K and a pressure of 1 atm. The supersaturation at the centerline of the chamber, to which the sample aerosol is exposed, is a function of axial temperature gradient and flow rate of the sample gas. As a result, the supersaturation inside the growth chamber of the CCNc can be varied by either adjusting the sample flow rate (Q) or the stream-wise temperature gradient (ΔT). A detailed description of the working principal and thermodynamic model is described in Roberts and Nenes.[131] Depending on the size and chemical composition of the individual particles, once exposed to supersaturated conditions, particles will start to grow due to condensation of water vapor molecules onto their surfaces. This process will lead to a growth in size until particles are activated into liquid droplets, which are detected by an optical particle counter (OPC) at the outlet of the CCNc.

During laboratory experiments (Paper II and III) CCN activity of size-selected exhaust particles was determined using the single column CCNc. Before reaching the CCNc, exhaust particles were dried using silica gel diffusion dryers and size-selected by a DMA (Model 3080L, TSI Inc., USA), which selected d_{mo} between 50 nm and 250 nm. To measure the total number of particles entering the CCNc (N_{P}) and derive activated fractions (AF), the ratio between activated particles and the total amount of particles, a CPC (Model 3775, TSI Inc., USA) was operated parallel to the CCNc.

In order to perform continuous measurements of SS spectra for size-selected particles, the CCNc was operated in Scanning Flow CCN Analysis (SFCA) mode.[132] In this method,

SS inside the growth chamber is continuously adjusted by ramping the sample flow rate Q_{CCNc} from 0.2 to 1.0 l min^{-1} over 120 s, while a constant ΔT is maintained. The minimum and maximum flow rates were kept constant for 30 s. To avoid large pressure variations in the sampling line due to adjustments of the Q_{CCNc}, which could influence measurements of other instruments, a mass flow controller (MFC) was operated in parallel to the CCNc and kept the total flow rate ($Q_{\mathrm{CCNc}} + Q_{\mathrm{MFC}}$) at 1.0 l min^{-1}. Measurements of SS spectra were performed at ΔT = 4, 10 and 18°C, covering a SS range of about 0.07 - 2.4%. These values were determined by calibration measurements using ammonium sulfate $(NH_4)_2SO_4$ particles of the different sizes. These measurements allowed SS_c, defined as the SS where 50% of the size-selected singly charged particle population are activated into liquid droplets, to be determined. Values of SS_c were calculated by fitting sigmoidal functions to the measured activation curves following Moore and Nenes,[132]

$$\frac{N_{\mathrm{CCN}}}{N_{\mathrm{P}}} = a_0 + \frac{a_1 - a_0}{1 + (Q_{\mathrm{CCNc}}/Q_{50})^{-a_2}}\,, \tag{3.6}$$

where a_0, a_1, a_2 and Q_{50} are the minimum, maximum, slope, and inflection point respectively. Q_{50} values were converted to SS_c using instrument calibration data (see e.g., Figure S2 in Paper II). The resulting SS_c values were subsequently converted into κ values using,

$$\kappa = \frac{4A^3}{27 d_{mo}^3 ln^2(1 + SS_c/100\%)}\,, \text{ with } A = \frac{4\sigma_w M_w}{RT\rho_w}\,, \tag{3.7}$$

where experimentally determined SS_c is given in %, σ_w = 71.99 mN m^{-1} is the surface tension of water at 25°C, M_w is the molar mass of water, R is the universal gas constant, T is the absolute temperature and ρ_w is the density of water at 25°C (0.997 g cm^{-3}).[10]

3.1.8 Ice Nucleation Measurements

Ice nucleation experiments (Paper III) were conducted using the Portable Ice Nucleation Chamber II (PINCii), a newly developed continuous flow diffusion chamber (CFDC) described in detail by Castarède et al.[133] The measurement principals of CFDCs are similar to those of the CCNc but adjusted to enable studying ice formation at temperatures as low as ≈-50°C.[134–136] Here, the operational and measurement principal is briefly explained based on the design of PINCii. For detailed descriptions of the instrument, including instrument dimensions, components and instrument characterization experiments, see Castarède et al.[133]

The centerpiece of PINCii is the main chamber, a 1 m long growth chamber, connected to a 0.42 m long evaporation section. Both sections consist of parallel, individually

temperature-controlled wall plates. During initialization of freezing experiments the main chamber is continuously flushed with filtered ambient air at a flow rate of 10 l min^{-1}. Simultaneously, all wall sections are cooled to -15° C. Once the wall temperatures have stabilized at this set point temperature, the chamber is filled with distilled water from its outlet and immediately drained once the water reaches the top of the main chamber. The wall temperatures cause water to freeze and form a thin layer of ice (≈1 mm), which is sufficiently thick to provide the chamber with water vapor via sublimation for at least 4 to 5 operational hours. The freezing process also causes wall temperatures to rise due to the release of latent heat, approaching 0° C. Subsequently, the wall sections are re-cooled to -5° C and further cooled in 5° C steps until experimental temperature set points are reached. Once these set points are reached, a sample flow of 1 l min^{-1}, which is confined between two particle-free sheath air flows of 4.5 l min^{-1} respectively, is introduced to the growth chamber. For freezing experiments the growth section plates are set to different temperatures, resulting in horizontal temperature and humidity gradients. The ice coated walls ensure that at each wall the vapor pressure is at the relevant equilibrium saturation vapor pressure. The gradient and again the differential diffusion of heat and vapor cause the aerosol flow to be exposed to supersaturated conditions with respect to ice and/or liquid water. The value of supersaturation to which the aerosol is exposed, depends on the magnitude of the temperature gradient. Depending on the aerosol particle type, different T and RH might induce liquid droplet activation and freezing, which both result in particle growth. Since chamber conditions can induce both ice crystal and liquid droplet nucleation, the sample flow is guided through an evaporation section, where both wall plates are set to one temperature. Thus, the vapor pressure in the evaporation section is uniformly the equilibrium saturation vapor pressure over ice at the chosen temperature, and therefore subsaturated with respect to liquid water. This causes liquid droplets to evaporate and shrink in size, which makes it possible to discriminate them from ice crystals. At the outlet of the main chamber, particle concentrations are detected by a size-discriminating OPC (Model Remote 3104, Lighthouse Worldwide Solutions, USA).

Ice nucleation measurements, which were conducted only in conjunction with the 50% load experiments, were performed by doing ramps of relative humidity with respect to ice (RH_i) for three to four constant lamina temperatures. During these ramps or scans wall temperatures are continuously adjusted to maintain a constant lamina temperature but increase the RH_i in the lamina from ≈110% to 160%. Experiments were performed at temperatures between -26°C and -50°C. From the five size channel OPC, signals for particles >3 μm were used as the criterion for ice crystals detection. Between each lamina temperature change, PINCii's inlet valve was switched to sample filtered ambient air for 15 minutes to obtain information on background ice crystal number concentrations, which

were later used to correct data during analysis. Before entering PINCii, particles in the sample flow were dried using a diffusion dryer and size-selected using a DMA (Model 3080L, TSI, USA) to generate a monodisperse aerosol of d_{mo} = 200 nm. Similar to CCNc operation, a CPC (Model 3010, TSI, USA), measured downstream of the DMA and in parallel with PINCii to infer activated fractions.

3.1.9 Calculation of Emission Factors

Calculating emission factors (EF) is a standard method for normalizing emissions of various pollutants by the amount of fuel consumed (pollutant per kg of fuel) or the energy delivered by an engine during operation (pollutant per kWh). Using EFs enable intercomparison of emission results between different fuel and engine types, and across literature. In the investigations presented here, EFs were calculated using the formulation,

$$\mathrm{EF}_x = \frac{Q_{\mathrm{exh}} C_x}{A_i} \ , \tag{3.8}$$

where Q_{exh} is the exhaust gas flow in $\mathrm{m^3\ h^{-1}}$, C_x is the number or mass concentration of a variable x per $\mathrm{m^3}$, and A_i is the load and fuel dependent engine parameter used to normalize emissions, i.e. the fuel consumption in $\mathrm{kg\ h^{-1}}$ or energy output in kWh.

Particle number (PN) emission factors ($\mathrm{EF_{PN}}$), were derived from numerical integration of particle number size distributions and corrected for dilution factors and diffusional losses. Particle mass (PM) emission factors ($\mathrm{EF_{PM}}$) were calculated by converting particle number size distributions into mass distributions by either assuming standard density for all particles ($\mathrm{EF_{PM,\rho_0}}$) or using average or interpolated ρ_{eff} values for individual particle modes ($\mathrm{EF_{PM,\rho_{eff}}}$). While quantitative particle emissions from marine engines are often dominated by ultrafine particles below 100 nm, particles above 1 μm in diameter are often co-emitted and while these particles are often low in number relative to the ultrafine particulates, they can have a significant impact on the mass emissions. It is therefore important to stress, that the method to measure particle mass emissions applied here has an upper size limit between ≈500 and 700 nm, which leads to a systematic underestimation of mass emissions. Exhaust particle mass emissions are often carried out by gravimetric analysis, where exhaust particles are collected onto filters, which are later on weighed. This type of analysis was not applied here.

In order to estimate CCN emission factors ($\mathrm{EF_{CCN}}$), a simple model was applied, which was adopted from Kristensen et al. [137] and slightly modified in Paper II and III. Here, κ values for the entire size range of measured particle size distributions were derived by fitting exponential functions to data (Paper II) or interpolating results (Paper III) obtained from CCNc measurements. Fitted and interpolated κ values were converted into

size-dependent critical SS for size distributions following Petters and Kreidenweis [10] This enables the fraction of the size distribution which activates into droplets at a given supersaturation to be calculated. Activated fractions were then numerically integrated to derive number concentration of CCN (N_{CCN}). These were then converted into CCN emission factors ($\mathrm{EF}_{\mathrm{CCN}}$) using a modified version of Equation 3.8

$$\mathrm{EF}_{\mathrm{CCN}} = \frac{Q_{\mathrm{exh}} N_{\mathrm{CCN}}(SS)}{\mathrm{FC}} , \tag{3.9}$$

where $N_{\mathrm{CCN}}(SS)$ is the number concentration of CCN as a function of SS in $\#\ \mathrm{m}^{-3}$, Q_{exh} is the exhaust gas flow rate in $\mathrm{m}^3\ \mathrm{h}^{-1}$ and FC is the load and fuel dependent fuel consumption in $\mathrm{kg\ h}^{-1}$.

3.2 Large-Eddy Simulation Experiments

The aim in Paper IV is to investigate how ship aerosol emissions under current IMO FSC regulations may potentially impact the properties of Arctic mixed-phase clouds. This is achieved by utilizing experimental results from Paper I to III as input parameters in a cloud-resolving large-eddy simulation (LES) model. The model was set up to simulate a low-level, stratiform mixed-phase cloud, which was observed during an field campaign in the Arctic. [119,120] Cloud perturbations by ship emissions were then studied by adding additional ship aerosol particles (experimental results from Paper I to III) to the simulated cloud case.

3.2.1 MISU MIT Cloud and Aerosol Model (MIMICA) - Model Overview

Large-eddy simulations (LES) are useful tools for simulating atmospheric cloud and boundary layer processes, due to their high-resolution scale. In these types of atmospheric models turbulent structures as large as 1 km in scale are generally resolved within the model but other subgrid scale processes, such as microphysical processes, need to be parametrized. In Paper IV we employed the MISU MIT Cloud and Aerosol (MIMICA) LES model. MIMICA was primarily designed to study clouds at higher latitudes and has already been applied in a variety of cloud studies, ranging from mid-latitude, marine stratocumulus clouds [138,139] to Arctic mixed-phase clouds. [140–144] Here, only a brief overview of the model is provided. For a more detailed model description, the reader is referred to Savre et al. [138]

For the simulations, a 3-D domain consisting of $96 \times 96 \times 128$ grid cells with periodic boundaries was used. Near the surface and within the cloud layer vertical grid spacing (dz) was more refined. In the remaining domain, a sine-squared function calculated dz. The

grid possessed a uniform horizontal resolution of $dx = dy = 62.5$ m and variable vertical resolution of 7.5 m $\leq dz \leq$ 25 m. The total domain size was 6 km × 6 km × 1.7 km.

Within MIMICA aerosol particles were represented by lognormal distributions, defined by a count median diameter (CMD), geometric standard deviation (σ_g) and a particle number concentration (N_p). Corresponding particle densities and κ values were assigned to each aerosol mode and depended on the particle type. Microphysical schemes were implemented for five hydrometeor classes, including liquid cloud droplets, raindrops, ice crystals, graupel (rimed ice) and snow. The mass mixing ratios and number densities of each hydrometeor class were predicted using a two-moment bulk microphysics scheme.[145,146] Diffusional growth processes including condensation/evaporation of liquid drops and deposition/sublimation of ice crystals were computed following Pruppacher and Klett[11] The mass of cloud droplets and raindrops is affected by different processes, including *autoconversion* (cloud droplets with a radius of 25 μm are automatically converted into rain drops), *accretion* (growth of raindrops due to coalescence with cloud droplets) and *self-collection* (growth of cloud droplets/raindrops due to coalescence with hydrometeors of the same class), and are modelled following Seifert and Beheng.[145,146] In a similar way, these processes also apply for ice- and mixed-phase hydrometeors.[147] Cloud droplet formation was modelled using κ-Köhler theory and is therefore, dependent on pre-existing aerosol particles or CCN, as well as simulated supersaturations with respect to liquid water (SS).[10] While MIMICA offers options to use different heterogeneous ice nucleation parametrizations, herein, a diagnostic ice crystal number concentration was used. The approach was to simulate heterogeneous ice formation processes by assuming an ice crystal number concentration of 200 m^{-3} for grid cells with temperatures below 0°C and when sufficient supercooled cloud water is present.[144]

3.2.2 Mixed-Phase Cloud Case Study

The reference mixed-phase cloud case is based on observational data recorded during the Arctic Summer Cloud Ocean Campaign (ASCOS), an field campaign conducted in the central Arctic in 2008.[119,120] The aim of the campaign was to improve the general understanding regarding the formation and life-cycle of Arctic low-level summer clouds. The campaign employed a wide range of instruments measuring meteorological parameters, aerosol and CCN characteristics, and concentrations of trace gases among others. The case employed in this study is a mixed-phase stratocumulus, which was observed between August 30th and August 31st.[120] The same case has been used in investigations of central Arctic clouds.[140–144] Meteorological data, including temperature and humidity profiles, were used to initialize all model runs.

3.2.3 Implementation of Experimental Results and LES Simulation Overview

In order to investigate how ship emissions perturb the mixed-phase cloud, results from Paper I to III were incorporated into MIMICA as additional aerosol parameters. In each case an aerosol mode with case-specific ρ_{eff} and κ values was assigned.

All model runs were performed with hygroscopic (κ = 1), marine seaspray as background aerosol (BG). The BG aerosol was assigned to two aerosol modes, Aitken (Ait) and accumulation mode (Acc). The reference simulation without ship aerosol is referred to as Mix. From Paper I and II, results from HGO, MGO and SWS were adopted into the model. For simplification these are referred to as HiS (high FSC; corresponding to HGO), LoS (low FSC; corresponding to MGO) and WS (wet scrubber; corresponding to SWS) in the modelling study. From Paper III results for HiS and WS measurements (not to be confused with the newly introduced nomenclature for Paper I and II LES cases), obtained at 50% engine load, were investigated. In these instances, only the more hygroscopic and dominant sulfate particle mode was included in the model. Ship aerosol cases from Paper III are labeled HiS_sul and WS_sul respectively. BG aerosol was present in all model runs. The number concentrations N_p of both BG aerosol modes was set to 30 cm^{-3}. Ship aerosol experiments were performed with $N_{p,\text{ship}}$ = 100 cm^{-3} and $N_{p,\text{ship}}$ = 1000 cm^{-3}. In the WS case (Paper I and II), $N_{p,\text{ship}}$ of both corresponding aerosol modes was adjusted to accommodate for the particle number concentration increase, observed during laboratory experiments. For each case, simulations with low and high N_p are labeled with _lo and _hi respectively. An overview of aerosol particle modes used in the simulations is given in Table 3.2. Aerosol particle number concentrations were evenly distributed over the entire domain and remained constant during the full simulation period, meaning there were no aerosol sources and sinks during the simulations. Each case was simulated for 16 hours, with the first four hours considered model spin-up that was excluded from the analysis.

3.2.4 Relevant Model Output Variables

All MIMICA simulations were run with the full microphysics scheme, meaning that all five classes of hydrometeors were included. For each class, the model calculated the mass mixing ratios and number densities, from which the respective volumetric number (N_x) and mass concentrations (Q_x) were derived, where x is replaced by c for cloud droplets, r for raindrops, i for ice crystals, g for graupel and s for snow. Q_c and Q_i are also known as liquid (LWC) and ice water content (IWC) of the cloud respectively. Together with N_c and N_i, LWC and IWC can be used to calculate the average size of the respective hydrometeors, which is an important parameter for initiation of precipitation and for cloud albedo.[148] The mean cloud droplet radius r_v can be calculated as,

Table 3.2: Properties of marine background (BG) and ship aerosol used as model input parameters, including the count median diameter (CMD) and geometric standard deviation (σ_g) of the size distributions, particle density (ρ_{eff}) and aerosol hygroscopicity (κ). HiS, LoS, and WS represent ship aerosol from measurements of high (HGO) and low sulfur content fuels (MGO), and wet scrubbing (SWS) respectively (Paper I and II). The HiS_sul and WS_sul cases represent sulfate particle modes of high FSC fuel combustion and exhaust gas wet scrubbing from Paper III. The WS case is composed of a bimodal distribution, hence, the two separate aerosol modes listed. For each ship exhaust sensitivity test two sets of simulations with either low or high ship aerosol number concentrations were performed. Corresponding simulations with low and high concentrations (N_p) are additionally labeled with _lo and _hi respectively. Reproduced from Paper IV.

Case	CMD [nm]	σ_g	ρ_{eff} [g cm^{-3}]	κ	N_p [cm^{-3}]
BG (Ait)	32	1.1	2.18	1	30
BG (Acc)	93	1.5	2.18	1	30
LoS	45	1.6	0.91	0.04	100/1000
HiS	45	1.6	1.02	0.11	100/1000
WS (Mode 1)	22	1.2	1.18	0.22	131.3/1313
WS (Mode 2)	64	1.3	1.09	0.16	36.7/367
HiS_sul	18	1.15	1.6	0.64	100/1000
WS_sul	39	1.22	1.6	0.64	100/1000

$$r_v = \left(\frac{3}{4} \frac{Q_c}{\pi \rho_w N_c} \right)^{1/3}, \tag{3.10}$$

where Q_c is the cloud liquid water content, ρ_w is the density of water (10^6 g m^{-3}) and N_c is the cloud droplet number concentration. The formation of precipitation is dependent on collisions between hydrometeors (collision-coalescence). An additional aerosol particle load (increase in CCN number concentrations) can lead to increased N_c with smaller droplet diameters. Smaller cloud droplets reduce the collision efficiency and therefore, reduce rain formation rates. This effect can extend the lifetime of the cloud, as it reduces the loss of cloud water through precipitation. The effect is also known as the cloud-lifetime effect.[8] Alternatively, if the liquid water content remains constant, while the cloud layer is polluted with additional aerosol particles, an increase in N_c and reduction of their respective sizes, may also lead to an increase in cloud albedo (α).[7]

Liquid and ice water path (LWP and IWP) are the vertically integrated LWC and IWC of the cloud. LWP is useful in deriving the cloud drop effective radius r_e, which is an important parameter for precipitation and can be utilized to determine α. Freud and

Rosenfeld [149] found that r_e is related to r_v,

$$r_e \sim 1.08\, r_v \ . \tag{3.11}$$

From Equation 3.11, the cloud optical depth (τ) can be derived following Stephens, [150]

$$\tau = \frac{3}{2}\frac{\mathrm{LWP}}{r_e \rho_w} \ , \tag{3.12}$$

where LWP is the liquid water path in g m^{-2}. With Equation 3.12 α is approximated as

$$\alpha = \frac{(1-g)\tau}{1+(1-g)\tau} \ , \tag{3.13}$$

where the scattering asymmetry factor $g = 0.85$ for the scattering of solar radiation by clouds. [151]

4

Thesis Findings and Discussion

The ultimate goal of this research has been to investigate, whether increased shipping emissions may lead to climate feedbacks in the Arctic due to changes in (radiative) properties of Arctic mixed-phase clouds. Results presented in this thesis take into account international shipping regulations, which aim to reduce ship exhaust emissions of SO_x to the atmosphere, and outcomes that emerge from two possible pathways to comply with the regulation. Those are, utilization of low FSC fuels and a combination of high FSC fuel with exhaust wet scrubbing. It is essential to first characterize how compliance measures affect the physicochemical properties of exhaust particles. This was done in a series of controlled laboratory engine experiments. Results from these experiments were subsequently used in a cloud-resolving LES model to study aerosol-cloud interactions between ship exhaust particles and an Arctic mixed-phase cloud given the presented compliance scenarios.

4.1 Laboratory Studies - Impacts of Compliance Measures on Exhaust Particle Emissions

Aims of the laboratory engine experiments were to characterize impacts of FSC reduction and wet scrubbing on exhaust particle properties using different laboratory diesel engines and different fuels of varying FSC. Particle size distributions give an overview of the bulk physical exhaust particle characteristics, yield insight into possible formation mechanisms and allow for comparison with other relevant studies. More detailed exhaust particle information, such as the effective density, illuminate particle composition(s) and the amount of condensed material in the particle phase. Moreover, combined with spectroscopy we learn about the structure and morphology of the particles. Chemical characterization of exhaust particles is fundamental to understanding particle formation processes and their sources. In addition, it allows us to understand the potential role of the exhaust particles in the climate system. Finally, the CCN and ice nucleation (IN) activity of exhaust particles are measured, which give us direct insight into how they might impact cloud formation and properties. Calculation of PN, PM and CCN emission allows us to estimate the potential

health and climate impacts of the investigated compliance measures.

Paper I and II present data from initial laboratory engine experiments utilizing fuel types of varying FSC and exhaust wet scrubbing. In Paper I and II a variety of aerosol and gas instrumentation was used to measure particle size distributions, ρ_{eff}, chemical compositions and hygroscopicities of exhaust particles under a single engine load.

Paper III was both a consolidation and enhancement of the initial studies with key extensions in the experimental setups and investigation regimes. First, the engine employed during experiments described in Paper III had significantly greater power output, which has potential implications for exhaust emissions. Moreover, the impact of three different engine loads on physicochemical properties of exhaust particles was investigated. Chemical characterization of exhaust particles was expanded with EDXRF analysis. Lastly, the IN activity of exhaust particles was investigated, alongside their CCN activities.

4.1.1 Particle Size Distributions

Fuels used across all laboratory experiments shared similar properties (Table 3.1). That said, PSDs were significantly affected by individual test-bed engines. The results presented in Paper I and II (Figure 4.1), demonstrate that for all fuels tested (HGO, MGO and HVO) the measured PSDs were quite similar. In all three instances, PSDs possess unimodal distributions centered around 50 nm. While these observations generally concur with those measured for other ship engines, exhaust particle emissions presented in other studies often also display a smaller particle mode in the range of 10 to 20 nm, formed from sulfurous or other inorganic and organic compounds.[36,152–155] Results for HGO, MGO and HVO displayed larger variability in connection with variations in combustion conditions, as highlighted by the two distinct HGO cases. Surprisingly, no clear differences between PSDs from combustion of HGO and the two low FSC fuels was observed.

The impact of wet scrubbing on HGO exhaust is pronounced. In both fresh- and seawater scrubbing cases, an additional particle mode centered around ≈20 nm is observed. Additional tests performed with the wet scrubber and a low FSC fuel, did not result in this additional particle mode (see Supplemental Information of Paper I). Therefore, we infer that exhaust particles in this dominant mode probably contain sulfurous compounds.

In contrast to results from Paper I, measurements reported in Paper III show a clear difference between exhaust particle PSDs from combustion of low (LoS) and high FSC fuels (HiS). Whereas emissions of LoS resulted in unimodal PSDs, HiS combustion yielded a bimodal PSD, with a dominant mode (orders of magnitude larger) around 20 nm (Figure 4.2), similar to those measured for other marine diesel engines operating on high FSC fuels.[152,153] Downstream of the scrubber, the dominant HiS particle mode was shifted towards larger sizes and reduced in amplitude, in a similar fashion to what Jeong et al.[68]

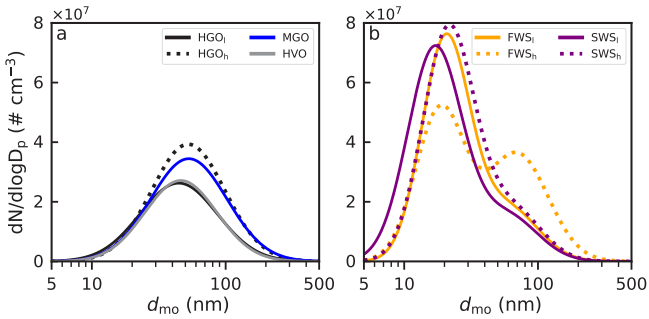

Figure 4.1: Lognormal least squares fits representing particulate emissions for all five fuel and aftertreatment cases retrieved from measured particle size distributions (PSD). All PSDs have been corrected for diffusion losses and dilution factors.[117] HGO, HVO and MGO designate exhaust particles produced from the combustion of the respective fuels, whereas FWS and SWS indicate HGO combustion in conjunction with wet scrubbing using either sea- (SWS) or freshwater (FWS). In both WS cases bimodal lognormal distributions have been fitted to the data points (b). Variations in combustion conditions for HGO, FWS and SWS, characterized by changes in CO_2 emissions, are denoted by subscript l, for relatively low CO_2 concentrations (HGO_l) and subscript h, for relatively high CO_2 concentrations (HGO_h). Fits shown in this figure are reproduced from data presented in Paper I. Reproduced from Paper II.

observed for wet scrubber measurements. Therein, the authors concluded that this shift is caused by coagulation of sulfate particles inside the scrubber.[68]

In all three cases, particle modes around 50 nm display a clear declining trend with increasing engine load. Exhaust particles within this mode likely consist of solid, carbonaceous soot particles. On the other hand, smaller particle modes appear to follow an increasing trend with increasing engine load. For LoS nucleation mode particle concentrations were observed to increase with increasing engine load. Similar trends were seen for HiS and WS. Higher engine loads, generally produce larger concentrations of gaseous SO_2, which can lead to enhanced formation of sulfate particles.

4.1.2 Effective Densities

Despite being a good estimate for density and mass of exhaust particles, ρ_{eff} also yields insight into the particle morphology. By comparing ρ_{eff} for equally sized particles, one can derive potential differences in their chemical compositions and estimate the amount of condensable/volatile material in the particle phase. Moreover, by assuming a homogeneous exhaust particle chemical composition, one can assess the shape and morphology of the particles by determining and comparing ρ_{eff} for different particle mobility diameters. If

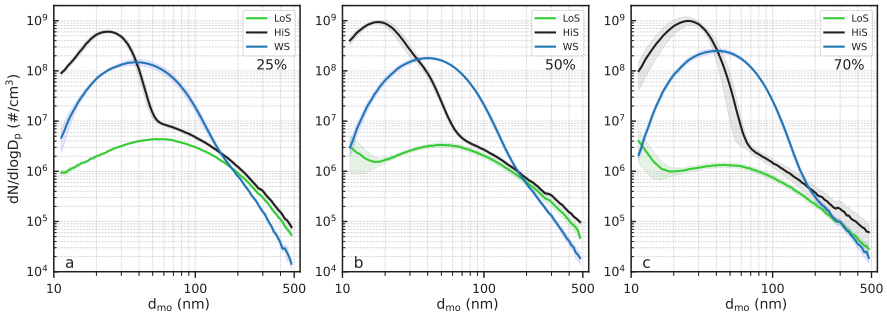

Figure 4.2: Averaged particle size distributions measured with the SMPS for the low FSC fuel (LoS), the high FSC fuel (HiS) and where HiS exhaust gas is passed through the wet scrubber using seawater (WS) are shown in panels (a) to (c). Respective panels show size distributions measured for different engine load regimes, 25%, 50% and 70%. The shaded areas depict ± one standard deviation in measurement uncertainty. Reproduced from Paper III.

a declining trend for ρ_{eff} with increasing mobility diameter is observed, it generally implies that the particles are becoming less dense with increasing size, which is typical for freshly emitted soot particles. On the other hand, if ρ_{eff} remains constant, one can assume that the exhaust particles are spherical and/or liquid droplets.

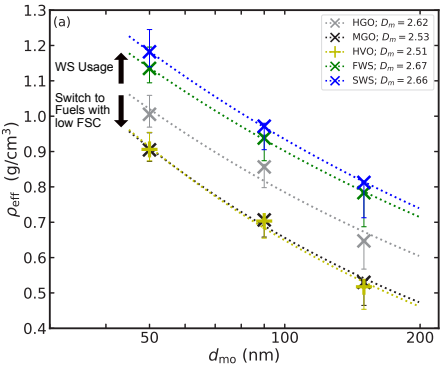

Figure 4.3: Effective densities (ρ_{eff}) determined for the three fuels (HGO, MGO and HVO) as well as both WS cases using HGO and either sea- (SWS) or freshwater (FWS) plotted as a function of mobility diameter with the measurement uncertainty given by the whiskered error bars. The mass-mobility power law fittings are shown as dotted lines with the resulting fractal dimensions (D_m) given in the legend. Reproduced from Paper I.

In Figure 4.3 ρ_{eff} measurements are shown for HVO, MGO, HGO and both wet scrubber cases, FWS and SWS. In all cases, a declining trend with increasing particle size is observed, which implies that exhaust particles are becoming less dense with increasing size, which is typical for soot particles.[127,156] It was, however, not possible to compare particles $\lesssim 20$ nm due to experimental restrictions. This small particle size range would be of particular interest, given that they likely represent newly formed particle modes downstream of the scrubber.

Direct comparisons between HGO and the two low FSC fuels, show that HGO particles are in general more dense, which is likely due to the additional sulfur in the particle phase, although other substances cannot not be excluded. Exhaust particles processed by the wet scrubber are more dense than HGO particles. Considering the high humidity and a strong exhaust temperature reduction from >200°C to ≈ 40°C inside the scrubber, it is very likely that more material condensed onto the particles.

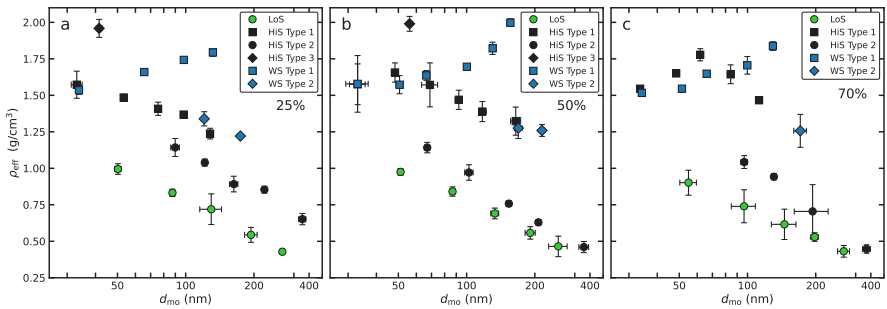

Figure 4.4: Measured effective densities (ρ_{eff}) for the fuels LoS and HiS and the HiS + WS case as a function of particle mobility diameter for an engine load of (a) 25%, (b) 50% and (c) 70%. Error bars represent ± two standard deviations. Classification into different modes was based on observed trends in the raw data output (see Figures S7 to S9 in Paper III). Reproduced from Paper III.

The range and spread of ρ_{eff} measurements increased during the final laboratory engine campaign, which is shown in Figure 4.4. Herein, LoS particles display similar declining trends in ρ_{eff} to the data presented in Figure 4.3. We therefore assume, that LoS particles in the measured PSDs mainly consist of soot particles. The multimodal character of measured PSDs of HiS and WS are reflected in the heterogeneous ρ_{eff} data distribution. In the HiS and WS cases, several particle types could be identified (see Paper III), which correspond to individual PSD modes (Figure 4.2). HiS Type 2 particles (≈60 nm to 350 nm) display a similar trend to LoS particles, i.e., ρ_{eff} declines with increasing particle size. At the same particle size, HiS and LoS display similar offsets to those between

HGO and MGO/HVO particles (Figure 4.3). Meaning that HiS soot particles appear to be more dense compared to those from low FSC fuel combustion. HiS Type 1 particles display a less clear trend. First, ρ_{eff} of Type 1 particles is significantly larger than values of Type 2 particles, reaching a maximum value of 1.78 g cm^{-3}. The differences in trends of Type 1 particles for the different engine loads makes it difficult to assess, whether these particles are more spherical or more fractal-like particles, which become less dense with increasing size. From the data analysis we could identify a third particle mode, which had ρ_{eff} value of ≈1.98 g cm^{-3}. For reference, sulfuric acid has a material density of 1.83 g cm^{-3} and pure soot is estimated to have a density of ≈1.83 g cm^{-3}.[157] It is therefore possible, that these particles consist of sulfate particles, sulfuric acid droplets and/or coated soot particles. Nevertheless, results for Type 3 particles exert a bias that cannot be fully explained. Identified WS particle types display similar behaviors. The values of Type 1 WS particles coincide with Type 1 HiS particles but diverge at sizes above 80 nm and display an increasing trend in ρ_{eff} with particle size. It is noteworthy that ρ_{eff} of ≈34 nm HiS and WS particles are nearly identical, suggesting that the same type of particles are being emitted. Only a few data points for Type 2 WS particles could be identified. The ρ_{eff} values of these particles are substantially lower than those of Type 1 particles.

4.1.3 Chemical Characterization

Two methods were used to determine the chemical compositions of exhaust particle emissions. Scanning transmission X-ray microscopy coupled with NEXAFS is used to obtain detailed information on chemical bonding, structure and morphology of single particles. Energy dispersive X-ray fluorescence, on the other hand, yields chemical fingerprints of bulk aerosol properties collected on filters. Results presented here and obtained from STXM and NEXAFS analysis that are reported in Paper III, match those published in Paper II. EDXRF measurements were only conducted and presented for comparison in Paper III.

In general, combustion of low FSC fuels resulted in emissions of mostly carbonaceous, soot particles (Paper II and III). Figure 4.5 shows a STXM image and corresponding carbon and oxygen K-edge NEXAFS spectra of an exemplary soot particle emitted from LoS combustion (Paper III). The particle displays distinct morphological soot characteristics, such as a fractal-like structure and a fluffy texture (Figure 4.5 a). In Figure 4.5 b the absorption peak around 285.4 eV corresponds to carbon-carbon double bonds (C=C), which are characteristic for black carbon.[129,158] The broader absorption peak above 291 eV likely corresponds to carbon-carbon single bonds (C-C).[129] The oxygen K-edge exhibits absorption features, associated with the carbonyl group (C=O; Figure 4.5 c).[129,159]

Exhaust particles from high FSC combustion exhibit more compositional heterogene-

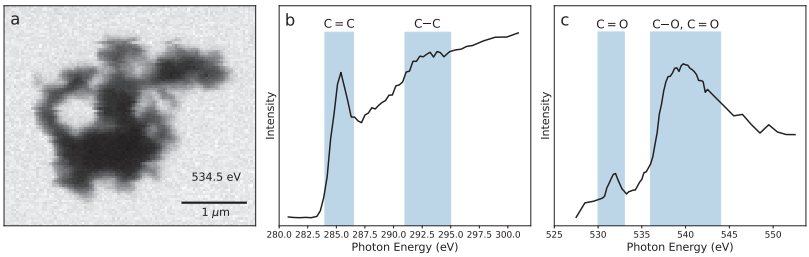

Figure 4.5: A scanning transmission X-ray microscopy (STXM) image and corresponding near-edge absorption fine structure (NEXAFS) spectra of a typical LoS exhaust particle. (a) A X-ray microscopy image taken of the respective particle at the oxygen K-edge at 534.5 eV. NEXAFS spectra acquired for the particle at (b) the carbon K-edge and (c) the oxygen K-edge. The blue shaded areas in panel (b) and (c) mark absorption features related to different functional groups displayed over the corresponding areas. The range for the shaded areas were visually estimated from Moffet et al. [129] Reproduced from Paper III.

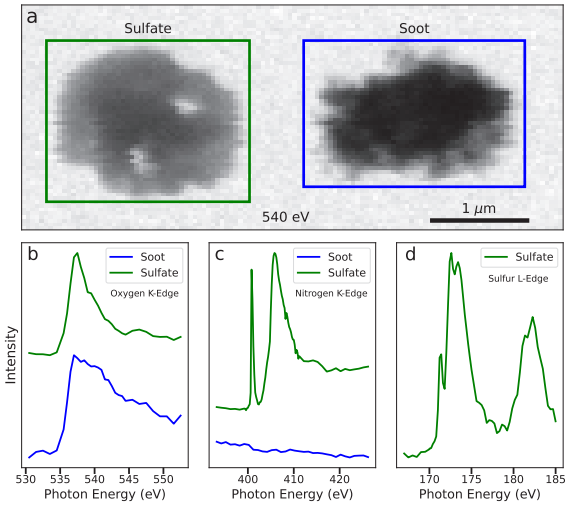

Figure 4.6: STXM image and NEXAFS spectra from HiS exhaust particles. (a) STXM images taken at 540 eV showing a sulfate-type and soot particle. NEXAFS spectra at (b) the oxygen K-edge, (c) the nitrogen K-edge and (d) the sulfur L-edge. Spectra shown in panels (b) to (d) represent the average of whole particles, although during the analysis process all particles were inspected for spectral heterogeneity. Reproduced from Paper III.

ity. During STXM analyses, two distinct particle types, soot (Paper II and III) and sulfate particles (Paper III) were observed. One key difference in the composition of soot particles from low and high FSC combustion, was the presence of sulfates in the particle phase (Paper II and III). Figure 4.6 shows a STXM image of HiS combustion soot and sulfate particles side by side. The sulfur L-edge spectra of the sulfate particle (Figure 4.6 d) shows absorption features characteristic of atmospherically-relevant sulfate particles.[160] We were able to conclude from direct comparisons between oxygen K-edge spectra obtained for the LoS soot particle and, the HiS soot and sulfate particle, as well as a comparison with literature,[161] that sulfate is present in the HiS soot particle (Paper III).

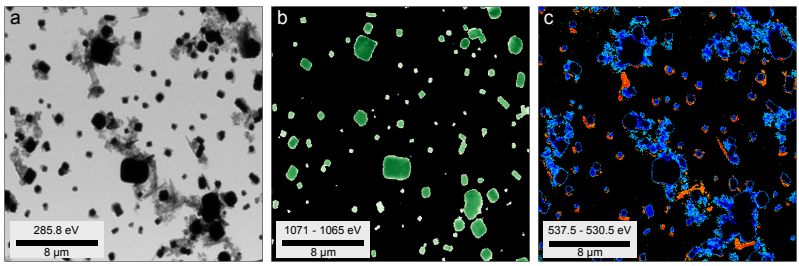

Figure 4.7: STXM images of particles from wet scrubber exhaust taken at different energies. (a) Single energy image around the carbon K-edge (285.8 eV) showing different particle types present on the grid. (b) Differential energy image at the sodium K-edge (1071 eV – 1065 eV) where different shades of green indicate the intensity of measured Na signal. (c) Differential energy image at the oxygen K-edge (537.5 eV – 530.5 eV), where hues of red indicate presence of oxygen-rich sulfates and mineral particles and bluish hues highlight oxygen-containing soot particles. In (b) and (c) images taken within the same absorption edge were pixel-aligned and background corrected signals of the lower (pre-edge) energies were subtracted from signals obtained around absorption peaks (higher energy values). The choice of the two respective energy values were based on carbon and sodium NEXAFS spectra typical for the respective particle types. Reproduced from Paper III.

Wet scrubbing was found to lead to significant changes in exhaust particles' mixing states (Paper II and III). Alongside soot and sulfate particles, wet scrubbing led to emissions of oxygen and calcium containing mineral particles as well as sodium chloride particles. Figure 4.7 shows WS particle clusters where mixtures of salt, soot and mineral are displayed.

The key results from EDXRF measurements (Paper III) are summarized in Table 4.1. The main finding is that wet scrubbing leads to enhanced emissions of sulfur in the particle phase, as well as to minor increases in chlorine, potassium and iron, when compared to HiS and LoS results. These results support the hypothesis that the dominant particle mode measured during the measurement outlined in Paper III (Figure 4.2), consists of sulfate particles and that the shift in CMD and σ_g of the corresponding mode, was likely due to

Table 4.1: Summary of particulate matter related emission factors measured for the three different cases and engine loads normalized by load-dependent fuel consumption. Emission factors of S, Cl, K, Ca and Fe were derived from filter-based EDXRF measurements of PM2.5 sampled using a cyclone impactor. The uncertainties are given as ± two standard deviations. Reproduced form Paper III.

Case	Load	S μg kg^{-1}	Cl μg kg^{-1}	K μg kg^{-1}	Ca μg kg^{-1}	Fe μg kg^{-1}
LoS	25	0.92 ± 0.32	0.10 ± 0.07	0.03 ± 0.02	0.19 ± 0.10	0.33 ± 0.18
	50	0.36 ± 0.13	0.00 ± 0.01	0.00 ± 0.00	0.04 ± 0.02	0.13 ± 0.07
	70	0.18 ± 0.07	0.02 ± 0.01	0.01 ± 0.01	0.02 ± 0.01	0.06 ± 0.04
HiS	25	23.13 ± 5.98	0.03 ± 0.01	0.02 ± 0.01	0.15 ± 0.09	0.33 ± 0.23
	50	20.71 ± 5.89	0.00 ± 0.00	0.05 ± 0.02	0.30 ± 0.10	0.50 ± 0.20
	70	24.91 ± 6.29	0.01 ± 0.01	0.00 ± 0.00	0.09 ± 0.04	0.40 ± 0.14
WS	25	38.63 ± 9.45	1.25 ± 0.32	0.14 ± 0.09	0.51 ± 0.17	0.51 ± 0.25
	50	38.23 ± 9.70	0.95 ± 0.28	0.32 ± 0.10	0.66 ± 0.19	0.62 ± 0.18
	70	31.14 ± 8.39	0.60 ± 0.16	0.07 ± 0.04	0.31 ± 0.09	0.93 ± 0.29

coagulation of sulfate particles.

4.1.4 CCN Activity

Fuel sulfur reduction and wet scrubbing effects on physicochemical properties of exhaust particles are reflected in the CCN activity results. In the previous sections it was shown that exhaust particles from high FSC fuel combustion consist of sulfate particles and soot particles with traces of sulfates. When exhaust particles from low FSC fuel combustion were analyzed, we found exclusively carbonaceous soot particles, which were also less dense compared to HiS soot particles and had no detectable amounts of sulfate. Wet scrubbing affected the mixing state of exhaust particles significantly. Alongside soot and sulfate particles, sodium chloride and mineral particles were emitted. Moreover, scrubbed soot particles were more dense than HiS particles, which suggests that more condensable material partitioned into the particle phase. These observations have implications for the hygroscopicity of the particles.

In Figure 4.8 κ values of HGO, MGO and SWS, and FWS, particles are shown. We show that the two investigated compliance measures have opposing effects on the CCN activity of ship engine exhaust particles. These observations also agree with the results shown in the previous sections. As shown in Figure 4.8, the CCN activity is substantially

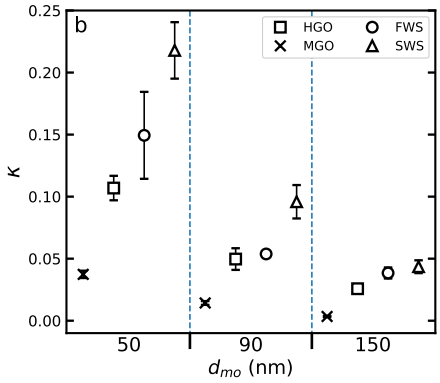

Figure 4.8: κ values of fresh exhaust particles obtained for mobility diameters of 50 nm, 90 nm and 150 nm. HGO and MGO designate exhaust particles produced from the combustion of the respective fuels, whereas FWS and SWS indicate HGO combustion in conjunction with wet scrubbing using either sea- (SWS) or freshwater (FWS). The CCN activity was below the detection limit for HVO particles, and therefore HVO related data points are not present in the figure. Data points are calculated mean values with whiskers indicating measurement uncertainties given by ± one standard deviation. Reproduced from Paper II.

reduced when switching to low FSC fuels, as can be seen from direct comparisons between κ values of HGO and MGO particles. This can be explained by the relative absence of sulfates and other water soluble compounds in the particle phase. Values for HVO particles are missing in the figure because no CCN activity was observed for HVO particles. A key fuel composition difference between MGO and HVO, was the substantially higher aromatic content in MGO. We therefore hypothesize that the aromatic content of the fuel affects the particle composition and can to a degree facilitate droplet activation. Wet scrubbing, strongly facilitated CCN activation, as is seen from the high κ values compared to those of HGO particles. Considering the previously observed impacts of wet scrubbing on exhaust particle emissions, i.e., particles with more condensed/water soluble material and enhanced mixing with salt particles, one would expect that these changes increase CCN activity.

In Paper III similar observations were made, albeit changes in CCN activity between HiS and WS are less pronounced compared to Paper II (Figure 4.9). Similar to Paper II, low FSC fuel combustion, which resulted predominantly in emissions of soot particles absent sulfates, reduced the hygroscopicity across the inspected size range. The effect of wet scrubbing on the CCN activity is most pronounced in the 50 nm to 100 nm size range, which coincides with the observed shifts of the dominant particle mode. Comparing κ values of 50 nm WS and HiS particles and, taking into account similarities in ρ_{eff} and

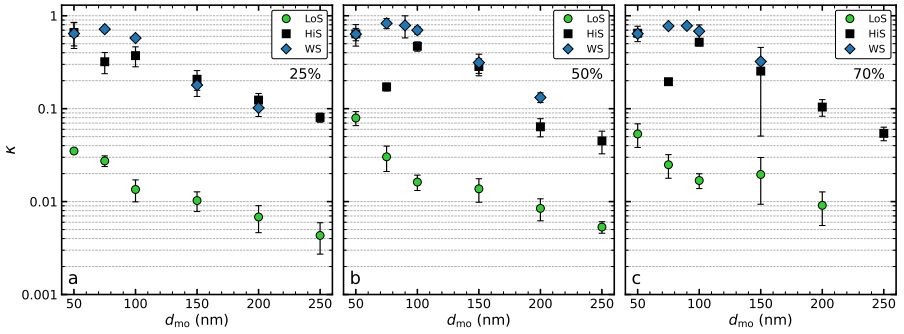

Figure 4.9: CCN activity expressed as the mean hygroscopicity parameter (κ) value for particle mobility diameters between 50 and 250 nm. LoS represents combustion of low FSC fuel, HiS of non-compliant high FSC fuel and in WS, HiS exhaust was processed by the wet scrubber. Panels (a) to (c) show results for engine loads ranging from 25% to 70% (as indicated). The error bars represent ± two standard deviations of measurement uncertainty. Reproduced from Paper III.

results obtained from STXM/NEXAFS analysis, we hypothesize that 50 nm particles share the same chemical composition. No immediate correlation between engine load and CCN activity was found for any of the cases.

4.1.5 IN Activity

For Paper III the IN abilities of the exhaust particles were also investigated. Given the fact, that compliance measures had distinct impacts on CCN activity, one might expect to observe similar results for IN. In Figure 4.10 the freezing onset conditions for 200 nm LoS, HiS and WS exhaust particles are shown. The data show at which temperature and RH_i 1% of the total size-selected particle population is activated into ice crystals. At temperatures between -35 and -50° C particles only exhibited ice nucleation onsets close to liquid water saturation or around homogeneous freezing conditions. At higher temperatures no apparent ice nucleation was observed from any of the three cases. It has been previously shown that sulfuric acid and organic coatings on soot particles can influence IN activity, either by filling pores and thus, inhibiting pore condensation freezing, or by facilitating water uptake due to the addition of more hygroscopic material.[28] While ship plumes have previously been found to enhance INP concentrations,[162] our results show that FSC reduction and wet scrubbing have no apparent influence on the exhaust particles' freezing abilities. That said, we cannot exclude that long-term atmospheric aging processes could affect particles in different ways.[26]

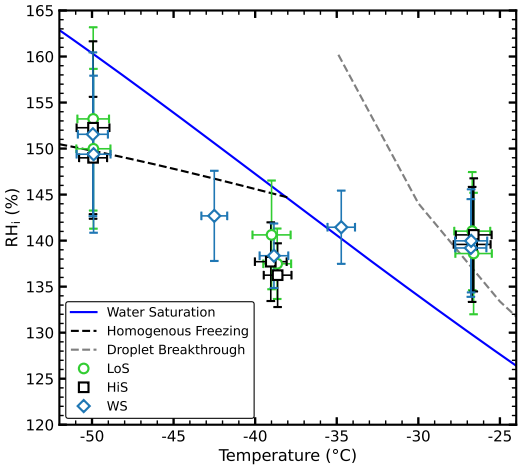

Figure 4.10: Summary of 200 nm particle freezing experiments from −26°C to −50°C. The freezing onset was defined as the point where the activated fraction, i.e., the ratio between the concentration of ice crystals exceeding 3 μm and the total particle concentration measured with the CPC, exceeded 1%. The solid blue line indicates water saturation, the dashed blue line represents the homogeneous freezing threshold for 200 nm particles according to Koop et al. [15] (calculated with a water activity (Δa_w) of 0.2946) and the grey dashed line represents the experimentally determined droplet breakthrough conditions for PINCii. [133] Reproduced from Paper III.

4.1.6 Emission Factors

Particle number (EF_{PN}), particle mass (EF_{PM}), and CCN emission factors (EF_{CCN}) from Paper I, II and III, reveal dependencies on engine type and load (Table 4.2). One key finding is that switching to low FSC generally decreased both number and mass emissions of exhaust particles. While this relationship is less pronounced in Paper I, where particle exhaust emissions were subject to less stable combustion conditions, it is very clear for results reported in Paper III. Results in Paper III show that FSC reduction was characterized by an absence of sulfate particles, which dominated PN emissions from HiS fuel combustion. For wet scrubbing the net impact on EF_{PN} and EF_{PM} emissions depended strongly on the engine type. In Paper I, wet scrubbing led to the formation of an additional ultrafine particle mode, which resulted in increased EF_{PN}. As wet scrubbing was found to mostly affect exhaust particles in size ranges, which contribute only little to the total mass, the impact on EF_{PM} was less pronounced (Paper I). In Paper III, wet scrubbing shifted the HiS sulfate mode (increase in CMD) and reduced its amplitude. This led to a reduction

in EF_{PN} but, due to the shift in size, to an increase in EF_{PM}. Engine load dependencies are less clear. While the soot mode was observed to be reduced with increasing engine load for all cases, the impact on smaller, non-soot particles is less clear (Paper III). In summary, we observe a reduction in both EF_{PN} and EF_{PM}, when high FSC is replaced by SECA-compliant low FSC fuels. Reducing the sulfur content of marine fuels is therefore a viable solution to reducing PM emissions from ships. Our observations regarding the impact of wet scrubbing on exhaust particle emissions, mirror those of other studies, where large variability in terms of particle removal efficiency is seen (see Section 1.2.1). While wet scrubbing helps in reducing SO_2 emissions and thus, inhibits formation of secondary aerosol, it might not be the most favorable solution in mitigating primary exhaust particle emissions.

The impact of compliance measures on CCN emissions can have significant implications for atmospheric processes and the net impact of shipping activity on the climate system. In our measurements we found that combustion of low FSC fuels led in general to a decrease in CCN number emissions, due to emissions of mostly hydrophobic soot particles. This reduction was especially pronounced when high FSC fuel combustion was accompanied by abundant sulfate particle emissions (Paper III). On the other hand, wet scrubbing increased CCN emissions in most cases. Observed EF_{CCN} increases were caused by a general increase in particle hygroscopicity (Paper II and III) and by shifts in particle size distributions towards larger sizes, possibly caused by coagulation of particles inside the scrubber. These CCN emissions results highlight that investigated compliance measures have the potential to impact the (Arctic) climate system in different ways. While BC deposition on snow and ice surfaces might play a larger role in low FSC fuel combustion, wet scrubber emissions have a stronger potential to impact cloud formation and properties, which may lead to alterations in radiative processes.

Table 4.2: Summary of particulate matter and CCN related emission factors normalized by fuel consumption. Particle number (EF_{PN}) and particle mass emission factors (EF_{PM}) are derived from integration of measured particle size distributions. EF_{PM} are calculated using the average ρ_{eff} for individual particle modes ($EF_{PM,\rho_{eff}}$). The uncertainties are given as ± two standard deviations. Data reproduced from Paper I, II and III.

Case	Load (%)	EF_{PN} 10^{14} # kg^{-1}	$EF_{PM,\rho_{eff}}$ mg kg^{-1}	$EF_{CCN,0.3\%}$ 10^{13} # kg^{-1}	$EF_{CCN,0.7\%}$ 10^{13} # kg^{-1}
HVO	32	3.73 ± 0.16	58.07 ± 2.78	-	-
MGO	32	4.98 ± 0.39	128.26 ± 14.33	0.01	0.11
HGO_l	32	4.08 ± 0.29	88.35 ± 9.04	0.07	0.83
HGO_h	32	5.48 ± 0.14	161.80 ± 8.00	0.15	1.66
FWS_l	32	7.67 ± 0.68	79.85 ± 12.99	0.07	0.79
FWS_h	32	7.29 ± 0.57	202.02 ± 12.33	0.27	2.11
SWS_l	32	6.91 ± 0.17	70.99 ± 2.35	0.07	1.25
SWS_h	32	8.57 ± 0.65	94.37 ± 3.93	0.09	1.57
LoS	25	1.18 ± 0.04	62.49 ± 2.36	0.20	1.13
	50	0.73 ± 0.23	34.70 ± 10.50	0.18	0.75
	70	0.33 ± 0.33	11.08 ± 2.16	0.08	0.29
HiS	25	69.90 ± 8.90	198.23 ± 32.08	7.19	51.76
	50	80.68 ± 14.55	126.01 ± 28.73	3.22	33.27
	70	77.52 ± 30.11	164.58 ± 44.30	1.76	77.32
WS	25	26.93 ± 5.11	388.36 ± 105.96	43.22	146.75
	50	23.44 ± 2.73	333.14 ± 31.17	38.77	136.26
	70	28.19 ± 4.83	358.92 ± 30.05	45.41	166.25

4.2 Mixed-Phase Cloud Responses Induced by Ship Aerosol Perturbations

The laboratory engine studies enabled us to construct a good overview of impacts of FSC reduction and wet scrubbing on the exhaust particle properties. The results yielded essential information for implementation of ship exhaust particle information into the cloud-resolving LES model MIMICA. This allowed us to investigate the overarching research question of this study, that is, how ship particle exhaust emissions in the Arctic might impact mixed-phase cloud properties. We investigated the impacts on microphysical cloud properties, i.e., the impact on distribution of different hydrometeors in the cloud. Using these results we could further explore how IMO regulation policies impact macrophysical cloud properties, including radiative properties that give us insight into possible climate effects.

4.2.1 Impact of FSC Reduction and Wet Scrubbing on Liquid and Ice Water Path

The time evolution of the domain-averaged LWP and IWP are shown in Fig. 4.11 and compared to ASCOS observations. The general overestimate in LWP compared to observational data is due to the use of prescribed aerosol particle concentrations, which was found to yield a larger LWP compared to using interactive aerosol concentrations.[140,142] In ship cases with sufficiently large particle number concentrations ($\geq$ 1000 cm^{-3}; HiS_hi, WS_hi, and WS_sul_hi), the LWP was found to be increased compared to the reference Mix case (Figure 4.11 a and b). This agrees with a similar model study by Possner et al.,[112] where ship-related CCN emissions were also found to increase LWP. In contrast to Paper IV, Possner et al.[112] utilized prescribed aerosol specifications of ship emissions based on **?**, which did not take into account different compliance measures and assume exhaust particles to have a soluble fraction of 0.62%. The LWP increase is absent in LoS_hi and HiS_sul_hi, suggesting that in these cases ship exhaust particles were too hydrophobic (LoS_hi; κ=0.04) or too small (HiS_sul_hi; CMD=18 nm) to induce this effect.

In contrast to results for the LWP, no effect on the modeled IWP was observed (Figure 4.11 c and d). This is mainly due to the implementation of prognostic N_i, which excludes direct effects by additional ship aerosol particles. Here, ship exhaust perturbations can only impact graupel and snow by influencing the availability of water vapor and accretion efficiency of the hydrometeors.

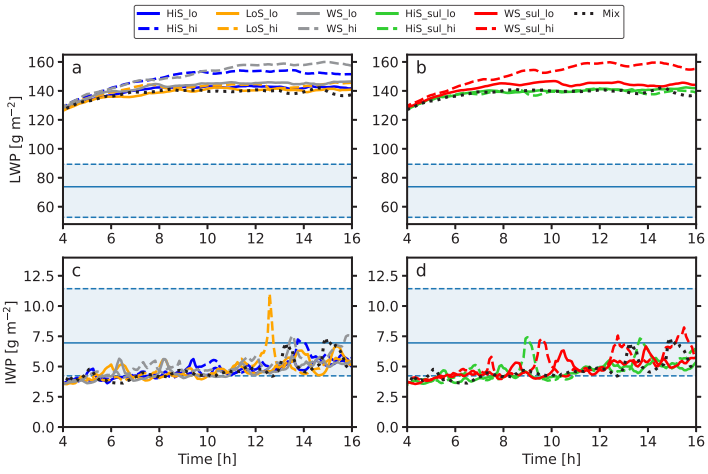

Figure 4.11: Time evolution of the simulated domain-averaged (a and b) liquid water path (LWP) and (c and d) ice water path (IWP). Mix refers to the reference case with background aerosol only. Mix refers to the reference case with seaspray background aerosol only. HiS, LoS, and WS represent ship aerosol from measurements of high and low sulfur content fuels and wet scrubbing respectively (Paper I and Paper II). The HiS_sul and WS_sul cases represent sulfate particle modes of high FSC fuel combustion and exhaust gas wet scrubbing from Paper III. The label additions _lo and _hi signify the ship aerosol concentrations used in the individual model runs. The blue shaded area refers to the retrieved LWP and IWP from microwave radiometer measurements (median over the observation period; the corresponding dashed lines are the 25th/75th percentiles) during the ASCOS campaign.[119,120] The first four hours are considered a spin-up period of the model and are removed from the figures. Reproduced from Paper IV.

4.2.2 Impact of FSC Reduction and Wet Scrubbing on Hydrometeors

In accordance with results reported for LWP and IWP, ship perturbations were mostly found to affect cloud droplet (N_c) and raindrop concentrations (N_r; Figure 4.12). When ship aerosol particles were added into the model domain, generally, more smaller cloud droplets (Figure 4.12 a and f) and less larger raindrops were formed (Figure 4.12 b and g). Similar to results shown in Figure 4.11, this model response was largely dependent on the ship exhaust particle concentrations, CMD and κ. The WS_sul_lo case was the only low concentration sensitivity case able to induce a moderate cloud response with respect to hydrometeor concentrations. Moreover, we found that the CMD of ship exhaust particles had a stronger influence on the cloud than larger hygroscopicities, as can be seen when comparing LoS_1k (CMD = 45 nm; κ = 0.04) and HiS_sul_1k (CMD = 18 nm; κ = 0.64).

This agrees with similar model responses reported by Christiansen et al.[141] who found particle hygroscopicity to be of smaller importance when Acc mode aerosol particles are present for the same cloud case.

Ship exhaust cases that affected N_c were also found to induce a delay in rain formation onsets alongside general reductions in N_r. With larger numbers of cloud droplets, the amount of water vapor available for condensation per particle is reduced. This limits the growth of droplets and therefore, their auto-conversion rates, i.e., conversion into raindrops. Cloud drop effective radii r_e are reduced by additional ship exhaust particles (Table 4.3), agreeing with observed reductions in N_r due to reduced droplet coalescence.

As ice crystals are mainly prescribed (N_i), ship exhaust particles were only found to exert moderate impacts on graupel (N_g; Figure 4.12 d and i) and snow concentrations (N_s; Figure 4.12 e and j). All simulations showed similar cloud depths and evolutions (Figure 4.12, although, data indicate that ship perturbations induced moderate cloud deepening. Cloud depths ranged between 535 m (Mix) and 570 m (WS_sul_hi).

Table 4.3: Overview of mean LWP, IWP, surface precipitation, net longwave radiation at the surface (Net LW), cloud effective radius (r_e) and cloud albedo (α) over the last four hours of simulation time. The label additions _lo and _hi signify the ship aerosol concentrations used in the individual model runs. Reproduced from Paper IV.

Case	LWP [g m^{-2}]	IWP [g m^{-2}]	Surface precipitation [mm d^{-1}]	Net LW at surface [W m^{-2}]	r_e [μm]	α
Mix	139.3	5.5	0.06	-14.6	3.52	0.90
LoS_lo	140.7	5.3	0.06	-14.5	3.51	0.90
LoS_hi	143.6	5.5	0.05	-14.4	3.43	0.90
HiS_lo	142.5	5.1	0.06	-14.5	3.50	0.90
HiS_hi	152.8	5.6	0.03	-14.2	3.29	0.91
WS_lo	145.4	5.1	0.06	-14.4	3.46	0.91
WS_hi	158.6	5.9	0.02	-13.9	3.16	0.92
HiS_sul_lo	141.0	5.0	0.07	-14.6	3.53	0.90
HiS_sul_hi	139.8	5.4	0.06	-14.6	3.52	0.90
WS_sul_lo	144.6	5.4	0.05	-14.4	3.44	0.91
WS_sul_hi	158.0	6.2	0.02	-14.0	3.16	0.92

4.2.3 Impact of FSC Reduction and Wet Scrubbing on Macrophysical Cloud Properties

The results discussed in the previous two sections show that ship exhaust perturbations had the tendency to generate optically thicker clouds and to reduce rain formation.

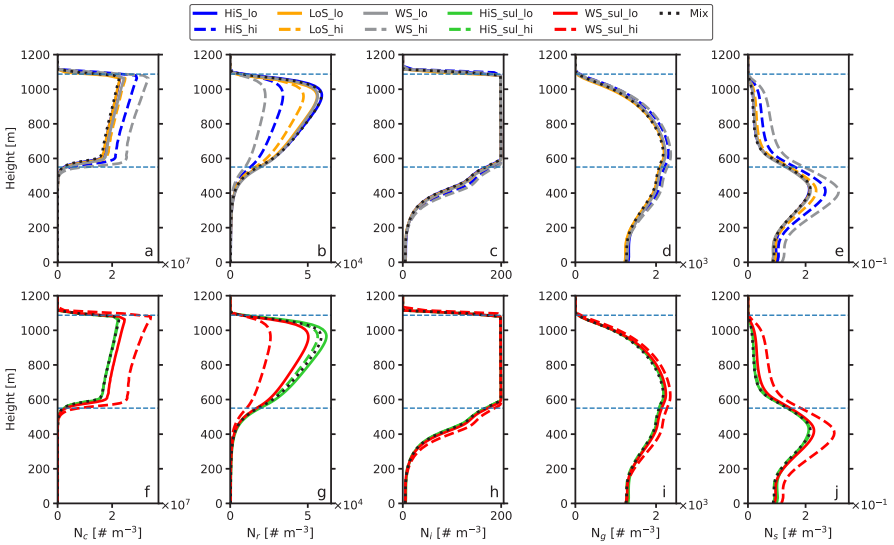

Figure 4.12: Vertical profiles of horizontally averaged (a and f) N_c, (b and g) N_r, (c and h) N_i, (d and i) N_g and (e and j) N_s averaged over the last four simulation hours. averaged over the last four simulation hours. The light blue, dashed line represents the average cloud bottom and top height calculated for the reference case (Mix). HiS, LoS, and WS represent ship aerosol from measurements of high and low sulfur content fuels and wet scrubbing respectively from Paper I and II. The HiS_sul and WS_sul cases represent sulfate particle modes of high FSC fuel combustion and exhaust gas wet scrubbing from Paper III. The label additions _lo and _hi signify the ship aerosol concentrations used in the individual model runs. Reproduced from Paper IV.

These results have implications for cloud radiative effects and processes at the surface, which help in identifying potential climate impacts from shipping in the Arctic.

Ship exhaust particles generally led to reductions in rain drop formation (Figure 4.12) and in r_e (Table 4.3). Consequently, surface precipitation was also reduced for ship exhaust cases with high particle number concentrations (Table 4.3 and Figure 4.13 a and b). These results suggest that ship exhaust emissions may sustain the cloud for longer times compared to the unperturbed reference case, although longer simulation durations are required in order to draw definitive conclusions. The shipping-induced increases in LWP and reductions in r_e also resulted in increased α (Table 4.3). In general, larger α values lead to increased reflection and scattering of incoming solar radiation and can therefore play a substantial role on the surface radiative balance during the Arctic summer months. Here, only small adjustments in α were observed from ship exhaust perturbations (0.90 to 0.92), which

was likely due to the already high α value in Mix. It is important to note though, that the magnitude of shortwave (SW) radiative cooling from cloud albedo adjustments also depends on the properties of underlying surfaces. When the surface is covered by ice, clouds lead to lower contrast compared to open sea or land surfaces and therefore, cloud albedo effects are of smaller importance in the Arctic.

Net fluxes of SW and longwave (LW) radiation at the surface were calculated by subtracting net upwelling fluxes from net downwelling fluxes. Negative values imply net upwelling radiation, hence, radiative surface cooling. Net SW radiative fluxes at the surface are positive for all cases and remain mostly unaffected by ship exhaust perturbations (Figure 4.13 e and f). This result agrees with the relatively small adjustments in α and suggests that ship exhaust emissions may not lead to SW radiative cooling due to enhancements of cloud reflectivity. It is important to note that the impact of increased ship exhaust emissions on net SW may change substantially with cloud properties. That said, for most cases this may not be of major importance in the Arctic climate system.

A larger impact from ship exhaust perturbations was modeled for LW radiation at the surface (Table 4.3 and Figure 4.13 c and d). Net LW is negative in all model runs, which implies net upwelling LW radiation. Ship cases which were found to significantly impact the LWP of the cloud, also led to a reduction in LW radiative cooling at the surface, i.e., net LW became less negative. This effect is especially pronounced for wet scrubber cases with high exhaust particle concentrations (WS_hi and WS_sul_hi). The largest difference in net LW at the surface was modelled for WS_hi, where net radiative cooling was reduced by 0.7 W m^{-2}.

In conclusion, our results suggest that Arctic ship exhaust emissions may lead to diminished radiative longwave cooling and enhanced surface warming due to an increases in LWP, which enhances re-emission of LW radiation to the surface. Nevertheless, this effect is mostly observed for ship exhaust cases with high particle concentrations and strongly dependent on the CMD of exhaust particle size distributions. Here, we only tested one specific cloud case, therefore, the impact of ship exhaust emissions may change with ambient conditions and cloud properties.

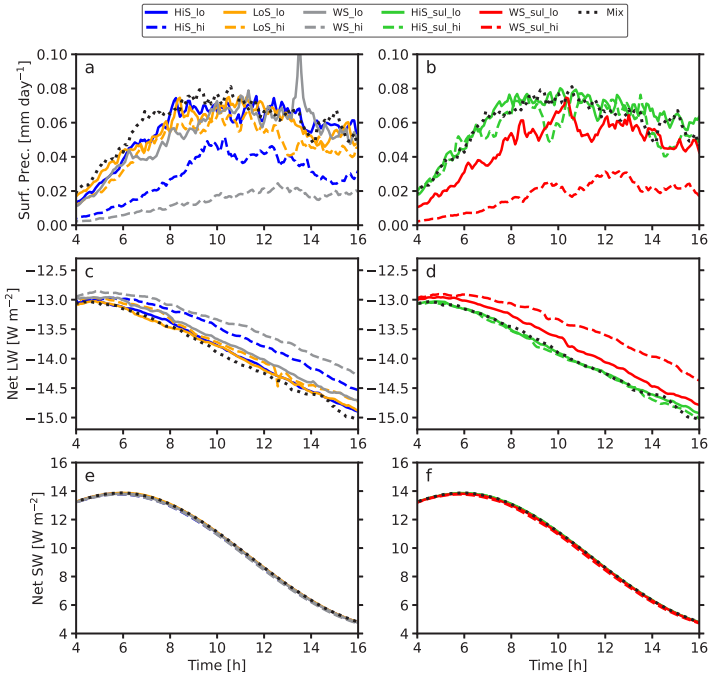

Figure 4.13: Time evolution of the simulated domain-averaged (a and b) surface precipitation, (c and d) net longwave radiation at the surface (Net LW) and (e and f) net shortwave radiation at the surface (Net SW) for the set of simulations. Net radiative fluxes are calculated by subtracting the upwelling radiative flux from the downwelling flux (e.g., LW_{down}-LW_{up}), hence, a negative value implies net outgoing radiation. Mix refers to the reference case with background aerosol only. Mix refers to the reference case with seaspray background aerosol only. HiS, LoS, and WS represent ship aerosol from measurements of high and low sulfur content fuels and wet scrubbing respectively (Paper I and II). The HiS_sul and WS_sul cases represent sulfate particle modes of high FSC fuel combustion and exhaust gas wet scrubbing from Paper III. The label additions _lo and _hi signify the ship aerosol concentrations used in the individual model runs. The first four hours are considered a spin-up period of the model and are removed from the figures. Reproduced and modified from Paper IV.

5

Conclusions and Outlook

5.1 Conclusions

The aim of this work has been to contribute to understanding how international marine fuel policies affect physicochemical properties of ship engine exhaust particles. These results are useful for projecting how changes (increases) in Arctic shipping activity may lead to changes in Arctic cloud properties and therefore, affect climatological feedbacks in an environment, that is already experiencing unprecedented climate warming. The Arctic is characterized by a very sensitive climate system, where changes in individual system processes, may result in cascading feedbacks, that can further amplify warming. It is therefore important that we improve our understanding of potential feedbacks including from increased ship emissions, which might help to limit detrimental climate impacts. To answer the research questions outlined in Section 2 we employed methods that allowed us to investigate the topic from the nanometer scale, the typical size of ship engine exhaust particles, to the regional scale, encompassing tens of square kilometers, representative of the extent of Arctic mixed-phase clouds.

Given the context of current international marine fuel regulations, we focused on two possible compliance pathways, i.e., utilization of fuels with reduced sulfur content and the combination of high FSC fuel usage with wet scrubbing, to inhibit emissions of SO_x to the atmosphere. The experiments using multiple marine test-bed engines, different fuels and a laboratory wet scrubber were reported in Paper I to III. Here, main findings and answers to our main research questions are briefly summarized.

Results reported in Paper I, II and III revealed that FSC reduction and exhaust wet scrubbing have substantial impacts on physicochemical properties of exhaust particles that vary substantially with engine type. Whereas combustion of high FSC fuel was found to emit a variety of exhaust particles, including soot particles with traces of sulfate and sulfate particles, FSC reduction resulted primarily in emissions of soot particles absent of sulfate. For wet scrubbing, the impact on properties was more varied compared to low FSC fuel combustion and strongly engine-dependent. In the first set of experiments (Paper I), we

report that wet scrubbing can lead to the formation of an additional nucleation mode. In Paper III high FSC fuel combustion resulted in bimodal size distributions, consisting of a sulfate mode around 20 nm and a soot mode around 45 nm. When high FSC fuel exhaust was processed by the wet scrubber, a shift of this sulfate mode was observed (increase in CMD), which was likely caused by coagulation of particles within the scrubber (Paper III). Wet scrubbing was also found to increase the particle densities and substantially impact the chemical mixing state of exhaust particles. In addition to soot and sulfate particles, wet scrubbing led to enhanced emissions of salt and mineral particles (Paper II and III).

Fuel sulfur content reduction and wet scrubbing have opposing effects on the CCN activity of exhaust particles. In general, the CCN activity was reduced when the sulfur content of the fuel was reduced. Contrarily, wet scrubbing was found to facilitate liquid droplet formation of exhaust particles. While FSC is a main driver of CCN activity of engine exhaust particles, other fuel properties, such as aromatic content, may also play a significant role (compare MGO and HVO in Paper II). Observations of CCN activity agreed with results regarding the chemical composition of the particles, such as the absence of sulfate in particles from combustion of fuels with reduced FSC and larger amounts of water-soluble material in particle emissions from wet scrubbing. Unlike CCN activity, ice nucleation experiments revealed that compliance measures did not affect the IN activity of exhaust particles. In most cases, ice nucleation was only observed close to liquid water saturation or around homogeneous freezing conditions. We can therefore say, that soot remains a poor INP at temperatures in the mixed-phase cloud regime.

Quantification of exhaust particle and CCN emissions is essential in estimating climate- and health-related impacts from shipping activity. In general, low FSC fuel combustion resulted in lower PN emissions compared to equivalent emissions from high FSC fuels. The magnitude of this reduction strongly depended on the PSDs exhibited by the different fuel types. The strongest reductions are reported in Paper III ($\geq$95%) due to the absence of dominant sulfate particle modes when low FSC fuel is utilized. Particle mass emissions were generally reduced when low FSC fuels were used, due to reduced number emissions and lower particle effective densities. The net impact on PN and PM emission from wet scrubbing is less obvious and varied substantially with experiments. In Paper I and II increased PN but slightly reduced PM emissions are reported, driven by the additional formation of 20 nm particles and slight reduction in larger soot mode particles. On the other hand, results reported in Paper III show a reduction in PN but increase in PM emissions due to the shift in size of the already present sulfate particle mode. It is important to note though that our analysis focused on submicron exhaust particles. We can therefore not say how compliance measures affect particles ≥ 1 μm, which are comparatively few in numbers but can have a large impact on total mass emissions. In comparison to combustion

of non-compliant, high FSC fuel, significant reductions in CCN number emissions for low FSC fuels and generally, increased CCN emissions for scrubbed exhaust were observed. In conclusion, these results suggest that FSC reduction may lead to beneficial health effects but to diminished direct and indirect radiative cooling from exhaust particle emissions. Wet scrubbing, on the other hand, could lead to enhanced radiative cooling due to increased CCN emissions but the impact on health is subject to larger uncertainties as PN emissions were found to increase and/or decrease depending on engine type.

Using different engines adds uncertainty to the results but also likely better represents the range of realistic outputs from ocean-going vessels. It is also important to note, that laboratory measurements are constrained by resources and operational costs. We acknowledge that the relevant investigation of atmospheric aging of exhaust particles was not conducted in these studies. While it is of particular relevance to the understanding of fundamental particle formation processes and to assess the role of exhaust particles in atmospheric processes, it was beyond the scope of this study but should be considered in future work.

By performing the laboratory engine experiments, we were able to constrain the potential range of ship particle emissions in the Arctic. Using this information in the MIMICA LES model, we tried to assess the impact of ship exhaust particles on an Arctic mixed-phase cloud, which is based on observations from the ASCOS icebreaker campaign.[119,120]

General observations made for ship exhaust-induced changes in cloud properties included increased cloud droplet number concentrations and reduced raindrop formation, leading to increased LWP, reduced surface precipitation and possibly, to extended cloud lifetimes. In the context of Arctic Amplification, the most relevant impact from ship emissions was found to be the reduction of LW radiative cooling at the surface. In our investigations, changes in macrophysical properties led to enhanced re-emission of LW radiation to the surface. Increased ship exhaust emissions may therefore enhance surface warming in the Arctic. Excluding results from high FSC fuel combustion, our results suggest that wet scrubbing has a larger potential to cause the aforementioned changes in mixed-phase cloud properties. Low FSC fuel combustion is less likely to trigger these changes as exhaust particles are generally more hydrophobic and PSDs are often found to have smaller CMDs.

The magnitude of the changes in micro- and macrophysical cloud states correlated with particle hygroscopicity and, even more strongly, with the size of emitted exhaust particles. In most cases, significant cloud perturbations were only observed for relatively high particle concentrations, which might have real-world implications for spatially-constrained perturbations, like ship-tracks. Cloud properties are in general also strongly depend on ambient aerosol concentrations. Here, we simulated only one specific cloud case with

ship exhaust particles. The properties of Arctic clouds can vary substantially, thus more work is needed to get a more complete picture of the potential climate feedbacks from ship emissions. While most model experiments yielded quite muted cloud responses, results still suggest, that depending on which fuel type and/or exhaust-aftertreatment systems will become dominant in Arctic shipping, it can have different implications for aerosol-cloud feedbacks. In order to estimate the overall impact of future Arctic shipping, one would have to implement future ship traffic scenarios, have better estimates for future fuel type usage and exhaust emission characteristics and expand the area of research to a much larger area, e.g., by using atmospheric models that cover larger spatial domains. While this was not within the scope of this project, it is of great interest for future studies.

5.2 Future Perspectives

It should be stated, that this work does not endorse or advocate for any of the investigated compliance measures. Here, we only explored a few potential outcomes out of a multitude of possibilities encountered on the open sea. Both studied compliance measures, can have advantages and disadvantages, depending on the area of focus.

Our results suggest that wet scrubber usage may reduce or increase particles number emissions, adding to the uncertainty displayed in other studies. It is obvious that wet scrubbing related ship exhaust emissions require more attention from the scientific community and possibly, stricter regulation, that constrain the impact(s) on particle exhaust emissions more clearly. We found that reducing the sulfur content of marine fuels, leads to reduction of particle number emissions, which is in agreement with previously published results,[45,51,80] and is therefore a viable option to mitigate the health impact of ship exhaust emissions. In light of the decarbonization of the shipping sector, other alternative fuel options should be explored. Moreover, a transition away from fossil fuels, would likely result in the largest long-term climate benefits.

While low FSC fuels yielded reductions in PN emissions compared to wet scrubbing, we showed that compliance measures have opposing effects on the cloud activity of exhaust particles. Transitioning towards low FSC fuels would likely reduce radiative cooling from ship exhaust aerosol-cloud interactions, due to emission of predominantly hydrophobic soot particles. On the other hand, wet scrubbing may lead to enhanced shipping-induced climate cooling, as ship exhaust emissions generally tend to have a net cooling effect on the global climate. That said, it is important to highlight that wet scrubbing shifts a significant fraction of the pollution from the atmosphere to the marine environment and therefore, is far from being an ideal solution.

With the changing landscapes we face, both in a literal sense and also regarding fuel

type utilization in the maritime shipping sector, it is necessary that more research focuses on potential, unanticipated climatic feedbacks from ship exhaust emissions. Here, we show that international policies trying to mitigate the burden of shipping-related air pollution on human health, may lead to secondary, climatic responses, which are not prioritized. It would therefore be beneficial to expand the work presented here, by implementing alternative fuel types, that were not discussed here, and also, to expand the model simulations to include other cloud cases. The Arctic is a unique test-ground, due to strong couplings to process-feedbacks in the climate system and its comparably pristine atmosphere, where ship exhaust emissions may perturb background concentrations of atmospheric constituents substantially, thus leading to stronger feedbacks.[100] Nonetheless, a majority of ship traffic occurs at lower latitudes, where exhaust emissions also lead to perturbations in marine low-level clouds and cause climate feedbacks, potentially with global implications.

Shipping activity in the Arctic requires attention not only from the scientific community, but also from various stakeholders and more importantly, from policy makers. While our modelling results are rather inconclusive with respect to whether increased ship exhaust emissions may lead to substantial perturbations in Arctic mixed-phase clouds and whether this may lead to enhanced climatic feedbacks, it is important to stress that this study was performed using one specific cloud case and experimental data from two engines. Given the wide range of observations existing in the real world, our results depict only a small subset in a vast range of outcomes.

Increased Arctic shipping activity also bears other potential risks to the environment, which have not been investigated here. This includes, for example, increased risks for oil spills due to shipping accidents, the disturbance of ecosystems and increased emissions of black carbon, which can deposit onto snow and ice, and enhance melting. The IMO and its members are aware of related risks. As one of the first steps, MARPOL agreed to adopt a ban on the carriage and usage of heavy fuel oils with densities and kinematic viscosities exceeding 900 kg m^{-3} and 150 mm^2 s^{-1} respectively, for ships operating in polar waters. This will come into effect in June 2024.[116] Moreover, Resolution MEPC.342(77) urges member states to use distillate, or other cleaner fuels or propulsion methods, for ships operating in the Arctic.[163] As of now, this is not mandatory. At the 80th session of the Marine Environment Protection Committee (MEPC), Canada outlined a potential proposal for a Canadian Arctic Emission Control Area. The proposal would require ships, trafficking in Arctic waters under Canadian authority, to adhere to SECA regulations and also, to utilize exhaust after-treatments that reduce NO_x emissions.[164] At the same MEPC session, the organizations Friends of the Earth International (FOEI), World Wildlife Fund (WWF), Pacific Environment and the Clean Shipping Coalition (CSC) suggested different BC control measures, to reduce the impact of ship BC emissions on the Arctic environment.

The document suggests to make it mandatory for ships to use distillate or alternative fuels, and to establish a BC emission control area for the Arctic, which would require ships to use specified fuels and would prohibit the usage of wet scrubbers. More proposed measures are outlined in the document.[165] While suggestions like these seem like a step in the right direction, the process of implementing such regulations can take a substantial amount of time. The Russian Federation, for example, published a comment regarding the mandatory use of distillate fuels for ships navigating Arctic waters, and are skeptical and believe that more scientific proof is required, to clearly show the benefits of distillates compared to more conventional HFO.[166] It is very possible that regulatory changes may affect Arctic shipping in the future.

The results and methods presented in this thesis may help future research, investigating the impact of ship exhaust emissions on Arctic clouds and its climate system. More extensive work is needed to gain greater insight into possible outcomes and to more accurately quantify the net climate impact. Since discussed IMO regulations apply worldwide, this thesis may also give guidance to research aiming to assess the impact of ship exhaust emissions on the global climate.

Bibliography

[1] Freud, E., Krejci, R., Tunved, P., *et al.* Pan-Arctic aerosol number size distributions: seasonality and transport patterns. *Atmospheric Chemistry and Physics*, 17(13): 8101–8128, 2017.

[2] Pernov, J. B., Beddows, D., Thomas, D. C., *et al.* Increased aerosol concentrations in the High Arctic attributable to changing atmospheric transport patterns. *npj Climate and Atmospheric Science*, 5(1):62, 2022.

[3] Dall´Osto, M., Beddows, D. C. S., Tunved, P., *et al.* Arctic sea ice melt leads to atmospheric new particle formation. *Scientific Reports*, 7(1):3318, 2017.

[4] IPCC. *Climate change 2021 – The physical science basis: Working Group I contribution to the Sixth Assessment Report of the Intergovernmental Panel on Climate Change*. Cambridge University Press, 2021. doi: 10.1017/9781009157896.

[5] Tan, I., Oreopoulos, L., and Cho, N. The role of thermodynamic phase shifts in cloud optical depth variations with temperature. *Geophysical Research Letters*, 46 (8):4502–4511, 2019.

[6] Zelinka, M. D., Myers, T. A., McCoy, D. T., *et al.* Causes of higher climate sensitivity in CMIP6 models. *Geophysical Research Letters*, 47(1):e2019GL085782, 2020.

[7] Twomey, S. The influence of pollution on the shortwave albedo of clouds. *Journal of the Atmospheric Sciences*, 34(7):1149–1152, 1977.

[8] Albrecht, B. A. Aerosols, cloud microphysics, and fractional cloudiness. *Science*, 245(4923):1227–1230, 1989.

[9] Seinfeld, J. H. and Pandis, S. N. *Atmospheric chemistry and physics: From air pollution to climate change*. J. Wiley, Hoboken, N.J., 2006.

[10] Petters, M. D. and Kreidenweis, S. M. A single parameter representation of hygroscopic growth and cloud condensation nucleus activity. *Atmospheric Chemistry and Physics*, 7(8):1961–1971, 2007.

[11] Pruppacher, H. R. and Klett, J. D. *Microphysics of clouds and precipitation*, volume 18. Springer Dordrecht, 1997.

[12] Petzold, A., Gysel, M., Vancassel, X., *et al.* On the effects of organic matter and sulphur-containing compounds on the CCN activation of combustion particles. *Atmospheric Chemistry and Physics*, 5(12):3187–3203, 2005.

[13] Henning, S., Ziese, M., Kiselev, A., *et al.* Hygroscopic growth and droplet activation of soot particles: uncoated, succinic or sulfuric acid coated. *Atmospheric Chemistry and Physics*, 12(10):4525–4537, 2012.

[14] Wittbom, C., Eriksson, A. C., Rissler, J., *et al.* Cloud droplet activity changes of soot aerosol upon smog chamber ageing. *Atmospheric Chemistry and Physics*, 14 (18):9831–9854, 2014.

[15] Koop, T., Luo, B., Tsias, A., and Peter, T. Water activity as the determinant for homogeneous ice nucleation in aqueous solutions. *Nature*, 406(6796):611–614, 2000.

[16] Korolev, A. V., Isaac, G. A., Cober, S. G., *et al.* Microphysical characterization of mixed-phase clouds. *Quarterly Journal of the Royal Meteorological Society*, 129 (587 PART A):39–65, 2003.

[17] Vali, G., DeMott, P. J., Möhler, O., and Whale, T. F. Technical Note: A proposal for ice nucleation terminology. *Atmospheric Chemistry and Physics*, 15(18):10263–10270, 2015.

[18] Hallett, J. and Mossop, S. C. Production of secondary ice particles during the riming process. *Nature*, 249(5452):26–28, 1974.

[19] Lloyd, G., Choularton, T. W., Bower, K. N., *et al.* The origins of ice crystals measured in mixed-phase clouds at the high-alpine site Jungfraujoch. *Atmospheric Chemistry and Physics*, 15(22):12953–12969, 2015.

[20] Hoose, C. and Möhler, O. Heterogeneous ice nucleation on atmospheric aerosols: A review of results from laboratory experiments. *Atmospheric Chemistry and Physics*, 12(20):9817–9854, 2012.

[21] Després, V. R., Huffman, J. A., Burrows, S. M., *et al.* Primary biological aerosol particles in the atmosphere: A review. *Tellus B: Chemical and Physical Meteorology*, 64(1):15598, 2012.

[22] Kulkarni, G., Liu, S., Nandasiri, M., *et al.* Ice nucleation activity of diesel soot particles at cirrus relevant temperature conditions: Effects of hydration, secondary organics coating, soot morphology, and coagulation. *Geophysical Research Letters*, 43:3580–3588, 2016.

[23] Mahrt, F., Marcolli, C., David, R. O., *et al.* Ice nucleation abilities of soot particles determined with the Horizontal Ice Nucleation Chamber. *Atmospheric Chemistry and Physics*, 18(18):13363–13392, 2018.

[24] Vergara-Temprado, J., Holden, M. A., Orton, T. R., *et al.* Is black carbon an unimportant ice-nucleating particle in mixed-phase clouds? *Journal of Geophysical Research: Atmospheres*, 123(8):4273–4283, 2018.

[25] Kanji, Z. A., Welti, A., Corbin, J. C., and Mensah, A. A. Black carbon particles do not matter for immersion mode ice nucleation. *Geophysical Research Letters*, 47 (11):1–9, 2020.

[26] Mahrt, F., Alpert, P. A., Dou, J., *et al.* Aging induced changes in ice nucleation activity of combustion aerosol as determined by near edge X-ray absorption fine structure (NEXAFS) spectroscopy. *Environmental Science: Processes & Impacts*, 22(4):895–907, 2020.

[27] Mahrt, F., Kilchhofer, K., Marcolli, C., *et al.* The impact of cloud processing on the ice nucleation abilities of soot particles at cirrus temperatures. *Journal of Geophysical Research: Atmospheres*, 125(3):1–23, 2020.

[28] Gao, K. and Kanji, Z. A. Impacts of cloud-processing on ice nucleation of soot particles internally mixed with sulfate and organics. *Journal of Geophysical Research: Atmospheres*, 127(22):e2022JD037146, 2022.

[29] Gao, K., Zhou, C.-W., Meier, E. J. B., and Kanji, Z. A. Laboratory studies of ice nucleation onto bare and internally mixed soot–sulfuric acid particles. *Atmospheric Chemistry and Physics*, 22(8):5331–5364, 2022.

[30] UNCTAD. Review of maritime transport 2023, 2022.

[31] Heywood, J. B. *Internal combustion engine fundamentals*. McGraw-Hill, New York (N.Y.), 1988. doi: 10.1016/s1350-4789(10)70041-6.

[32] Atkinson, R. Atmospheric chemistry of VOCs and NOx. *Atmospheric Environment*, 34(12):2063–2101, 2000.

[33] Tree, D. R. and Svensson, K. I. Soot processes in compression ignition engines. *Progress in Energy and Combustion Science*, 33(3):272–309, 2007.

[34] Popovicheva, O., Kireeva, E., Shonija, N., *et al.* Ship particulate pollutants: Characterization in terms of environmental implication. *Journal of Environmental Monitoring*, 11(11):2077–2086, 2009.

[35] Moldanová, J., Fridell, E., Popovicheva, O., *et al.* Characterisation of particulate matter and gaseous emissions from a large ship diesel engine. *Atmospheric Environment*, 43(16):2632–2641, 2009.

[36] Anderson, M., Salo, K., Hallquist, Å. M., and Fridell, E. Characterization of particles from a marine engine operating at low loads. *Atmospheric Environment*, 101(2015):65–71, 2015.

[37] Eichler, P., Müller, M., Rohmann, C., *et al.* Lubricating oil as a major constituent of ship exhaust particles. *Environmental Science & Technology Letters*, 4(2):54–58, 2017.

[38] Corbett, J. J., Winebrake, J. J., Green, E. H., *et al.* Mortality from ship emissions: A global assessment. *Environmental Science & Technology*, 41(24):8512–8518, 2007.

[39] Liu, H., Fu, M., Jin, X., *et al.* Health and climate impacts of ocean-going vessels in East Asia. *Nature Climate Change*, 6(11):1037–1041, 2016.

[40] Jonson, J. E., Gauss, M., Schulz, M., *et al.* Effects of global ship emissions on European air pollution levels. *Atmospheric Chemistry and Physics*, 20(19):11399–11422, 2020.

[41] International Maritime Organisation (IMO). RESOLUTION MEPC.176(58) - Revised MARPOL Annex VI. 2008.

[42] International Maritime Organization (IMO). RESOLUTION MEPC.361(79) - Mediterranean Sea Emission Control Area for sulphur oxides and particulate matter, 2022.

[43] Det Norske Veritas (DNV) group. Alternative fuels insight. URL `https://afi.dnv.com`. Accessed on 2024-01-02.

[44] Zetterdahl, M., Moldanová, J., Pei, X., *et al.* Impact of the 0.1% fuel sulfur content limit in SECA on particle and gaseous emissions from marine vessels. *Atmospheric Environment*, 145:338–345, 2016.

[45] Seppälä, S. D., Kuula, J., Hyvärinen, A.-P., *et al.* Effects of marine fuel sulfur restrictions on particle number concentrations and size distributions in ship plumes in the Baltic Sea. *Atmospheric Chemistry and Physics*, 21(4):3215–3234, 2021.

[46] Yu, C., Pasternak, D., Lee, J., *et al.* Characterizing the particle composition and cloud condensation nuclei from shipping emission in Western Europe. *Environmental Science & Technology*, 54(24):15604–15612, 2020.

[47] Yu, C., Pasternak, D., Lee, J., *et al.* Correction to "Characterizing the particle composition and cloud condensation nuclei from shipping emission in Western Europe". *Environmental Science & Technology*, 57(20):7888–7889, 2023.

[48] Anastasopolos, A. T., Sofowote, U. M., Hopke, P. K., *et al.* Air quality in Canadian port cities after regulation of low-sulphur marine fuel in the North American Emissions Control Area. *Science of The Total Environment*, 791:147949, 2021.

[49] Wu, Z., Zhang, Y., He, J., *et al.* Dramatic increase in reactive volatile organic compound (VOC) emissions from ships at berth after implementing the fuel switch policy in the Pearl River Delta Emission Control Area. *Atmospheric Chemistry and Physics*, 20(4):1887–1900, 2020.

[50] Sofiev, M., Winebrake, J. J., Johansson, L., *et al.* Cleaner fuels for ships provide public health benefits with climate tradeoffs. *Nature Communications*, 9(1):406, 2018.

[51] Kuittinen, N., Jalkanen, J.-P., Alanen, J., *et al.* Shipping remains a globally significant source of anthropogenic PN emissions even after 2020 sulfur regulation. *Environmental Science & Technology*, 55(1):129–138, 2021.

[52] Zhai, J., Yu, G., Zhang, J., *et al.* Impact of ship emissions on air quality in the Greater Bay Area in China under the latest global marine fuel regulation. *Environmental Science & Technology*, 57(33):12341–12350, 2023.

[53] Lehtoranta, K., Aakko-Saksa, P., Murtonen, T., *et al.* Particulate mass and nonvolatile particle number emissions from marine engines using low-sulfur fuels, natural gas, or scrubbers. *Environmental Science & Technology*, 53(6):3315–3322, 2019.

[54] Gronholm, T., Makela, T., Hatakka, J., *et al.* Evaluation of methane emissions originating from LNG ships based on the measurements at a remote marine station. *Environmental Science and Technology*, 55(20):13677–13686, 2021.

[55] Balcombe, P., Heggo, D. A., and Harrison, M. Total methane and CO_2 emissions from liquefied natural gas carrier ships: The first primary measurements. *Environmental Science & Technology*, 56(13):9632–9640, 2022.

[56] Karle, I. M. and Turner, D. Seawater scrubbing - reduction of SOx emissions from ship exhausts, 2007. URL `https://research.chalmers.se/publication/106400/file/106400_Fulltext.pdf`. Accessed on 2024-01-02.

[57] Oikawa, K., Yongsiri, C., Takeda, K., and Harimoto, T. Seawater flue gas desulfurization: Its technical implications and performance results. *Environmental Progress*, 22(1):67–73, 2003.

[58] Andreasen, A. and Mayer, S. Use of seawater scrubbing for SO2 removal from marine engine exhaust gas. *Energy and Fuels*, 21(6):3274–3279, 2007.

[59] Lloyd's Register Group. *Understanding exhaust gas treatment systems - Guidance for shipowners and operators*. London, 2012.

[60] International Maritime Organisation (IMO). RESOLUTION MEPC.340(77) - 2021 Guidelines for Exhaust Gas Cleaning Systems, 2021.

[61] Lunde Hermansson, A., Hassellöv, I.-M., Moldanová, J., and Ytreberg, E. Comparing emissions of polyaromatic hydrocarbons and metals from marine fuels and scrubbers. *Transportation Research Part D: Transport and Environment*, 97:102912, 2021.

[62] Ytreberg, E., Hansson, K., Hermansson, A. L., *et al.* Metal and PAH loads from ships and boats, relative other sources, in the Baltic Sea. *Marine Pollution Bulletin*, 182:113904, 2022.

[63] International Council on Clean Transportation. Global update on scrubber bans and restrictions, 2023. URL `https://theicct.org/wp-content/uploads/2023/06/Scrubbers_policy_update_final.pdf`. Accessed on 2024-01-02.

[64] Fridell, E. and Salo, K. Measurements of abatement of particles and exhaust gases in a marine gas scrubber. *Proceedings of the Institution of Mechanical Engineers, Part M: Journal of Engineering for the Maritime Environment*, 230(1):154–162, 2016.

[65] Winnes, H., Fridell, E., and Moldanová, J. Effects of marine exhaust gas scrubbers on gas and particle emissions. *Journal of Marine Science and Engineering*, 8(4): 299, 2020.

[66] Zhou, J., Zhou, S., and Zhu, Y. Characterization of particle and gaseous emissions from marine diesel engines with different fuels and impact of after-treatment technology. *Energies*, 10(8):1110, 2017.

[67] Yang, J., Tang, T., Jiang, Y., *et al.* Controlling emissions from an ocean-going container vessel with a wet scrubber system. *Fuel*, 304:121323, 2021.

[68] Jeong, S., Bendl, J., Saraji-Bozorgzad, M., *et al.* Aerosol emissions from a marine diesel engine running on different fuels and effects of exhaust gas cleaning measures. *Environmental Pollution*, 316:120526, 2023.

[69] Järvinen, A., Lehtoranta, K., Aakko-Saksa, P., *et al.* Performance of a wet electrostatic precipitator in marine applications. *Journal of Marine Science and Engineering*, 11(2):393, 2023.

[70] Lieke, K. I., Rosenørn, T., Pedersen, J., *et al.* Micro- and nanostructural characteristics of particles before and after an exhaust gas recirculation system scrubber. *Aerosol Science and Technology*, 47(9):1038–1046, 2013.

[71] Nations, U. Green Shipping Challenge, 2023. URL `https://greenshippingchallenge.org`. Accessed on 2024-01-02.

[72] International Maritime Organisation (IMO). Resolution mepc.377(80) - 2023 imo strategy on reduction of ghg emissions from ships, 2023.

[73] Coakley, J. A., Bernstein, R. L., and Durkee, P. A. Effect of ship-stack effluents on cloud reflectivity. *Science*, 237(4818):1020–1022, 1987.

[74] Hobbs, P. V., Garrett, T. J., Ferek, R. J., *et al.* Emissions from ships with respect to their effects on clouds. *Journal of the Atmospheric Sciences*, 57(16):2570–2590, 2000.

[75] Durkee, P. A., Noone, K. J., Ferek, R. J., *et al.* The impact of ship-produced aerosols on the microstructure and albedo of warm marine stratocumulus clouds: A test of MAST hypotheses 1i and 1ii. *Journal of the Atmospheric Sciences*, 57(16): 2554–2569, 2000.

[76] Lauer, A., Eyring, V., Hendricks, J., *et al.* Global model simulations of the impact of ocean-going ships on aerosols, clouds, and the radiation budget. *Atmospheric Chemistry and Physics*, 7(19):5061–5079, 2007.

[77] Eyring, V., Isaksen, I. S., Berntsen, T., *et al.* Transport impacts on atmosphere and climate: Shipping. *Atmospheric Environment*, 44(37):4735–4771, 2010.

[78] Lund, M. T., Eyring, V., Fuglestvedt, J., *et al.* Global-mean temperature change from shipping toward 2050: Improved representation of the indirect aerosol effect in simple climate models. *Environmental Science & Technology*, 46(16):8868–8877, 2012.

[79] Lund, M. T., Aamaas, B., Stjern, C. W., *et al.* A continued role of short-lived climate forcers under the Shared Socioeconomic Pathways. *Earth System Dynamics*, 11(4): 977–993, 2020.

[80] Lack, D. A., Cappa, C. D., Langridge, J., *et al.* Impact of fuel quality regulation and speed reductions on shipping emissions: Implications for climate and air quality. *Environmental Science & Technology*, 45(20):9052–9060, 2011.

[81] Gryspeerdt, E., Smith, T. W. P., O'Keeffe, E., *et al.* The impact of ship emission controls recorded by cloud properties. *Geophysical Research Letters*, 46(21):12547–12555, 2019.

[82] Yuan, T., Song, H., Wood, R., *et al.* Global reduction in ship-tracks from sulfur regulations for shipping fuel. *Science Advances*, 8(29):1–9, 2022.

[83] Watson-Parris, D., Christensen, M. W., Laurenson, A., *et al.* Shipping regulations lead to large reduction in cloud perturbations. *Proceedings of the National Academy of Sciences*, 119(41), 2022.

[84] Manshausen, P., Watson-Parris, D., Christensen, M. W., *et al.* Invisible ship tracks show large cloud sensitivity to aerosol. *Nature*, 610(7930):101–106, 2022.

[85] Diamond, M. S. Detection of large-scale cloud microphysical changes within a major shipping corridor after implementation of the International Maritime Organization 2020 fuel sulfur regulations. *Atmospheric Chemistry and Physics*, 23(14):8259–8269, 2023.

[86] Serreze, M. C. and Barry, R. G. *The Arctic climate system*. Cambridge University Press, Cambridge, 2006.

[87] Intrieri, J. M., Fairall, C. W., Shupe, M. D., *et al.* An annual cycle of Arctic surface cloud forcing at SHEBA. *Journal of Geophysical Research: Oceans*, 107(C10): SHE 13–1–SHE 13–14, 2002.

[88] Shupe, M. D. and Intrieri, J. M. Cloud radiative forcing of the Arctic surface: The influence of cloud properties, surface albedo, and solar zenith angle. *Journal of Climate*, 17(3):616–628, 2004.

[89] Shupe, M. D., Matrosov, S. Y., and Uttal, T. Arctic mixed-phase cloud properties derived from surface-based sensors at SHEBA. *Journal of the Atmospheric Sciences*, 63(2):697–711, 2006.

[90] Morrison, H., De Boer, G., Feingold, G., *et al.* Resilience of persistent Arctic mixed-phase clouds. *Nature Geoscience*, 5(1):11–17, 2012.

[91] Solomon, A., Feingold, G., and Shupe, M. D. The role of ice nuclei recycling in the maintenance of cloud ice in Arctic mixed-phase stratocumulus. *Atmospheric Chemistry and Physics*, 15(18):10631–10643, 2015.

[92] Bekryaev, R. V., Polyakov, I. V., and Alexeev, V. A. Role of polar amplification in long-term surface air temperature variations and modern Arctic warming. *Journal of Climate*, 23(14):3888–3906, 2010.

[93] Screen, J. A. and Simmonds, I. The central role of diminishing sea ice in recent Arctic temperature amplification. *Nature*, 464(7293):1334–1337, 2010.

[94] IPCC. *Climate change 2013 – The physical science basis: Working Group I contribution to the Fifth Assessment Report of the Intergovernmental Panel on Climate Change*. Cambridge University Press, 2014. doi: 10.1017/CBO9781107415324.

[95] Serreze, M. C. and Barry, R. G. Processes and impacts of Arctic amplification: A research synthesis. *Global and Planetary Change*, 77(1-2):85–96, 2011.

[96] Kay, J. E. and Gettelman, A. Cloud influence on and response to seasonal Arctic sea ice loss. *Journal of Geophysical Research: Atmospheres*, 114(D18):2009JD011773, 2009.

[97] Pithan, F. and Mauritsen, T. Arctic amplification dominated by temperature feedbacks in contemporary climate models. *Nature Geoscience*, 7(3):181–184, 2014.

[98] Morrison, A. L., Kay, J. E., Frey, W. R., *et al.* Cloud response to Arctic sea ice loss and implications for future feedback in the CESM1 Climate Model. *Journal of Geophysical Research: Atmospheres*, 124(2):1003–1020, 2019.

[99] Schmale, J., Zieger, P., and Ekman, A. M. L. Aerosols in current and future Arctic climate. *Nature Climate Change*, 11(2):95–105, 2021.

[100] Mauritsen, T., Sedlar, J., TjernstrÃm, M., *et al.* An Arctic CCN-limited cloud-aerosol regime. *Atmospheric Chemistry and Physics*, 11(1):165–173, 2011.

[101] ACIA. *Impacts of a warming Arctic: Arctic climate impact assessment*. Cambridge University Press, Cambridge, 2005.

[102] Lasserre, F. and Pelletier, S. Polar super seaways? Maritime transport in the Arctic: an analysis of shipowners' intentions. *Journal of Transport Geography*, 19(6): 1465–1473, 2011.

[103] Song, S., Chen, Y., Chen, X., *et al.* Adapting to a foggy future along trans-Arctic shipping routes. *Geophysical Research Letters*, 50(8):e2022GL102395, 2023.

[104] Paxian, A., Eyring, V., Beer, W., *et al.* Present-day and future global bottom-up ship emission inventories including polar routes. *Environmental Science & Technology*, 44(4):1333–1339, 2010.

[105] Corbett, J. J., Lack, D. A., Winebrake, J. J., *et al.* Arctic shipping emissions inventories and future scenarios. *Atmospheric Chemistry and Physics*, 10(19): 9689–9704, 2010.

[106] Peters, G. P., Nilssen, T. B., Lindholt, L., *et al.* Future emissions from shipping and petroleum activities in the Arctic. *Atmospheric Chemistry and Physics*, 11(11): 5305–5320, 2011.

[107] Theocharis, D., Pettit, S., Rodrigues, V. S., and Haider, J. Arctic shipping: A systematic literature review of comparative studies. *Journal of Transport Geography*, 69:112–128, 2018.

[108] Hansen, J. and Nazarenko, L. Soot climate forcing via snow and ice albedos. *Proceedings of the National Academy of Sciences*, 101(2):423–428, 2004.

[109] Browse, J., Carslaw, K. S., Schmidt, A., and Corbett, J. J. Impact of future Arctic shipping on high-latitude black carbon deposition. *Geophysical Research Letters*, 40(16):4459–4463, 2013.

[110] Namazi, M., Von Salzen, K., and Cole, J. N. S. Simulation of black carbon in snow and its climate impact in the Canadian Global Climate Model. *Atmospheric Chemistry and Physics*, 15(18):10887–10904, 2015.

[111] Christensen, M. W., Suzuki, K., Zambri, B., and Stephens, G. L. Ship track observations of a reduced shortwave aerosol indirect effect in mixed-phase clouds. *Geophysical Research Letters*, 41(19):6970–6977, 2014.

[112] Possner, A., Ekman, A. M. L., and Lohmann, U. Cloud response and feedback processes in stratiform mixed-phase clouds perturbed by ship exhaust. *Geophysical Research Letters*, 44(4):1964–1972, 2017.

[113] Gilgen, A., Huang, W. T. K., Ickes, L., *et al.* How important are future marine and shipping aerosol emissions in a warming Arctic summer and autumn? *Atmospheric Chemistry and Physics*, 18(14):10521–10555, 2018.

[114] Stephenson, S. R., Wang, W., Zender, C. S., *et al.* Climatic responses to future trans-Arctic shipping. *Geophysical Research Letters*, 45(18):9898–9908, 2018.

[115] Eirund, G. K., Possner, A., and Lohmann, U. Response of Arctic mixed-phase clouds to aerosol perturbations under different surface forcings. *Atmospheric Chemistry and Physics*, 19(15):9847–9864, 2019.

[116] International Maritime Organisation (IMO). RESOLUTION MEPC.329(76) - Prohibition on the use and carriage for use as fuel of heavy fuel oil by ships in Arctic waters, 2021.

[117] Santos, L. F. E. d., Salo, K., and Thomson, E. S. Quantification and physical analysis of nanoparticle emissions from a marine engine using different fuels and a laboratory wet scrubber. *Environmental Science: Processes & Impacts*, 24:1769–1781, 2022.

[118] Santos, L. F. E. d., Salo, K., Kong, X., *et al.* Changes in CCN activity of ship exhaust particles induced by fuel sulfur content reduction and wet scrubbing. *Environmental Science: Atmospheres*, 3(1):182–195, 2023.

[119] Tjernström, M., Birch, C. E., Brooks, I. M., *et al.* Meteorological conditions in the central Arctic summer during the Arctic Summer Cloud Ocean Study (ASCOS). *Atmospheric Chemistry and Physics*, 12(15):6863–6889, 2012.

[120] Tjernström, M., Leck, C., Birch, C. E., *et al.* The Arctic Summer Cloud Ocean Study (ASCOS): Overview and experimental design. *Atmospheric Chemistry and Physics*, 14:2823–2869, 2014.

[121] Aliabadi, A. A., Thomas, J. L., Herber, A. B., *et al.* Ship emissions measurement in the Arctic by plume intercepts of the Canadian Coast Guard icebreaker Amundsen from the Polar 6 aircraft platform. *Atmospheric Chemistry and Physics*, 16(12): 7899–7916, 2016.

[122] Moldanová, J., Fridell, E., Winnes, H., *et al.* Physical and chemical characterisation of PM emissions from two ships operating in European Emission Control Areas. *Atmospheric Measurement Techniques*, 6(12):3577–3596, 2013.

[123] TSI Incorporation. Electrostatic Classifier model 3082 Scanning Mobility Particle Sizer™ (SMPS™) spectrometer model 3938, 1966.

[124] Hinds, W. C. *Aerosol technology: Properties, behavior, and measurement of airborne particles*. Wiley, New York (N.Y.), 1999.

[125] Tavakoli, F. and Olfert, J. S. An instrument for the classification of aerosols by particle relaxation time: Theoretical models of the aerodynamic aerosol classifier. *Aerosol Science and Technology*, 47(8):916–926, 2013.

[126] Tavakoli, F. and Olfert, J. S. Determination of particle mass, effective density, mass-mobility exponent, and dynamic shape factor using an aerodynamic aerosol classifier and a differential mobility analyzer in tandem. *Journal of Aerosol Science*, 75:35–42, 2014.

[127] Park, K., Cao, F., Kittelson, D. B., and McMurry, P. H. Relationship between particle mass and mobility for diesel exhaust particles. *Environmental Science and Technology*, 37(3):577–583, 2003.

[128] Wobrauschek, P., Streli, C., and Lindgren, E. S. Energy dispersive, X-ray fluorescence analysis. *Encyclopedia of analytical chemistry*, pages 1–17, 2010.

[129] Moffet, R. C., Tivanski, A. V., and Gilles, M. K. *Fundamentals and applications in aerosol spectroscopy*. CRC Press; Taylor & Francis Group, Boca Raton, FL, 2011.

[130] Hitchcock, A. axis 2000 - Analysis of X-ray images and spectra. URL `http://unicorn.mcmaster.ca/axis/aXis2000-IDLVM.html`. Accessed on 2024-01-02.

[131] Roberts, G. C. and Nenes, A. A Continuous-Flow Streamwise Thermal-Gradient CCN chamber for atmospheric measurements. *Aerosol Science and Technology*, 39 (3):206–221, 2005.

[132] Moore, R. H. and Nenes, A. Scanning flow CCN analysis - A method for fast measurements of CCN spectra. *Aerosol Science and Technology*, 43(12):1192–1207, 2009.

[133] Castarède, D., Brasseur, Z., Wu, Y., *et al.* Development and characterization of the Portable Ice Nucleation Chamber 2 (PINCii). 16(16):3881–3899, 2023.

[134] Rogers, D. C. Development of a Continuous Flow Thermal Gradient Diffusion Chamber for ice nucleation studies. *Atmospheric Research*, 22:149–181, 1988.

[135] Stetzer, O., Baschek, B., Lüönd, F., and Lohmann, U. The Zurich Ice Nucleation Chamber (ZINC) - A new instrument to investigate atmospheric ice formation. *Aerosol Science and Technology*, 42(1):64–74, 2008.

[136] Kanji, Z. A. and Abbatt, J. P. The university of toronto continuous flow diffusion chamber (UT-CFDC): A simple design for ice nucleation studies. *Aerosol Science and Technology*, 43(7):730–738, 2009.

[137] Kristensen, T. B., Falk, J., Lindgren, R., *et al.* Properties and emission factors of cloud condensation nuclei from biomass cookstoves – observations of a strong dependency on potassium content in the fuel. *Atmospheric Chemistry and Physics*, 21(10):8023–8044, 2021.

[138] Savre, J., Ekman, A. M. L., and Svensson, G. Technical note: Introduction to MIMICA, a large-eddy simulation solver for cloudy planetary boundary layers. *Journal of Advances in Modeling Earth Systems*, 6(3):630–649, 2014.

[139] Bulatovic, I., Ekman, A. M. L., Savre, J., *et al.* Aerosol indirect effects in marine stratocumulus: The importance of explicitly predicting cloud droplet activation. *Geophysical Research Letters*, 46(6):3473–3481, 2019.

[140] Stevens, R. G., Loewe, K., Dearden, C., *et al.* A model intercomparison of CCN-limited tenuous clouds in the high Arctic. *Atmospheric Chemistry and Physics*, 18 (15):11041–11071, 2018.

[141] Christiansen, S., Ickes, L., Bulatovic, I., *et al.* Influence of Arctic microlayers and algal cultures on sea spray hygroscopicity and the possible implications for mixed-phase clouds. *Journal of Geophysical Research: Atmospheres*, 125(19), 2020.

[142] Bulatovic, I., Igel, A. L., Leck, C., *et al.* The importance of Aitken mode aerosol particles for cloud sustenance in the summertime high Arctic – a simulation study supported by observational data. *Atmospheric Chemistry and Physics*, 21(5):3871–3897, 2021.

[143] Sotiropoulou, G., Ickes, L., Nenes, A., and Ekman, A. M. L. Ice multiplication from ice–ice collisions in the high Arctic: sensitivity to ice habit, rimed fraction, ice type and uncertainties in the numerical description of the process. *Atmospheric Chemistry and Physics*, 21(12):9741–9760, 2021.

[144] Frostenberg, H. C., Welti, A., Luhr, M., *et al.* The chance of freezing – a conceptional study to parameterize temperature-dependent freezing by including randomness of ice-nucleating particle concentrations. *Atmospheric Chemistry and Physics*, 23(19): 10883–10900, 2023.

[145] Seifert, A. and Beheng, K. D. A double-moment parameterization for simulating autoconversion, accretion and selfcollection. *Atmospheric Research*, 59-60:265–281, 2001.

[146] Seifert, A. and Beheng, K. D. A two-moment cloud microphysics parameterization for mixed-phase clouds. Part 1: Model description. *Meteorol. Atmospheric Phys.*, 92(1-2):45–66, 2006.

[147] Wang, C. and Chang, J. S. A three-dimensional numerical model of cloud dynamics, microphysics, and chemistry: 1. Concepts and formulation. *Journal of Geophysical Research: Atmospheres*, 98(D8):14827–14844, 1993.

[148] Lohmann, U., Lüönd, F., and Mahrt, F. *An introduction to clouds: From the microscale to climate*. Cambridge University Press, Cambridge, 2016. doi: 10.1017/CBO9781139087513.

[149] Freud, E. and Rosenfeld, D. Linear relation between convective cloud drop number concentration and depth for rain initiation: Drop Concentration and rain initiation. *Journal of Geophysical Research: Atmospheres*, 117(D2), 2012.

[150] Stephens, G. L. Radiation profiles in extended water clouds. ii: Parameterization schemes. *Journal of Atmospheric Sciences*, 35(11):2123 – 2132, 1978.

[151] Meador, W. E. and Weaver, W. R. Two-stream approximations to radiative transfer in planetary atmospheres: A unified description of existing methods and a new improvement. *Journal of Atmospheric Sciences*, 37(3):630 – 643, 1980.

[152] Kasper, A., Aufdenblatten, S., Forss, A., *et al.* Particulate emissions from a low-speed marine diesel engine. *Aerosol Science and Technology*, 41(1):24–32, 2007.

[153] Streibel, T., Schnelle-Kreis, J., Czech, H., *et al.* Aerosol emissions of a ship diesel engine operated with diesel fuel or heavy fuel oil. *Environmental Science and Pollution Research*, 24(12):10976–10991, 2017.

[154] Alanen, J., Isotalo, M., Kuittinen, N., *et al.* Physical characteristics of particle emissions from a medium speed ship engine fueled with natural gas and low-sulfur liquid fuels. *Environmental Science & Technology*, 54(9):5376–5384, 2020.

[155] Momenimovahed, A., Gagné, S., Gajdosechova, Z., *et al.* Effective density and metals content of particle emissions generated by a diesel engine operating under different marine fuels. *Journal of Aerosol Science*, 151, 2021.

[156] Olfert, J. and Rogak, S. Universal relations between soot effective density and primary particle size for common combustion sources. *Aerosol Science and Technology*, 53(5):485–492, 2019.

[157] Ouf, F.-X., Bourrous, S., Fauvel, S., *et al.* True density of combustion emitted particles: A comparison of results highlighting the influence of the organic contents. *Journal of Aerosol Science*, 134:1–13, 2019.

[158] Braun, A. Carbon speciation in airborne particulate matter with C (1s) NEXAFS spectroscopy. *Journal of Environmental Monitoring*, 7(11):1059–1065, 2005.

[159] Tivanski, A. V., Hopkins, R. J., Tyliszczak, T., and Gilles, M. K. Oxygenated interface on biomass burn tar balls determined by single particle scanning transmission X-ray microscopy. *The Journal of Physical Chemistry A*, 111(25):5448–5458, 2007.

[160] Sarret, G., Connan, J., Kasrai, M., *et al.* Chemical forms of sulfur in geological and archeological asphaltenes from Middle East, France, and Spain determined by sulfur K- and L-edge X-ray absorption near-edge structure spectroscopy. *Geochimica et Cosmochimica Acta*, 63(22):3767–3779, 1999.

[161] Priestley, M., Pei, X., Ohigashi, T., *et al.* Transformation of morphological and chemical properties by coating materials on soot. *AIP Conference Proceedings*, 2990(1):020004, 2023.

[162] Thomson, E. S., Weber, D., Bingemer, H. G., *et al.* Intensification of ice nucleation observed in ocean ship emissions. *Scientific Reports*, 8(1):1111, 2018.

[163] International Maritime Organisation (IMO). RESOLUTION MEPC.342(77) - Protecting the Arctic from shipping black carbon emissions, 2021.

[164] International Maritime Organisation (IMO). MEPC 80/16/2 - Development of a proposal to designate a Canadian Arctic Emission Control Area, 2023.

[165] International Maritime Organisation (IMO). MEPC 80/9/1 - Reducing black carbon emissions in the Arctic, 2023.

[166] International Maritime Organisation (IMO). PPR 10/6/1 - Reduction of the impact on the Arctic of black carbon emissions from international shipping. 2023.